REALIZING COMBINED VALUE STREAMS FROM CUSTOMER-SIDE RESOURCES

by

Akintonde Olukunle Abbas

A dissertation submitted to the faculty of
The University of North Carolina at Charlotte
in partial fulfillment of the requirements
for the degree of Doctor of Philosophy in
Electrical Engineering

Charlotte

2022

Approved by:

Dr. Badrul Chowdhury

Dr. Valentina Cecchi

Dr. Robert Cox

Dr. Peter Schwarz

©2022
Akintonde Olukunle Abbas
ALL RIGHTS RESERVED

ABSTRACT

AKINTONDE OLUKUNLE ABBAS. Realizing combined value streams from customer-side resources. (Under the direction of DR. BADRUL CHOWDHURY)

The importance of flexible customer-side resources in transitioning to a clean energy future is becoming increasingly apparent. Flexible customer-side resources can resolve most issues associated with intelligent and low carbon power grids and, in the process, unlock new value streams for both resource owners and load-serving entities (LSEs) with access to those resources. However, most LSEs with access to numerous flexible customer-side resources often use them for single applications when these resources can provide multiple value streams simultaneously. This dissertation focuses on developing models and frameworks to help LSEs simultaneously capture multiple value streams from customer-side resources within their jurisdiction.

Firstly, a stochastic equivalent battery model (EBM) that provides a simple yet accurate representation of the overall power consumption flexibility associated with a commercial building is proposed. The proposed stochastic EBM combines model-based functional simulations and optimization techniques to quantify the overall flexibility of a commercial building with flexible resources such as heating, ventilation, and air-conditioning (HVAC), electric water heater (EWH), battery, and electric vehicle charging stations. Illustrative case studies showcasing how the proposed model fits into complex resource scheduling problems whose objectives either maximize or minimize some value reflecting the LSE's intended outcomes are also considered.

Secondly, a stochastic optimization framework is proposed to help an LSE capture value streams involving bulk power system support services from its residential customer-side resources. The specific value streams of interest are energy arbitrage, peak shaving, and market-based frequency regulation, while the customer-side resources are residential HVACs, EWHs, and behind-the-meter (BTM) storage. A

resource type-centric clustering method is employed. The proposed framework contains two parts. The first part involves a day-ahead resource scheduling problem that captures uncertainties in energy prices, regulation prices, and frequency regulation signals. A voltage sensitivity matrix-based approach is proposed to capture the impacts of resource control actions on system voltages. The second part includes two real-time resource dispatch algorithms capable of eliciting fast responses from the resources to frequency regulation signals from the market operator with minimal voltage violations. The scheduling model and dispatch algorithms are evaluated using a HELICS-based co-simulation platform and real-world market data from New York Independent System Operator (NYISO).

Thirdly, a stochastic optimization framework is proposed to help an LSE capture multiple value streams focused on distribution system operations from its residential customer-side resources. The value streams of interest are peak shaving, energy arbitrage, ramp rate reduction, loss reduction, and voltage management. The framework captures the impact of third-party aggregators on the LSE's network and includes two dispatch algorithms - decision rule-based dispatch and optimal real-time dispatch.

Finally, a framework to help LSEs compensate owners of customer-side resources for multiple value streams is proposed. The compensation sharing approach classifies the LSE's realized value into three categories - additive, super-additive and sub-additive. The appropriate compensation-sharing mechanism is then defined for each value category. A special component of the compensation sharing mechanism that provides additional social benefits, specifically credit rating improvement, for low and medium-income flexible resource owners is also proposed.

DEDICATION

This dissertation is dedicated to God Almighty and my mother, who have paved the path for my life's journey. This doctoral journey would have been impossible without your help, sacrifices, and guidance. I am eternally grateful.

ACKNOWLEDGEMENTS

To my advisor, Dr. Badrul Chowdhury, thank you for your support, guidance, mentorship, deep insights, and thorough feedback at each step of this Ph.D. journey. It was such an honor to have worked with you.

Also, I appreciate my committee members, Dr. Valentina Cecchi, Dr. Robert Cox, and Dr. Peter Schwarz, for all the interesting conversations and insights provided to improve this work.

To my amazing siblings, Omolola, Abiodun, Titilayo, Olayemi, and Boluwatife, thanks for your support and constant prayers. To my very special person, Abiola, you are simply the best. To all my amazing friends and colleagues, thanks for keeping me going.

I would also like to appreciate The United States Department of Energy, Duke Energy, National Renewable Energy Laboratory, UNCC Graduate School, and UNCC Energy Production and Infrastructure Center for all the funding to support my work. I am very grateful.

TABLE OF CONTENTS

LIST OF TABLES

LIST OF FIGURES

CHAPTER 1: INTRODUCTION

Flexible resources on the demand side of the grid can be described as the hidden gems of the clean energy transition. However, these gems are no longer staying hidden. Multiple enabling policies and technological advancements, including improved performance and reduced costs of computing, connectivity, and communication technologies, are unraveling the value hidden in these resources. For example, according to a Microsoft report, the average cost of internet-of-things (IoT) sensors declined by 200% between 2008 and 2014 [1]. On the policy front, policies like FERC Orders 2222 and 841 are unlocking multiple value streams for flexible customer-side resources [2]. Also, these enabling policies, coupled with cost reductions driven by technological advancements and increasing awareness of climate change and sustainability, encourage electricity consumers to invest in more flexible resources. As such, these flexible resources can provide value to the resource owners, load-serving entities (LSEs), and every other user connected to the power grid. Note that the LSE is any entity that is able to supply electricity to a group of consumers. For the resource owner, the value can be in energy cost reductions or additional incentives for participation in demand-side management programs. For the LSE, the value can be reduced operating costs or additional revenue streams. Reducing the LSE's operating costs could lead to overall energy bill reductions for other grid users.

According to the North American Electric Reliability Corporation, demand-side management practices can be grouped into two broad classes - Demand Response and Energy Efficiency [3]. While energy efficiency represents a static paradigm, demand response is more dynamic. The United States Federal Electricity Regulatory Commission (FERC) defines demand response as "changes in electricity usage by demand-side

resources from their normal consumption patterns in response to changes in the price of electricity over time, or to incentive payments designed to induce lower electricity use at times of high wholesale market prices or when system reliability is jeopardized " [4]. Although FERC's demand response definition tilts towards reducing electricity consumption, flexible customer-side resources can also provide upward flexibility. For example, the power consumption of a group of residential air-conditioners can be increased for a short period to track frequency regulation signals [5].

Furthermore, customer-side resources can provide multiple value streams simultaneously, as shown in [6–8]. However, LSEs often only capture single value streams from the flexible customer-side resources within their jurisdiction leading to an underutilization of these resources. As such, this dissertation provides tools to help LSEs address typical problems on the journey toward making the most of flexible customer-side resources within their jurisdictions.

The problems associated with capturing multiple value streams from flexible customer-side resources can be grouped into four general categories - Resource Modeling, Planning and Operations, Compensations, and Policy Considerations. While each of these categories is very important, this dissertation focuses on addressing some of the gaps in the first three categories (i.e., Resource Modeling, Planning and Operations, Compensations) with the assumption that favorable policies are in place. However, future work can focus on exploring new policies that can augment existing ones to fully unlock the potential value of flexible customer-side resources.

1.1 Resource Modeling

Accurate and simple models of the flexible customer-side resources are required to capture multiple value streams from these resources. Due to their relatively small sizes, flexible customer-side resources are often aggregated to provide significant value. These aggregations can be classified as homogeneous or heterogeneous depending on the nature of the multiple resources treated as one [9]. For example, an aggregation

of residential HVAC resources is a homogeneous aggregation, while an aggregation containing all flexible resources in a commercial building is heterogeneous. However, modeling each resource separately could be impractical, especially when the LSE considers multiple resources. As such, simple yet accurate aggregate models are highly desirable.

Extensive work has been done on aggregate models for both homogeneous and heterogeneous resource aggregations. The authors in [10] proposed an aggregate model for residential thermostatically controlled loads (TCLs). Also, the authors in [11–13] discuss different variations of the equivalent battery model (EBM) concept for capturing the overall flexibility associated with an aggregation of residential air conditioning units. Both stochastic and deterministic EBM representations have been proposed for aggregations of residential TCLs. EBM representations have also been proposed for commercial HVAC systems [8]. However, before this study, no EBM representation captured uncertainties associated with the operation of a commercial building and captured its overall flexibility. The second chapter of this dissertation provides a detailed discussion of the proposed stochastic EBM model for representing a commercial building's flexibility.

1.2 Planning and Operations

The planning process for an LSE covers different time scales. However, this dissertation focuses on planning from a day-ahead perspective. An exciting area of further research is how using flexible customer-side resources for combined value streams fits into an LSE's long-term planning framework.

LSEs need to know how best to operate the available flexible customer-side resources within their jurisdictions to capture the multiple value streams desired during the next operating day. This planning requirement applies to LSEs in regulated and deregulated electricity market environments. However, the planning details depend on the nature of the value streams of interest. The third and fourth chapters

provide novel day-ahead stochastic scheduling models that LSEs can use to plan for value streams relating to the bulk power system and distribution system operations, respectively.

In addition to planning, LSEs also need to know how to dispatch individual flexible customer-side resources to achieve the multiple value streams planned for in real time. This implies that the LSE requires a detailed understanding of different real-time resource dispatch algorithms. The LSE also needs to clearly understand the pros and cons of such resource dispatch algorithms. The third and fourth chapters also include detailed discussions about different real-time dispatch algorithms that LSEs can use to dispatch customer-side resources to capture multiple value streams focused on bulk power system and distribution system operations.

1.3 Compensation

The LSE also requires fair mechanisms to compensate the flexible customer-side resources for participating in their flexibility programs and providing multiple services. Also, the LSE can introduce innovative compensation dimensions to incentivize participation from a particular customer segment. The fifth chapter of this dissertation focuses on a practical game theory-based compensation framework that can be easily adapted to different LSEs. A novel concept of social compensation dimensions, specifically credit rating improvements, in addition to financial compensations for low and medium-income (LMI) flexible resource owners, is also introduced.

1.4 Dissertation Format

This dissertation follows a three-paper format allowed by UNCC's Graduate School. In reality, four papers were prepared for publication. Short descriptions of the chapters are provided below for context:

Chapter 1 is the introductory chapter and provides an overview and overall motivation for the dissertation.

Chapter 2 deals with a simplified representation of the overall flexibility associated with a commercial building considering uncertainties in the building's operating pattern. It is based on an article that has been prepared and will be submitted to the Applied Energy journal.

Chapter 3 deals with how LSEs can use customer-side resources, specifically residential HVACs, EWHs, and BTM batteries, for combined self-service and bulk power grid support applications. It is based on an article that has been published in the IEEE Transactions on Smart Grid journal [14].

Chapter 4 deals with how LSEs can use the same set of customer-side resources (i.e., residential HVACs, EWHs, and BTM batteries) for combined self-service and distribution grid operational services. It is based on an article that has been submitted to the IEEE Transactions on Smart Grid journal.

Chapter 5 deals with a compensation framework that LSEs can apply to compensate customer-side resources providing multiple services. It is based on an article that has also been submitted to the IEEE Transactions on Smart Grid journal.

Chapter 6 is the concluding chapter where the major contributions of the dissertation are reiterated along with ideas for further research.

REFERENCES

[1] Microsoft Corporation, "2019 manufacturing trends report," 2019. Available: https://info.microsoft.com/rs/157-GQE-382/images/EN-US-CNTNT-Report-2019-Manufacturing-Trends.pdf.

[2] Federal Energy Regulatory Commission, "FERC Order No. 2222: Fact Sheet," 2020. Available: https://www.ferc.gov/media/ferc-order-no-2222-fact-sheet.

[3] North American Electric Reliability Corporation, 2022. Available: https://www.nerc.com/.

[4] Federal Energy Regulatory Commission, "Assessment of Demand Response and Advance Metering." Available: https://www.ferc.gov/industries/electric/ indus-act/demand-response/dem-res-adv-metering.asp. Accessed: August 9, 2022.

[5] N. Lu, "An evaluation of the hvac load potential for providing load balancing service," *IEEE Transactions on Smart Grid*, vol. 3, no. 3, pp. 1263–1270, 2012. doi: 10.1109/TSG.2012.2183649.

[6] O. Megel, J.L Mathieu, and G. Andersson, "Scheduling distributed energy storage units to provide multiple services," in *2014 Power Systems Computation Conference*, pp. 1–7, 2014. doi: 10.1109/PSCC.2014.7038358.

[7] C. D. White and K. M. Zhang, "Using vehicle-to-grid technology for frequency regulation and peak-load reduction," *Journal of Power Sources*, vol. 196, no. 8, pp. 3972–3980, 2011. doi: https://doi.org/10.1016/j.jpowsour.2010.11.010.

[8] H. Hao, D. Wu, J. Lian, and T. Yang, "Optimal coordination of building loads and energy storage for power grid and end user services," *IEEE Transactions on Smart Grid*, vol. 9, no. 5, pp. 4335–4345, 2018. doi:10.1109/TSG.2017.2655083.

[9] A. Abbas and B. Chowdhury, "Using customer-side resources for market-based transmission and distribution level grid services - a review," *International Journal of Electrical Power Energy Systems*, vol. 125, p. 106480, 2021. doi: https://doi.org/10.1016/j.ijepes.2020.106480.

[10] W. Zhang, J. Lian, C. Chang, and K. Kalsi, "Aggregated modeling and control of air conditioning loads for demand response," *IEEE Transactions on Power Systems*, vol. 28, no. 4, pp. 4655–4664, 2013. doi: 10.1109/TPWRS.2013.2266121.

[11] H. Hao, B. M. Sanandaji, K. Poolla, and T. L. Vincent, "Aggregate flexibility of thermostatically controlled loads," *IEEE Transactions on Power Systems*, vol. 30, no. 1, pp. 189–198, 2015. doi: 10.1109/TPWRS.2014.2328865.

[12] H. Hao, A. Somani, J. Lian, and T. E. Carroll, Thomas, "Generalized aggregation and coordination of residential loads in a smart community," in *2015 IEEE International Conference on Smart Grid Communications (SmartGridComm)*, pp. 67–72, 2015. doi: 10.1109/SmartGridComm.2015.7436278.

[13] S. P. Nandanoori, I. Chakraborty, T. Ramachandran, and S. Kundu, "Identification and validation of virtual battery model for heterogeneous devices," in *2019 IEEE Power Energy Society General Meeting (PESGM)*, pp. 1–5, 2019. doi: 10.1109/PESGM40551.2019.8973978.

[14] A. Abbas and B. Chowdhury, "A stochastic optimization framework for realizing combined value streams from customer-side resources," *IEEE Transactions on Smart Grid*, vol. 13, no. 2, pp. 1139–1150, 2022. doi: 10.1109/TSG.2021.3135155, ©[2022] IEEE. Reprinted, with permission, from [A. Abbas, B. Chowdhury, A stochastic optimization framework for realizing combined value streams from customer-side resources, IEEE Transactions on Smart Grid, March 2022].

CHAPTER 2: CAPTURING OVERALL FLEXIBILITY OF COMMERCIAL BUILDINGS USING STOCHASTIC EQUIVALENT BATTERY MODELS

Typical flexible resources include heating, ventilation, and air conditioning (HVAC) systems and electric water heaters. In addition, other resources, such as batteries and electric vehicle charging stations, are becoming increasingly available in commercial buildings. Also, uncertainties are often associated with the operations of each of these resources. While an equivalent battery model (EBM) has proven to be a simple and effective tool for representing the flexibility associated with the power consumption of certain individually complex systems in commercial buildings, there is still a need for a model that provides a simple yet accurate representation of the overall flexibility and uncertainties associated with the operation of a commercial building. This chapter presents a stochastic equivalent battery model that meets the aforementioned need. The proposed model combines both model-based functional simulations and optimization techniques to quantify a commercial building's overall power consumption flexibility in the face of dominant uncertainties associated with building operations. We also present an illustrative case study demonstrating how the proposed model can be applied to complex resource scheduling problems.

Nomenclature

Parameters

$\Delta P_{lower,t,min/max}$ Lower limits for building's stochastic minimum and maximum flexibility limits

$\Delta P_{upper,t,min/max}$ Upper limits for building's stochastic minimum and maximum flexibility limits

$\eta_{ch,b}$ Battery charging efficiency

$\eta_{dis,b}$ Battery discharging efficiency

λ_t Electricity price at time t

a_0, a_1, a_2 Chiller model parameters

$A_{building,t,min/max}$ Stochastic limits for building's virtual discharge rate at time t

$A_{building,t}$ Building's virtual self-discharge rate at time t

C Water heater thermal capacitance

$C_i/C_{i,z}$ Internal thermal capacitance for building zone z

c_a Specific heat capacity of air

C_e Thermal capacitance for zone envelope

C_p Specific heat capacity of water

$e_{min/max}$ Slack variable limits

H_a	Ambient absolute humidity
H_s	Chiller absolute humidity setpoint
k_0, k_1, k_2	Fan model parameters
$P_{building,t,min/max}$	Building's total power limits at time t
$P_{ch,b,max}$	Maximum battery charging rate
$P_{dis,b,max}$	Maximum battery discharging rate
$P_{ev,max,t}$	Total EV worst case charging profile at time t
Q_D	Total zonal solar and internal heat gains at time t
Q_{infil}	Heating rate from air infiltration into a zone
$Q_{rh,sp,tot,t}$	Total base HVAC reheat rate at time t
$Q_{rh,sp,z,t}$	Base reheat rate for zone z at time t
$Q_{sen,sp,tot,t}$	Total base HVAC sensible cooling rate at time t
$Q_{sen,sp,z,t}$	Base sensible cooling rate for zone z at time t
R	Water heater thermal resistance
R_{ea}	Thermal resistance between zonal envelope and internal air stream
R_{ie}	Thermal resistance between zone air and zone envelope
R_j	Thermal resistance between neighboring zone j and the zone of interest
rh_{ind}	HVAC reheat system type indicator
$s_{w,1,t}$	Uncertainty associated with base temperature profile for water heater w at time t

$s_{w,2,t}$ Uncertainty associated with base heating rate for water heater w at time t

$s_{z,1,t}$ Uncertainty associated with base temperature profile of zone z at time t

$s_{z,2,t}$ Uncertainty associated with base cooling and heating rate for zone z at time t

T_a Ambient temperature

$T_{a,w}$ Water heater location ambient temperature

T_{in} Hot water supply temperature

T_s Cooling air supply setpoint

$T_{w,sp,t}$ Hot water base temperature at time t

$T_{z,sp,t}$ Base temperature profile for zone z at time t

$x_{b,max}$ Maximum battery energy

$x_{b,min}$ Minimum battery energy

$x_{building,t,min/max}$ Building's total virtual energy limits at time t

$x_{ev,max}$ EV charging budget

$x_{ev,util}$ Minimum expected EV charging budget utilization

Variables

$\Delta P_{building,t}$ Building's total flexibility at time t

$ch_{ind,t}$ Battery charging indicator at time t

$dis_{ind,t}$	Battery discharging indicator at time t
e_t	Slack variable at time t
m_z	Air mass flow rate for zone z
$P_{b,t}$	Battery power at time t
$P_{building,t}$	Building's total power consumption at time t
$P_{ch,b,t}$	Battery charging rate at time t
$P_{chiller,t}$	Chiller power consumption at time t
$P_{dis,b,t}$	Battery discharging rate at time t
$P_{ev,t}$	Total EV charging power at time t
$P_{fan,t}$	Fan power consumption at time t
$P_{HVAC,t}$	Total HVAC power consumption at time t
$P_{substation,t,s}$	Substation power at time t for scenario s
Q_c	Cooling rate supplied to a zone
$Q_{lat,chil,t}$	Chiller latent cooling rate at time t
$Q_{rh,tot,t}$	Total HVAC reheat rate at time t
$Q_{rh,z,t}$	Reheat rate for zone z at time t
Q_{rh}	Reheat rate supplied to a zone
$Q_{sen,chil,t}$	Chiller sensible cooling rate at time t
$Q_{sen,tot,t}$	Total HVAC sensible cooling rate at time t
$Q_{sen,z,t}$	Sensible cooling rate for zone z at time t

$Q_{w,sp,t}$	Hot water base heating rate at time t
$Q_{w,t}$	Hot water heating rate at time t
T_i/T_z	Internal temperature for a zone
$T_{avg,t}$	Average zonal temperature at time t
T_e	Envelope temperature for a zone
T_j	Internal temperature in neighboring zone j
$T_{mix,t}$	Mixed air temperature at time t
T_{rh}	Reheat temperature for a zone
$T_{w,t}$	Hot water temperature at time t
$x_{b,t}$	Battery energy at time t
$x_{building,t}$	Building's total virtual energy at time t
$x_{ev,t}$	Total EV charging budget utilization at time t
$x_{HVAC,t}$	Virtual HVAC energy variable at time t
$x_{w,t}$	Water heater virtual energy at time t
$x_{z,t}$	Virtual energy variable for zone z at time t

2.1 Introduction

2.1.1 Background and Motivation

Commercial buildings are major electricity consumers [1]. As such, any effective and sustainable decarbonization pathway must capture how commercial buildings consume electricity. Interestingly, electricity consumption patterns in most commercial buildings are becoming more flexible due to dynamic operating schedules and

the advent of a new crop of flexible energy-consuming devices [2]. This flexibility becomes very important under the smart grid paradigm, where demand could potentially tracks electricity generation.

Due to their large sizes, commercial buildings often contain multiple energy-consuming devices with various uses, operating patterns, flexibility, and complexity. Authors in [3] provide a simulation-based assessment of the power flexibility associated with cooling systems in commercial buildings across the United States. According to their results, the power consumption of cooling systems in commercial buildings across the United States can be increased by 46 GW and decreased by 40 GW during peak periods on peak summer days. A fraction of this flexibility can be harnessed to provide additional value streams for building operators and by extension, load-serving entities (LSEs). For example, several works have shown how commercial HVAC systems can provide frequency regulation services to support the bulk power grid. Authors in [4–6] present different experimental studies showing how commercial HVAC systems can be used for frequency regulation. Also, authors in [7] show how another resource, behind-the-meter (BTM) battery, can provide superlinear gains for building operators when used for combined peak load reduction and frequency regulation.

However, it is very challenging to model commercial buildings in detail in applications that require modeling the building's overall flexibility in addition to other resources like the distribution network supplying electricity to the building and other devices and loads connected to the network. For example, a Variable Air Volume (VAV) with Reheat HVAC system serving four thermal zones could have over forty variables for each time step. As such, a simple representation that quantifies the building's overall flexibility, considering the uncertainties associated with its resources, is required. Virtual or equivalent battery models (EBMs) are perfect candidates for the job. In fact, EBMs have been used extensively to model flexibilities associated with individual resources within a commercial building.

The authors in [8–10] use the equivalent battery model method to represent flexibilities associated with a group of residential thermostatically controlled loads (TCLs) without considering uncertainty. The authors in [11] capture uncertainties related to the operations of TCLs in their proposed variational autoencoder-based stochastic virtual battery model. However, the work focuses on aggregations of residential TCLs. The authors in [12] use equivalent battery models to quantify the regional potential of different residential TCLs for various grid-supporting services.

Generally, existing works on the usage of EBMs to quantify the flexibility of resources in commercial buildings have used either model-based functional simulations or optimization techniques. From the model-based functional testing standpoint, the authors in [13] present a technique for identifying virtual or equivalent battery models for commercial HVAC systems. The proposed technique assumes that there are known reference signals to which the HVAC system will be required to respond. While the proposed technique is interesting and showed promising results for the specific building examined, it has several limitations:

1. The technique focuses only on a single resource in the building (i.e., a commercial HVAC system) and does not necessarily reflect the overall building flexibility.

2. The technique assumes that the potential reference signals the commercial HVAC system will be required to respond to are known. This assumption makes the technique unsuitable for scheduling problems that seek to capture the commercial HVAC models in generating optimal resource operating schedules.

3. The flexibility limits are time-invariant, and the technique does not lend itself well to varying system parameters such as ambient temperature, internal heat gains, solar heat gains, etc. For example, the rate limits associated with the

EBM are only identified at the first timestep, which may be too conservative or outrightly infeasible at a later timestep.

4. The technique does not consider uncertainties associated with the HVAC operation.

From the optimization standpoint, the authors in [14] present a method for quantifying the flexibility of commercial HVAC systems. The authors in [15] also use an approach similar to that developed in [14] to explore the provision of ramping services from grid-interactive buildings. The proposed technique addresses most of the limitations of the model-based functional testing approach proposed in [13]. However, some limitations still exist:

1. The EBM focuses on commercial HVAC systems.

2. The proposed method is based on a simplified model for commercial HVAC systems, which may not be suitable for larger multi-zonal commercial buildings.

3. Uncertainties associated with the HVAC operation are not captured.

This work addresses all gaps mentioned above. Our main contributions are threefold.

1. Firstly, we propose a novel stochastic EBM that represents the overall flexibility associated with the power consumption of a multi-zonal commercial building, including HVAC, water heater, battery, and EV charging resources. The flexibility limits in the proposed model are time-varying and are quantified using a combination of model-based functional simulations and optimization techniques. The model-based functional simulations are primarily used to describe the impact of the dominant uncertainties associated with the building's resources. The procedure for generating the stochastic flexibility limits has also

been implemented in a Python-based package. To the best of our knowledge, this is the first work that provides such holistic perspectives.

2. Also, we show that the solution to a certain class of convex and feasible stochastic optimization problems approaches the solution to its deterministic counterpart if all uncertainties in the problem follow distributions with zero means. This contribution forms the basis for the stochastic flexibility characterization technique discussed in the paper.

3. Finally, we illustrate how the proposed stochastic EBM can be applied to complex stochastic resource scheduling problems.

2.2 Stochastic Equivalent Battery Model

The stochastic equivalent battery model representing the overall flexibility in electricity consumption of a commercial building takes the form shown in (2.1a) to (2.1h).

$$x_{building,t+1} = A_{building,t} x_{building,t} + \Delta P_{building,t} \Delta t \tag{2.1a}$$

$$P_{building,t} = f(\Delta P_{building,t}) \tag{2.1b}$$

$$x_{building,t,min} \leq x_{building,t} \leq x_{building,t,max} \tag{2.1c}$$

$$P_{building,t,min} \leq P_{building,t} \leq P_{building,t,max} \tag{2.1d}$$

$$\Delta P_{building,t,min} \leq \Delta P_{building,t} \leq \Delta P_{building,t,max} \tag{2.1e}$$

$$A_{building,t,min} \leq A_{building,t} \leq A_{building,t,max} \tag{2.1f}$$

$$\Delta P_{building,t,min} \, \epsilon \, [\Delta P_{lower,t,min}, \Delta P_{upper,t,min}] \tag{2.1g}$$

$$\Delta P_{building,t,max} \, \epsilon \, [\Delta P_{lower,t,max}, \Delta P_{upper,t,max}] \tag{2.1h}$$

In (2.1a), $x_{building,t}$ represents the building's overall virtual energy variable which captures occupant comfort limits and the state of charge associated with all flexible resources in the building. $\Delta P_{building,t}$ represents the direct flexibility associated with the resources in the building with respect to predefined base profiles. For example,

$\Delta P_{building,t}$ for a multi-zonal commercial building with a central HVAC system includes the change in the actual cooling or heating rate supplied to the zones within the building. However, the actual cooling or heating rate may or may not have a direct relationship with the electricity consumption of the HVAC system. This is because some components of the overall HVAC system could be non-electric, e.g., hot water reheat systems powered by gas-fired boilers. Also, the actual consumption of the HVAC system components powered by electricity depends on prevailing weather conditions. As such, the total electricity consumption, $P_{building,t}$, of the building, which is the variable of interest, can be expressed as a function of the actual flexibility as shown in (2.1b). Constraints (2.1c) to (2.1e) represent the limits for the energy, total electricity, and flexibility variables, respectively. While the limits in constraints (2.1c) and (2.1d) are deterministic values, the limits in constraint (2.1e) are stochastic values within confidence intervals shown in constraints (2.1g) and (2.1h). Constraint (2.1f) represents the stochastic limits for the building's virtual self-discharge rate.

In subsequent sections, each variable and parameter in model (2) will be examined in detail.

2.3 Resource Models

As pointed out in previous sections, we assume that the commercial building contains an HVAC system, water heating unit, electric vehicle charging stations, and battery energy storage. As such, each of these resources will contribute to the building's overall flexibility.

2.3.1 Commercial Building HVAC System

2.3.1.1 Commercial HVAC Model

Commercial buildings are often divided into multiple thermal zones, each representing a room or a group of rooms. The commercial HVAC systems' modeling includes modeling the building's thermal zones and related equipment, including chillers, boil-

ers, and fans. We assume the commercial HVAC system is a variable air volume (VAV) with a reheat system.

As shown in our previous work [16], each thermal zone in a commercial building can be satisfactorily modeled using a two-node RC network with additional terms to reflect inter-zonal thermal interactions, air infiltration, and internal and solar heat gains. Fig. 1 shows the two-node model for each zone, and (2.2a) - (2.2d) provides its mathematical representation.

$$C_i \frac{dT_i}{dt} = \frac{1}{R_{ie}}(T_a - T_i) + Q_c + Q_{rh} + Q_D + Q_{infil} + \sum_{j=1}^{J} \frac{1}{R_j}(T_j - T_i) \tag{2.2a}$$

$$Q_c = c_a m_z (T_s - T_i) \tag{2.2b}$$

$$Q_{rh} = c_a m_z (T_{rh} - T_s) \tag{2.2c}$$

$$C_e \frac{dT_e}{dt} = \frac{1}{R_{ie}}(T_i - T_e) + \frac{1}{R_{ea}}(T_a - T_e) \tag{2.2d}$$

In the two-node model, two state variables describe the time evolution of temperature within the zone, as shown in Fig. 2.1. The first state variable defines the zone's interior temperature T_i, and the other variable represents the temperature of the zone's envelope, T_e. The parameter R_{ie} reflects the thermal resistance between the zone's envelope and the air within the zone, while R_{ea} captures the resistance between the zone's envelope and ambient air. Parameters C_i and C_e represent the specific heat capacity of the air within the zone and the zone's envelope material, respectively. T_i depends on the ambient temperature, T_a, the cooling, and the reheat supplied to the zone represented by Q_c and Q_{rh} respectively. Furthermore, the internal thermal gains due to occupancy, equipment operation, and solar irradiance, which are lumped together as Q_D, also influence the temperature within the zone. Equation (2.2b) indicates that Q_c depends on the mass flow rate, m_z, and the temperature of

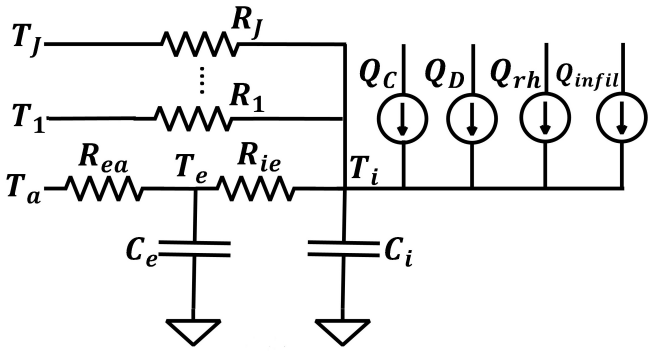

Figure 2.1: Two-node node model for a thermal zone

the conditioned air supplied to the zone, T_s. The zone's temperature is also impacted by thermal interactions with neighboring zones represented by the terms R_j and T_j. In addition to zonal thermal characteristics, other equipment associated with commercial HVAC systems are the chiller, the boiler, and the fan. The chiller model is shown in (2.3a) - (2.3d).

$$Q_{sen,cool} = c \sum_{z=1}^{n} m_z (T_{mix} - T_s) \tag{2.3a}$$

$$Q_{lat,cool} = l \sum_{z=1}^{n} m_z (H_a - H_s) \tag{2.3b}$$

$$Q_{cool} = Q_{sen,cool} + Q_{lat,cool} \tag{2.3c}$$

$$P_{chiller} = a_0 T_a + a_1 H_a + a_2 Q_{cool} \tag{2.3d}$$

Equations (2.3a) - (2.3d) show that a single chiller can serve multiple zones as indicated by mass flow rates for each zone m_z. Also, T_{mix} represents the resultant temperature of a mixture of return air from the zones and fresh external air that goes into the chiller. The total cooling load is the sum of the latent and sensible cooling loads, as shown in (2.3c). Given that the chiller's efficiency depends on the ambient conditions, the power consumption is modeled as shown in (2.3d), where a_o, a_1, and a_2 are model parameters. The boiler and chiller models are similar, excluding the latent heat term [16].

The fan's consumption is modeled as shown in (4) [17].

$$P_{fan} = k_2 \sum_{z=1}^{n} (m_z)^2 + k_1 \sum_{z=1}^{n} m_z + k_0 \tag{2.4}$$

2.3.1.2 Deterministic EBM Representation

The EBM representation discussed in this section includes detailed models for the associated HVAC equipment instead of simple flexibility limits.

The flexibility in the power consumption of any HVAC system serving a building depends on the thermal comfort limits of the occupants of the building. As such, each thermal zone within a building stores and releases thermal energy with respect to some base temperature setpoint or profile. Let the variable $x_{z,t}$ represent the thermal energy stored or released in thermal zone z at time t. $x_{z,t}$ can be defined mathematically as shown in (2.5a) where $T_{z,t}$ represents the temperature within the zone, and $T_{z,sp}$ represents the zone's base temperature profile. Considering (2.2a) and (2.5a), (2.2a) is re-written as (2.5b) to (2.5g).

$$x_{z,t} = C_{i,z}(T_{z,t} - T_{z,sp}) \tag{2.5a}$$

$$\frac{dx_{z,t}}{dt} = -a_z x_{z,t} + \Delta Q_{z,t} \tag{2.5b}$$

$$\Delta Q_{z,t} = Q_{z,t} - Q_{z,sp} \tag{2.5c}$$

$$a_z = \frac{1}{C_{i,z}}\left(\frac{1}{R_{ie,z}} + \frac{1}{R_1} + ... + \frac{1}{R_J}\right) \tag{2.5d}$$

$$Q_{z,t} = Q_{sen,z,t} + Q_{rh,z,t} \tag{2.5e}$$

$$Q_{z,sp,t} = Q_{sen,sp,z,t} + Q_{rh,sp,z,t} \tag{2.5f}$$

$$Q_{sen,sp,z,t} = c_a m_z (T_s - T_{z,sp}) \tag{2.5g}$$

In (2.5b), a_z, which depends on the zone's thermal parameters, represents the self-discharge rate of the zone's virtual energy represented by $x_{z,t}$. $Q_{z,t}$ represents the

thermal inputs into the zone, which includes the heating/cooling supplied by the HVAC system, and $Q_{z,sp,t}$ represents the zone's heating/cooling rate associated with the base temperature profile $T_{z,sp}$. An equivalent expression for $Q_{z,sp,t}$ can be obtained by setting T_i to $T_{z,sp,t}$ in (2.2a). Q_D and Q_{infil} are omitted from (2.5e) and (2.5f) because these two terms are parameters that will cancel each other out in (2.5c).

From (2.5a), $x_{z,t}$ can have both positive and negative values. Positive $x_{z,t}$ values can be due to the supply of heat (increased power consumption in winter seasons) or reduction in the supply of cold air (reduced power consumption in summer seasons) into the zone. On the other hand, negative $x_{z,t}$ values can be due to the supply of additional cold air (increased power consumption in summer seasons) or reduction in the supply of heat (reduced power consumption in winter season) into the zone. Therefore, defining a charging convention that depends only on $x_{z,t}$ is pertinent. We define charging as events that increase $x_{z,t}$ and discharging as events that reduce $x_{z,t}$. Equations (2.5b) - (2.5g) do not include the actual power consumption of the HVAC system. The power consumption equations are discussed later.

Considering a commercial building with n thermal zones connected to a single HVAC equipment, the battery representation for each zone can be combined to create the battery representation for the HVAC system, as shown in (2.6) to (2.7e). In (2.6) and (2.7), a_{HVAC} is the average of the virtual self-discharge rates for all zones connected to the HVAC equipment.

$$\frac{dx_{HVAC,t}}{dt} = -a_{HVAC}x_{HVAC,t} + \Delta Q_{tot,t} \tag{2.6}$$

Rewriting (2.6) in discrete form,

$$x_{HVAC,t+1} = (1 - a_{HVAC}\Delta t)x_{HVAC,t} + \Delta Q_{tot,t}\Delta t \tag{2.7a}$$

$$x_{HVAC,t} = \sum_{z=1}^{n} x_{z,t} \tag{2.7b}$$

$$\Delta Q_{tot,t} = Q_{tot,t} - Q_{base,tot,t} \tag{2.7c}$$

$$Q_{tot,t} = Q_{sen,tot,t} + Q_{rh,tot,t} \tag{2.7d}$$

$$Q_{base,tot,t} = Q_{sen,sp,tot,t} + Q_{rh,sp,tot,t} \tag{2.7e}$$

$Q_{sen,tot,t}$ represents the total sensible cooling the HVAC system provides to the zones. $Q_{sen,tot,t}$ can be approximated as shown in (2.8a). Also $Q_{rh,tot,t}$ can be approximated as shown in (2.8b).

$$Q_{sen,tot,t} = c_a m_{z,tot,t}(T_s - T_{avg,t}) \tag{2.8a}$$

$$Q_{rh,tot,t} = c_a m_{z,tot,t}(T_{rh,avg,t} - T_s) \tag{2.8b}$$

$Q_{rh,tot,t}$ represents the total heating supplied to the zones from the reheat coils, which can be electric or hot water driven. If the reheat coils are hot water-driven, the boiler provides the heat, and the contribution of the reheat power to the building's total electricity consumption depends on the boiler's fuel (i.e., electricity or natural gas-driven). However, most existing commercial buildings often use gas-fired boilers, and we adopt that configuration. Electric boilers can also be well represented with minimal adjustments.

Since the EBM representation will not explicitly include zonal temperatures, an approximate expression for $T_{avg,t}$ in terms of $x_{z,t}$ is generated from (2.5a) as shown in (2.9) where $C_{i,z,avg}$ is the average zonal capacitance.

$$T_{avg,t} = \frac{1}{n}\left(\frac{x_{HVAC,t}}{C_{i,z,avg}} + \sum_{z=1}^{n} T_{z,sp}\right) \tag{2.9}$$

As discussed earlier, the chiller cools down a stream of air, with a temperature $T_{mix,t}$, consisting of fresh ambient air, and return air from the thermal zones to a certain setpoint, T_s. Assuming that $T_{mix,t}$ represents an equal proportion of fresh

ambient air and return air from the thermal zones, $T_{mix,t}$ can be expressed mathematically as shown in (2.10).

$$T_{mix,t} = \frac{T_{avg} + T_a}{2} \tag{2.10}$$

The sensible ($Q_{sen,chil,t}$) and latent heat ($Q_{lat,chil,t}$) terms of the chiller's power consumption are calculated as shown in (2.11a) and (11b) respectively. The chiller's power consumption, $P_{chiller,t}$, can then be expressed as a function of $Q_{sen,chil,t}$, $Q_{lat,chil,t}$ and ambient conditions represented by T_a and H_a as shown in (2.3). The fan's power consumption, $P_{fan,t}$, is also expressed as a function of $m_{z,tot}$ as shown in (2.4). The summation of $P_{chiller,t}$, $P_{fan,t}$ and the reheat term (if electric) represents the total power consumption, $P_{HVAC,t}$, of the HVAC system.

$$Q_{lat,chil,t} = l m_{z,tot}(H_a - H_s) \tag{2.11a}$$

$$Q_{sen,chil,t} = c_a m_{z,tot}(T_{mix,t} - T_s) \tag{2.11b}$$

$$P_{chiller,t} = f(Q_{sen,chil,t}, Q_{lat,chil,t}, T_a, H_a) \tag{2.11c}$$

$$P_{fan,t} = f(m_{z,tot}) \tag{2.11d}$$

$$P_{HVAC,t} = P_{chiller,t} + P_{fan,t} + rh_{ind} Q_{rh,tot,t} \tag{2.11e}$$

The final deterministic EBM representation for the commercial HVAC system is given by equations (2.7a), (2.7c), (2.7d), and (2.8)-(2.11).

2.3.1.3 Stochastic EBM Representation

The EBM representation discussed in the previous section assumes that the HVAC's operating pattern and ambient conditions are known in a deterministic sense. However, this is not the case in reality. While several uncertainties are associated with commercial building operations, the uncertainties can be treated as variations to the sum of the Q_D and Q_{infil} parameters for each zone. These variations will, in turn,

affect each zone's base temperature profile $T_{z,sp,t}$ and the cooling/heating rate $Q_{z,sp,t}$ supplied by the HVAC system. Let us define two additional variables $T^{'}_{z,sp,t}$ and $Q^{'}_{z,sp,t}$ to reflect the variations in the base profiles due to the uncertainties.

$$T^{'}_{z,sp,t} = T_{z,sp,t} - s_{z,1,t} \tag{2.12a}$$

$$Q^{'}_{z,sp,t} = Q_{z,sp,t} - s_{z,2,t} \tag{2.12b}$$

Note that the signs in equations (2.12a) and (2.12b) are chosen arbitrarily and can be defined in any way desired. $s_{z,1,t}$ and $s_{z,2,t}$ represent zero-mean normally distributed uncertainties associated with the zone's temperature and thermal energy (i.e., cooling or heating) supply, respectively. However, if the zero mean assumption is not satisfied, the actual distributions can be normalized to a standard normal distribution with a zero mean value [18]. Also, the 95% confidence intervals are taken as the limits for the uncertainties $s_{z,1,t}$ and $s_{z,2,t}$ based on the normal distribution assumption. Based on the definitions in equations (2.12a) and (2.12b), a new representation of the zone's thermal energy that captures uncertainties can be expressed as shown in equation (2.13).

$$x^{'}_{z,t} = C_{i,z}(T_{z,t} - T^{'}_{z,sp,t}) \tag{2.13a}$$

$$x^{'}_{z,t} = C_{i,z}(T_{z,t} - T_{z,sp,t} + s_{z,1,t}) \tag{2.13b}$$

$$x^{'}_{z,t} = x_{z,t} + C_{i,z}s_{z,1,t} \tag{2.13c}$$

Also, the cooling/heating rate supplied by the HVAC system to the zone can be expressed with the associated uncertainties, as shown in (2.14).

$$\Delta Q^{'}_{z,t} = Q_{z,t} - Q^{'}_{z,sp,t} \tag{2.14a}$$

$$\Delta Q^{'}_{z,t} = \Delta Q_{z,t} + s_{z,2,t} \tag{2.14b}$$

Writing a new battery model using the stochastic terms $x^{'}_{z,t}$ and $\Delta Q^{'}_{z,t}$ produces (2.15).

$$\frac{dx^{'}_{z,t}}{dt} = -a_z x^{'}_{z,t} + \Delta Q^{'}_{z,t} \tag{2.15}$$

Substituting (2.13a) and (2.14b) into (2.15),

$$\frac{d(x_{z,t} + C_{i,z} s_{z,1,t})}{dt} = -a_z(x_{z,t} + C_{i,z} s_{z,1,t}) + \Delta Q_{z,t} + s_{z,2,t} \tag{2.16}$$

Assuming $\frac{dx_{z,t}}{dt} >> C_{i,z}\ \frac{ds_{z,1,t}}{dt}$, equation (2.16) can be re-written as follows.

$$\frac{dx_{z,t}}{dt} = a^{'}_{z,t} x_{z,t} + \Delta Q_{z,t} + s_{z,2,t} \tag{2.17a}$$

$$a^{'}_{z,t} = -a_z - a_z C_{i,z} \frac{s_{z,1,t}}{x_{z,t}} \tag{2.17b}$$

Rewriting (2.17) in discrete form,

$$x_{z,t+1} = A_{z,t} x_{z,t} + (\Delta Q_{z,t} + s_{z,2,t})\Delta t \tag{2.18a}$$

$$A_{z,t} = 1 + a^{'}_{z,t}\Delta t \tag{2.18b}$$

From equation (2.18b), the parameter $A_{z,t}$ is also a stochastic term since it depends on the $s_{z,1,t}$ which is stochastic. Taking the 95% confidence interval as the lower and upper limits for $s_{z,1,t}$, the limits on the parameter $A_{z,t}$ can also be estimated since the limits on the variable $x_{z,t}$ are also known. The limits on the variable $x_{z,t}$ depend on the thermal comfort limits allowable for the zone z and are calculated as shown in (2.19).

$$x_{z,t,max} = C_{i,z}(T_{z,max} - T_{z,sp,t}) \tag{2.19a}$$

$$x_{z,t,min} = C_{i,z}(T_{z,min} - T_{z,sp,t}) \tag{2.19b}$$

The stochastic battery representation for a commercial HVAC system serving n

zones can be obtained by summing the battery representations for the n zones, as shown in (2.20). $A_{HVAC,t}$ is taken as the average of $A_{z,t}$ for all connected zones. As such, the maximum and minimum limits for $A_{HVAC,t}$ (i.e., $A_{HVAC,t,max}$ and $A_{HVAC,t,min}$) correspond to the average maximum and minimum limits for all associated zones, respectively.

$$x_{HVAC,t+1} = A_{HVAC,t}x_{HVAC,t} + (\Delta Q_{tot,t} + s_{HVAC,2,t})\Delta t \tag{2.20a}$$

$$x_{HVAC,t} = \sum_{z=1}^{n} x_{z,t} \tag{2.20b}$$

$$s_{HVAC,2,t} = \sum_{z=1}^{n} s_{z,2,t} \tag{2.20c}$$

Equations (2.7c) to (2.11e) still apply to the stochastic representation. However, all variables are now scenario dependent i.e. the variables depend on specific realizations of $s_{HVAC,1,t}$ (i.e. $\sum_{n=1}^{z} s_{z,1,t}$) and $s_{HVAC,2,t}$. As such, any optimization problem based on the stochastic EBM representation of the HVAC system is stochastic. This inference is important and forms the basis for obtaining the building's flexibility limits and the final stochastic EBM representation.

2.3.2 Water Heater

2.3.2.1 Deterministic EBM Representation

The water heater is modeled as a single node RC network as shown in (2.21) [19].

$$C\frac{dT_w}{dt} = \frac{1}{R}(T_{a,w} - T_w) - m_w C_p(T_w - T_{in}) + Q_w \tag{2.21}$$

Let $x_{w,t}$ represent the water heater's virtual energy variable at time t. The variable $x_{w,t}$ can be defined mathematically as shown in (2.22), where $T_{w,sp,t}$ represents the

base water temperature setpoint or profile.

$$x_{w,t} = C(T_{w,t} - T_{w,sp,t}) \tag{2.22}$$

Considering (2.22), (2.21) is re-written as a battery model in (2.23a) to (2.23c). $Q_{w,sp,t}$ represents the water heater's heating power consumption corresponding to the base water temperature profile $T_{w,sp,t}$.

$$\frac{dx_{w,t}}{dt} = -a_w x_{w,t} + \Delta Q_{w,t} \tag{2.23a}$$

$$\Delta Q_{w,t} = Q_{w,t} - Q_{w,sp,t} \tag{2.23b}$$

$$a_w = \frac{1}{RC} \tag{2.23c}$$

Given that $x_{w,t}$ can have both positive and negative values, the same charging convention used for the HVAC system is adopted for the water heater for consistency, i.e., charging refers to events that increase $x_{w,t}$ and discharging refers to events that reduce $x_{w,t}$.

2.3.2.2 Stochastic EBM Representation

The main source of uncertainty associated with the water heater is the hot water consumption rate. This uncertainty affects the base temperature profile, $T_{w,sp,t}$, and the base power consumption, $Q_{w,sp,t}$, of the water heater.

Defining new variables to capture uncertainties in the water heater's base profiles,

$$T^{'}_{w,sp,t} = T_{w,sp,t} - s_{w,1,t} \tag{2.24a}$$

$$Q^{'}_{w,sp,t} = Q_{w,sp,t} - s_{w,2,t} \tag{2.24b}$$

Note that the same normal distribution and zero mean assumptions applied to the HVAC uncertainties also apply to $s_{w,1,t}$ and $s_{w,2,t}$.

A new battery model to reflect the water heater uncertainties is shown in (2.25) where $x^{'}_{w,t} = x_{w,t} + Cs_{w,1,t}$ and $\Delta Q^{'}_{w,t} = \Delta Q_{w,t} + s_{w,2,t}$.

$$\frac{dx^{'}_{w,t}}{dt} = -a_w x^{'}_{w,t} + \Delta Q^{'}_{w,t} \tag{2.25}$$

Substituting the definitions of $x^{'}_{w,t}$ and $\Delta Q^{'}_{w,t}$ into (2.25) and assuming that $\frac{dx_{w,t}}{dt}$ $>> C\ \frac{ds_{w,1,t}}{dt}$, (2.25) becomes (2.26).

$$\frac{dx_{w,t}}{dt} = a^{'}_{w,t} x_{w,t} + \Delta Q_{w,t} + s_{w,2,t} \tag{2.26a}$$

$$a^{'}_{w,t} = -a_w - \frac{s_{w,1,t}}{Rx_{w,t}} \tag{2.26b}$$

Rewriting (2.26) in discrete form,

$$x_{w,t+1} = A_{w,t} x_{w,t} + (\Delta Q_{w,t} + s_{w,2,t})\Delta t \tag{2.27a}$$

$$A_{w,t} = 1 + a^{'}_{w,t}\Delta t \tag{2.27b}$$

Note that $A_{w,t}$ is also stochastic and its limits ($A_{w,t,min}$ and $A_{w,t,max}$) can be obtained using the same procedure described for each thermal zone under section III.A.3.

2.3.3 Battery

The battery's charge or discharge can be scheduled as needed. As such, the battery is modeled as shown in (2.28) [20].

$$x_{b,t+1} = x_{b,t} + P_{b,t}\Delta t \tag{2.28a}$$

$$P_{b,t} = \eta_{ch,b} P_{ch,b,t} - \frac{1}{\eta_{dis,b}} P_{dis,b,t} \tag{2.28b}$$

$$x_{b,\min} \leq x_{b,t} \leq x_{b,\max} \tag{2.28c}$$

$$0 \leq P_{ch,b,t} \leq ch_{ind,t} P_{ch,b,\max} \tag{2.28d}$$

$$0 \leq P_{dis,b,t} \leq dis_{ind,t} P_{dis,b,\max} \tag{2.28e}$$

$$ch_{ind,t} + dis_{ind,t} \leq 1 \tag{2.28f}$$

2.3.4 Electric Vehicle Charging

While commercial buildings can have EV charging and vehicle-to-grid discharge capabilities, the focus is on EV charging. The charging patterns of EVs using the EV charging infrastructure associated with commercial buildings constitute the major sources of uncertainty. To take care of these charging pattern uncertainties, we assume that each commercial building offers EV charging as a complimentary service to the building's occupants, i.e., the building operator does not require EV users to pay for charging. Based on this assumption, each building has a daily EV charging budget, $x_{ev,max}$, a minimum expected EV charging budget utilization, $x_{ev,until}$, and a worst-case expected EV charging profile, $P_{ev,max,t}$. The minimum expected EV charging budget utilization can equal the daily EV charging budget. Also, the worst-case charging profile can be obtained from historical charging data. The parameters $x_{ev,max}$, $x_{ev,until}$, $P_{ev,max,t}$ provide the operating bounds which takes care of all EV charging uncertainties.

The building's total EV charging can be modeled using the set of equations in (2.29). Embedding (2.29) as constraints within an optimization framework provides the optimally managed EV charging profile that satisfies whatever objective being considered. $x_{ev,t}$ represents the portion of the EV charging energy budget used at time t. Equation (2.29b) shows that the minimum expected EV charging budget utilization would have been achieved at the end of the day.

$$x_{ev,t+1} = x_{ev,t} + P_{ev,t}\Delta t \tag{2.29a}$$

$$x_{ev,T} \geq x_{ev,util} \tag{2.29b}$$

$$0 \leq x_{ev,t} \leq x_{ev,\max} \tag{2.29c}$$

$$0 \leq P_{ev,t} \leq P_{ev,\max,t} \tag{2.29d}$$

2.4 Building's Stochastic Flexibility Limits

The foundation for the building's stochastic EBM representation with the flexibility limits explained in (2.1) has been established in section III. Considering equation (2.1a),

$$x_{building,t} = x_{HVAC,t} + x_{w,t} + x_{b,t} + x_{ev,t} \tag{2.30a}$$

$$A_{building,t} = mean(A_{HVAC,t}, A_{w,t},$$
$$A_{b,t} = 1, A_{ev,t} = 1) \tag{2.30b}$$

$$A_{building,t,min} = mean(A_{HVAC,t,min}, A_{w,t,min},$$
$$A_{b,t,min} = 1, A_{ev,t,min} = 1) \tag{2.30c}$$

$$A_{building,t,max} = mean(A_{HVAC,t,max}, A_{w,t,max},$$
$$A_{b,t,max} = 1, A_{ev,t,max} = 1) \tag{2.30d}$$

$$\Delta P_{building,t} = \Delta P_{flex,t} + s_{HVAC,2,t} + s_{w,2,t} \tag{2.30e}$$

$$\Delta P_{flex,t} = \Delta Q_{tot,t} + \Delta Q_{w,t} + P_{b,t} + P_{ev,t} \tag{2.30f}$$

$$P_{building,t} = P_{HVAC,t} + Q_{w,t} + P_{b,t} + P_{ev,t} \tag{2.30g}$$

Since the EV representation is in terms of energy budget utilization, there is no self-discharge rate associated with EV charging. Therefore, $A_{ev,t}$ equals 1. The battery's self-discharge rate is assumed to be negligible, making $A_{b,t}$ equal to 1. The stochastic optimization problem (2.31) provides a basis for obtaining the flexibility limits for variables $x_{building,t}$, $P_{building,t}$ and $\Delta P_{building,t}$ shown in equations (2.1c) to (2.1f).

$$min/max \sum_{t=1}^{T} E[P_{building,t}] \; or \; \sum_{t=1}^{T} E[x_{building,t}] \tag{2.31a}$$

subject to:

Overall building constraints: $(2.30a),\ (2.30f), (2.30g)$ for diff.

realizations of $s_{HVAC,1,t}, s_{HVAC,2,t}, s_{w,1,t}, s_{w,2,t}$ (2.31b)

HVAC constraints: $(2.20a)$, $(2.7c)$ $-$ $(2.11e)$ for different

realizations of $s_{HVAC,1,t}, s_{HVAC,2,t}, s_{w,1,t}, s_{w,2,t}$ (2.31c)

Water heater constraints: $(2.27a)$, $(2.23b)$ for different

realizations of $s_{HVAC,1,t}, s_{HVAC,2,t}, s_{w,1,t}, s_{w,2,t}$ (2.31d)

Battery constraints: $(2.28a)$ $-$ $(2.28f)$ for different

realizations of $s_{HVAC,1,t}, s_{HVAC,2,t}, s_{w,1,t}, s_{w,2,t}$ (2.31e)

EV charging constraints: $(2.29a)$ $-$ $(2.29d)$ for different

realizations of $s_{HVAC,1,t}, s_{HVAC,2,t}, s_{w,1,t}, s_{w,2,t}$ (2.31f)

The objective function (2.31a) either maximizes or minimizes the expected value of $P_{building,t}$ or $x_{building,t}$ depending on the limits of interest. The expectation operator in the objective function indicates that the variables $P_{building,t}$ or $x_{building,t}$ are scenario dependent i.e. the outcomes depend on the realizations of the uncertainties $s_{HVAC,1,t}$, $s_{HVAC,2,t}$, $s_{w,1,t}$, $s_{w,2,t}$. As such, the expected values of the limits are required. Since the building's total electricity consumption is often the variable of interest, maximizing or minimizing the expected value of $P_{building,t}$ also provides the needed limits for $\Delta P_{flex,t}$.

Solving the four stochastic optimization problems represented by (2.31) could be computationally challenging due to the need to create multiple scenarios based on the uncertainties $s_{HVAC,1,t}$, $s_{HVAC,2,t}$, $s_{w,1,t}$, and $s_{w,2,t}$. However, under certain conditions, the solutions to the stochastic optimization problems (2.31) approach the solutions to the deterministic counterparts (i.e. with $s_{HVAC,1,t} = s_{HVAC,2,t} = s_{w,1,t} = s_{w,2,t} = 0$). These conditions are stated in Theorem 1.

Let us consider the stochastic optimization problem shown in (2.32). $w(\gamma)$ and $x(\gamma)$ are scenario-dependent decision variables whose values depend on the specific

realization of uncertainty γ, normally distributed with a zero mean. Parameters h, W, A, K, and B are deterministic.

$$minimize\, E[w(\gamma)] \tag{2.32a}$$

subject to:

$$K + \gamma + x(\gamma) + Ww(\gamma) = h \tag{2.32b}$$

$$0 \leq w(\gamma) \leq A \tag{2.32c}$$

$$0 \leq x(\gamma) \leq B \tag{2.32d}$$

Problem (2.32) can be considered as a generic version of problem (2.31) with a linearized version of the quadratic fan model and relaxed binary variables associated with the battery. With these relaxations, each equality constraint in problem (2.31) can be viewed as the summation of scenario-dependent variables and uncertain parameters (i.e. (2.32b)), while the physical equipment limits or comfort-related limits are equivalent to the inequality constraints (i.e. (2.32c) to (2.32d)). Also, in reality, as long as the building is in operation, the total power consumption will always be greater than the minimum nameplate rating. Similarly, the total power consumption will always be less than the building's maximum power consumption rating. Therefore, constraint (2.32c) will be non-binding i.e. the parameters h, W, A, K, and B will be such that $w(\gamma)$ will always be greater than its minimum physical limit but less than its maximum physical limit. We can now state Theorem 1 relating to problem (2.32) and the proof is provided in the Appendix.

Theorem 1: *For a class of convex and feasible stochastic optimization problems described in Problem (2.32), the optimal solution (i.e., the minimum expected value of the scenario-dependent variable) approaches the optimal solution of the deterministic version of the problem (i.e., without the uncertainties) as the number of equally probable scenarios of the uncertainties increases if each uncertainty in the stochastic*

optimization problem follows a distribution with a zero mean.

Based on Theorem 1, the solutions of the deterministic counterparts to problem (2.32) provide the expected maximum and minimum flexibility limits for $x_{building,t}$, $P_{building,t}$ and $\Delta P_{flex,t}$. Note that the binary variables associated with the battery operation could be relaxed to preserve convexity. However, the capability of modern optimization solvers to solve problems with binary variables to optimality can be leveraged. Furthermore, each building will typically have a single battery storage system, so the number of binary variables remains manageable. Equation (2.30e) shows that $\Delta P_{building,t}$ is the summation of $\Delta P_{flex,t}$ and the uncertainties $s_{HVAC,2,t}$ and $s_{w,2,t}$. As such, the limits for $\Delta P_{building,t}$ can be obtained as stochastic parameters with lower and upper limits expressed as shown in (2.33).

$$\Delta P_{lower,t,min} = \Delta P_{flex,t,min} + s_{HVAC,2,t,min} + s_{w,2,t,min} \tag{2.33a}$$

$$\Delta P_{upper,t,min} = \Delta P_{flex,t,min} + s_{HVAC,2,t,max} + s_{w,2,t,max} \tag{2.33b}$$

$$\Delta P_{lower,t,max} = \Delta P_{flex,t,max} + s_{HVAC,2,t,min} + s_{w,2,t,min} \tag{2.33c}$$

$$\Delta P_{upper,t,max} = \Delta P_{flex,t,max} + s_{HVAC,2,t,max} + s_{w,2,t,max} \tag{2.33d}$$

The solutions of $P_{building,t}$ and $\Delta P_{flex,t}$ obtained by maximizing and minimizing $P_{building,t}$ in the deterministic version of problem (2.31) are used to obtain the parameters of a simple regression model, K_0 and K_1, that relates $P_{building,t}$ and $\Delta P_{building,t}$ as shown in (2.1b). This is because the values of the $\Delta P_{flex,t}$ in the deterministic problem are equivalent to the values of $\Delta P_{building,t}$ since the uncertainties are set to zero in the deterministic problem.

$$P_{building,t} = K_0 + K_1 \Delta P_{building,t} + e_t \tag{2.34a}$$

$$e_{min} \leq e_t \leq e_{max} \tag{2.34b}$$

The term e_t in (2.34) is a slack variable constrained by the maximum and minimum residuals from the regression model fitting procedure.

Based on the preceding discussions, the procedure for generating a stochastic equivalent battery model to capture the overall flexibility of a commercial building is described as follows.

1. Generate interval forecasts for each zone's total internal heat gains and hot water consumption rates. Set the mean values of the predictions as the base profiles.

2. Obtain the worst case charging profile for the EVs ($P_{ev,max}$) from historical data and set the daily EV energy budget ($x_{ev,max}$) and the minimum expected charging budget utilization ($x_{ev,util}$) .

3. Run building energy simulations with the base profiles in step 1 to establish the base profiles for the zonal temperatures ($T_{z,sp}$), hot water temperatures ($T_{w,sp}$), heating/cooling rate for each thermal zone ($Q_{z,sp}$) and the hot water heating rate ($Q_{w,sp}$).

4. Run multiple building energy simulations using parameters obtained by sampling the intervals in step 1.

5. Combine the simulation results from steps 3 and 4 to obtain the time-dependent mean and standard deviations of the uncertainties $s_{z,1,t}$, $s_{z,2,t}$, $s_{w,1,t}$, and $s_{w,2,t}$. If the uncertainties have non-zero means, transform the uncertainties to standard normally distributed values.

6. Obtain the limits for the building's virtual energy self-discharge rate, $A_{building,t}$, using equations (2.30c) and (2.30d)

7. Solve four deterministic optimization problems (i.e., deterministic versions of (2.31)) to obtain the building's flexibility limits. The objective functions of the

four optimization problems are $maximize \sum_{t=1}^{T} P_{building,t}$, $minimize \sum_{t=1}^{T} P_{building,t}$, $maximize \sum_{t=1}^{T} x_{building,t}$, and $minimize \sum_{t=1}^{T} x_{building,t}$. Note that if a maximization problem is solved first, the minimization problem is constrained with the optimal values from the maximization problem to ensure solution feasibility and vice versa.

8. Set the solutions of the optimization problems solved in step 7 as the limits for $x_{building,t}$ and $P_{building,t}$.

9. Obtain the limits for $\Delta P_{building,t}$ using equations (2.33a) to (2.33d).

10. Obtain the relationship between $\Delta P_{building,t}$ and $P_{building,t}$ using equation (2.34).

Note that, if necessary, the procedure described above can be applied multiple times to update the parameters of the stochastic equivalent battery model. This could be useful when the forecasts are unreliable. The main difference at every iteration will be the forecasts (internal heat gains, hot water consumption, worst-case charging profile) and input data (daily EV energy budget, minimum expected utilization) used.

2.5 Case Studies

2.5.1 Representative Buildings

We consider two commercial buildings to illustrate the proposed flexibility characterization procedure. The buildings were adapted from the United States Department of Energy Commercial Buildings database, and their characteristics are summarized in Fig. 2.2 [21]. Ambient conditions for Chicago reflected in the typical meteorological year (TMY3) file are assumed [22]. Specifically, all simulations are based on weather conditions for July 9 from the TMY3 weather file.

Also, the uncertainties associated with the internal heat gains and the hot water consumption rate are assumed to be ± 15% of the expected values. The daily EV charging budgets are assumed to be 196 kWh and 1402 kWh for buildings A and B,

	Overall	HVAC	Water heater	Battery	EVs
Building A	5,500ft^2 office; single floor; 4 occupied zones	VAV with electric reheat; 8 kW chiller and 1.5 kW fan	Electric; 200 gallons; 12.5 kW	6 kW / 12 kWh	4 charging points – 2 at 7 kW and 2 at 20 kW
Building B	50,045ft^2 warehouse; single floor; 3 occupied zones	VAV with hot water reheat; 300 kW chiller and 21 kW fan	Electric; 500 gallons; 30 kW	30 kW / 100 kWh	10 charging points, each at 20 kW rating

Figure 2.2: Building characteristics

respectively. For both buildings, the minimum EV charging budget utilization is zero. This implies that, if needed, the building's EV charging service can be unavailable to reduce the building's energy consumption to the barest minimum.

A Python-based commercial building simulation tool, previously benchmarked with EnergyPlus, was used to run all building energy simulations with 10-minute time steps [16]. Also, the flexibility limits characterization procedure, including the optimization problems, have been implemented in the Python-based commercial building simulation tool. The optimization problems were all solved using a Gurobi solver interfaced with the Pyomo package [23].

2.5.2 Stochastic EBM Representation Use Case

We consider a simple case study involving a small load serving entity (e.g., a utility cooperative) whose objective is to reduce the overall cost of the energy it purchases on behalf of its members. The load-serving entity's (LSE) network is assumed to be a modified version of the IEEE 33-bus network, with buildings A and B located at nodes 19 and 22, respectively. The LSE also operates a solar photovoltaic system on behalf of its members, as shown in Fig. 2.3. The LSE solves a day-ahead scheduling problem that determines the scheduled load profile for each member.

To simplify the illustration, we assume that the main uncertainties in the LSE's scheduling problem are those associated with the flexibilities of buildings A and B.

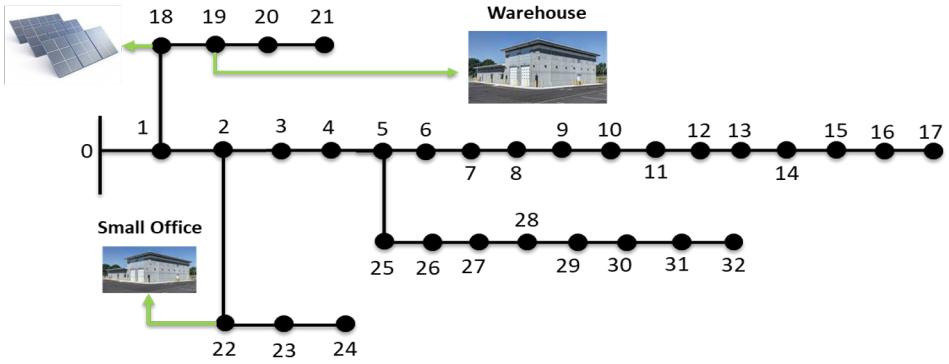

Figure 2.3: Illustrative LSE's network

Also, we assume that the LSE's members will follow any load profile provided to them by the LSE. Based on these assumptions, the LSE solves a stochastic day-ahead scheduling problem (2.34).

$$min. \sum_{t=1}^{T} E[\lambda_t P_{substation,t,s}] + \sum_{t=1}^{T} E[e_{A,t,s}] + \sum_{t=1}^{T} E[e_{B,t,s}] \tag{2.35a}$$

subject to:

$$\textbf{SOCP Power Flow Equations} \text{ (includes } P_{building,A(B),t,s}) \tag{2.35b}$$

$$\textbf{Building A Stochastic EBM: } (1a),\ (33), (1c)\ -\ (1h) \text{ for}$$

$$\text{different scenarios } s \tag{2.35c}$$

$$P_{building,A(B),t,s}) \tag{2.35d}$$

$$\textbf{Building B Stochastic EBM: } (1a),\ (33), (1c)\ -\ (1h) \text{ for}$$

$$\text{different scenarios } s \tag{2.35e}$$

Problem (2.34) minimizes the LSE's total energy cost. The prices were obtained from NYISO's 2019 data repository [24]. The expected values of the slack variables e_t associated with the stochastic EBM representations for the two buildings are also minimized. Power flows on the LSE's network are captured using the power flow equations' second-order conic relaxation (SOCP) [25]. Multiple scenarios as created

for the parameters $A_{building,t}$, $\Delta P_{building,t,min}$ and $\Delta P_{building,t,max}$. We assume that these scenarios are equally probable. The expected values of the variables $P_{building,A,t,s}$ and $P_{building,B,t,s}$ form the reference profiles which are provided for each building to follow. A receding horizon controller is then used to dispatch the individual resources in the building to track the provided reference signals in a co-simulation manner. Note that the controller and the co-simulation procedure have also been implemented within the Python-based commercial building simulation tool developed by the team.

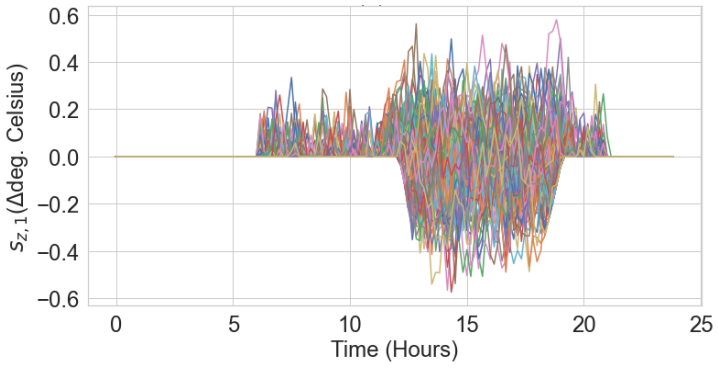

Figure 2.4: Plots of $s_{z,1,t}$ for a zone in building A

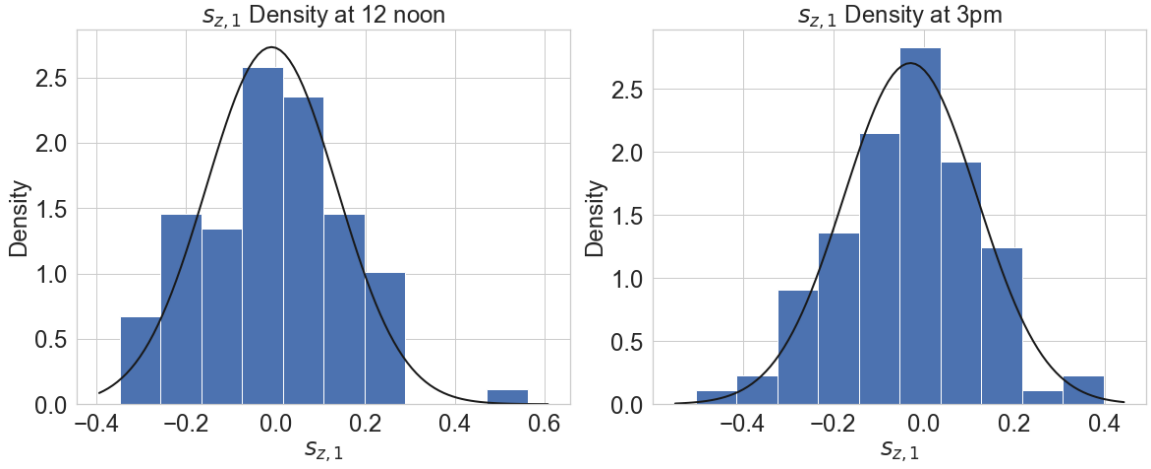

(a) 12 noon

(b) 3 pm

Figure 2.5: Distributions of $s_{z,1,t}$ at (a) 12 noon and (b) 3pm

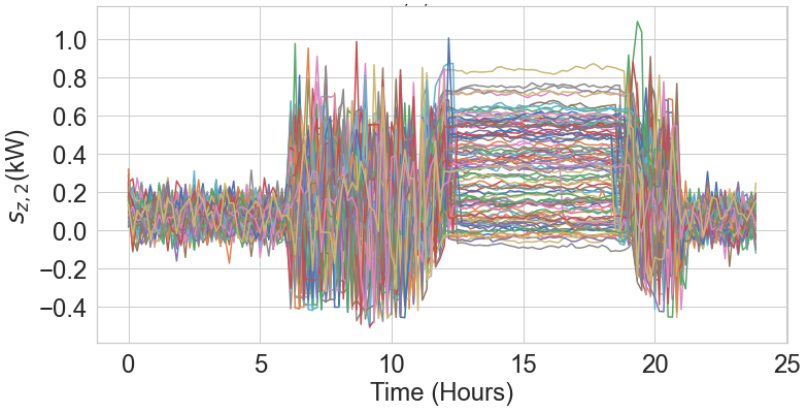

Figure 2.6: Plots of $s_{z,2,t}$ for a zone in building A

2.6 Results and Discussions

2.6.1 Uncertainties

Fig. 2.4 shows different time-dependent realizations of the uncertainty associated with the base temperature profile ($s_{z,1,t}$) for one of the zones in building A. These realizations are the outcomes of multiple building energy simulation runs using different values of solar and internal heat gain profiles (i.e., $\pm$ 15% of the base values). At first glance, we can infer that the uncertainties associated with the base temperature profile are more pronounced during the day. This is tied to the increased building occupancy levels during those periods. Fig. 2.5 provides a closer look at the distribution of the uncertainties at 12 noon and 3 pm. The distribution of the uncertainties at noon has a zero mean, while the distribution at 3 pm has a non-zero mean (precisely -0.04). Consequently, -0.04 can be added to the zone's base temperature profile, $T_{z,sp}$, at 3 pm to account for the non-zero assumption violation when solving the deterministic versions of the problem (2.31).

Fig. 2.6 shows the uncertainties associated with the base thermal heating/cooling rate supplied to the same zone by the HVAC system ($s_{z,2,t}$). As expected, there are more variations during the day when the zone is more occupied. The same procedure for correcting violations to the zero mean assumption is also applied to the values in Fig. 2.6.

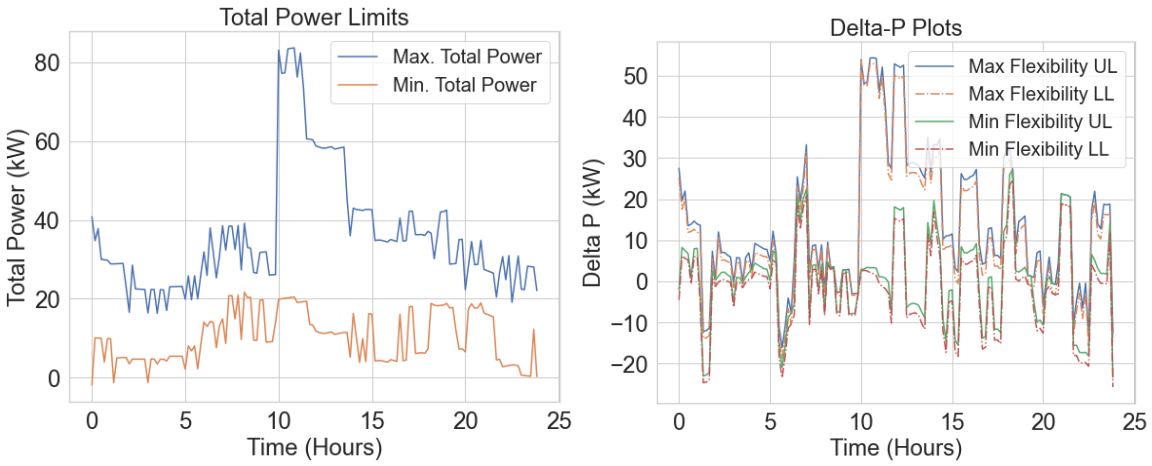

(a) $P_{building,A}$ limits (b) $\Delta P_{building,A}$ limits

Figure 2.7: (a) $P_{building,A}$ limits (b) $\Delta P_{building,A}$ limits

2.6.2 Flexibility Limits

Figures 2.7(a) and 2.7(b) show the limits for $P_{building,t}$ and $\Delta P_{building,t}$ for building A respectively. The base heating and cooling setpoints for the thermal zones in buildings A and B are 22.5^oC and 24^oC, respectively. For flexibility purposes, we assume that the temperature ranges for buildings A and B are 22^oC to 25^oC and 21^oC to 25^oC, respectively. The hot water temperature range is assumed to be 52^oC to 59^oC. The plots in Fig. 2.7(b) represent the upper and lower values of the maximum and minimum limits for $\Delta P_{building,t}$. A major observation is the step increase in the power limits at 10 am. This increase is due to the worst-case EV charging profile, which assumes that a significant number of EVs will be plugged in for charging at around 10 am. This charging assumption also impacted the virtual energy limits, as shown in Fig. 2.8(b), where the maximum energy limit increases at around 10 am. From Fig. 2.8(a), the variations in the virtual self-discharge rate are more pronounced during the day when the building's power consumption is generally more significant. The values of K_0 and K_1 for building A are 16.23 and 1.20, respectively.

Figures 2.9(a) and 2.9(b) show the limits for $P_{building,t}$ and $\Delta P_{building,t}$ for building B respectively. Since building B is a warehouse, we assume that the worst-case EV

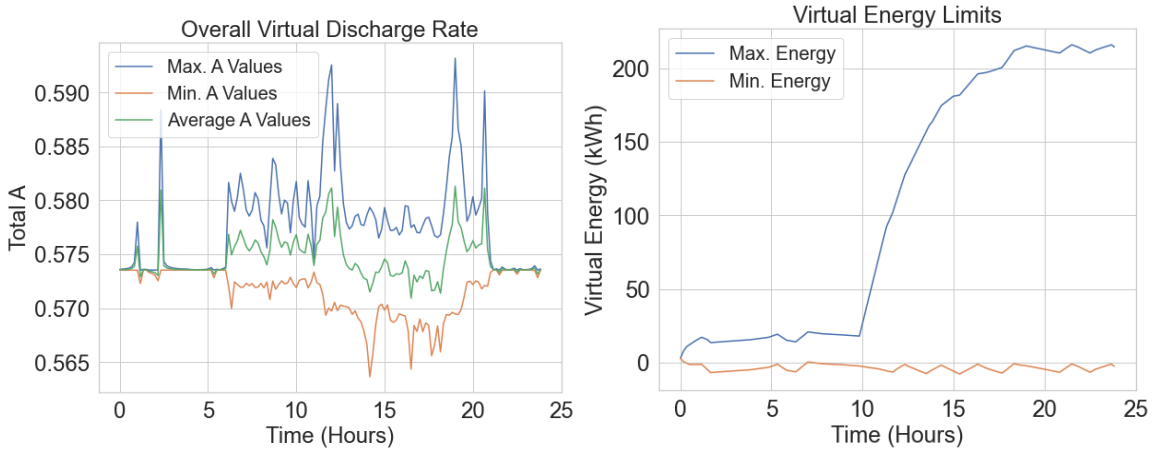

(a) $A_{building,A}$ limits

(b) $x_{building,A}$ limits

Figure 2.8: (a) Self-discharge limits (b) Virtual energy limits for building A

charging profile involves a significant charging activity in the early hours of the day, representing the charging of delivery trucks or vans associated with the warehouse facility. This assumption is reflected in Figures 2.9(a) and 2.9(b), with higher flexibility limits in the early hours of the day. Fig. 2.10(b) also reflects this assumption with a ramp in the maximum virtual energy limits in the early hours of the day. However, the virtual discharge rate (Fig. 2.10(a)) appears mostly constant. This is because of a number of reasons. Firstly, most of the zones in building B are windowless or without glass sections. As such, most of the zones have no solar heat gains. Secondly, due to ambient conditions and the relatively bigger size of the zones in the building, the uncertainties in the internal heat gains did not produce significant changes in base zone temperature across different scenarios. A combination of these factors results in smaller values of $s_{z,1,t}$ which leads to near constant A values for the building's HVAC system (based on equation (2.17b)), which is the dominant term in the overall $A_{building,t}$ term. The values of K_0 and K_1 for building B are 154.57 and 0.87, respectively.

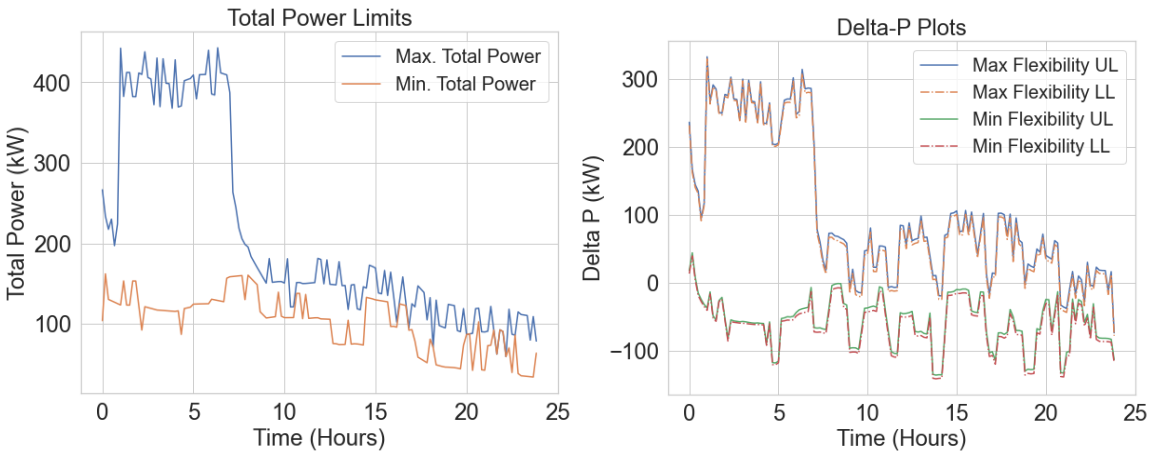

(a) $P_{building,B}$ limits (b) $\Delta P_{building,B}$ limits

Figure 2.9: (a) $P_{building,B}$ limits (b) $\Delta P_{building,B}$ limits

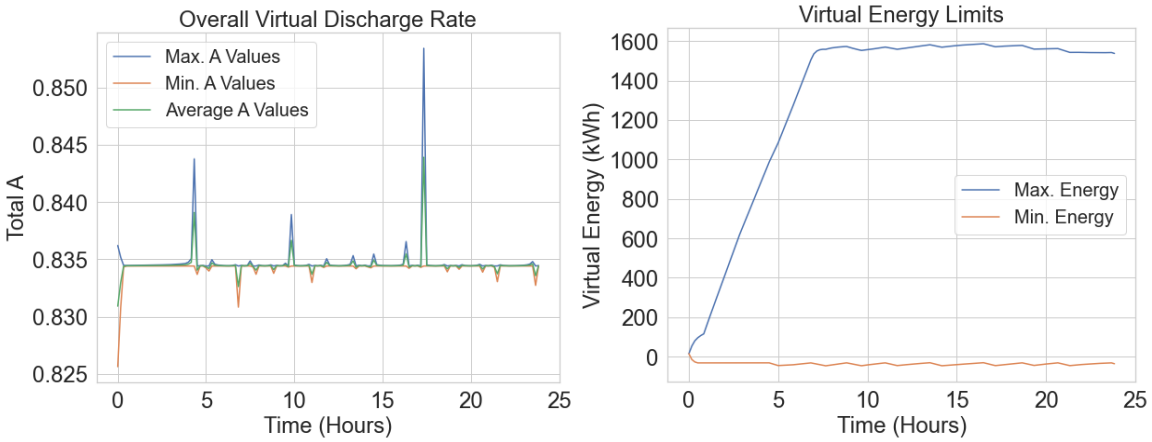

(a) $A_{building,B}$ limits (b) $x_{building,B}$ limits

Figure 2.10: (a) Self-discharge limits (b) Virtual energy limits for building B

2.6.3 Use Case Results

The solutions to Problem (2.34) provide the reference signals that the LSE provides for each building to follow. Since the scenarios considered are assumed to be equally probable, the average values of $P_{building,A,t,s}$ and $P_{building,B,t,s}$ over all scenarios s are taken as the reference signals for buildings A and B, respectively. Fig. 2.11 shows the reference signals and the total power profile of buildings A and B using the base internal and solar heat gain profiles. The normalized root-mean-square-error (RMSE) metric is used to evaluate the control performance for each building. The

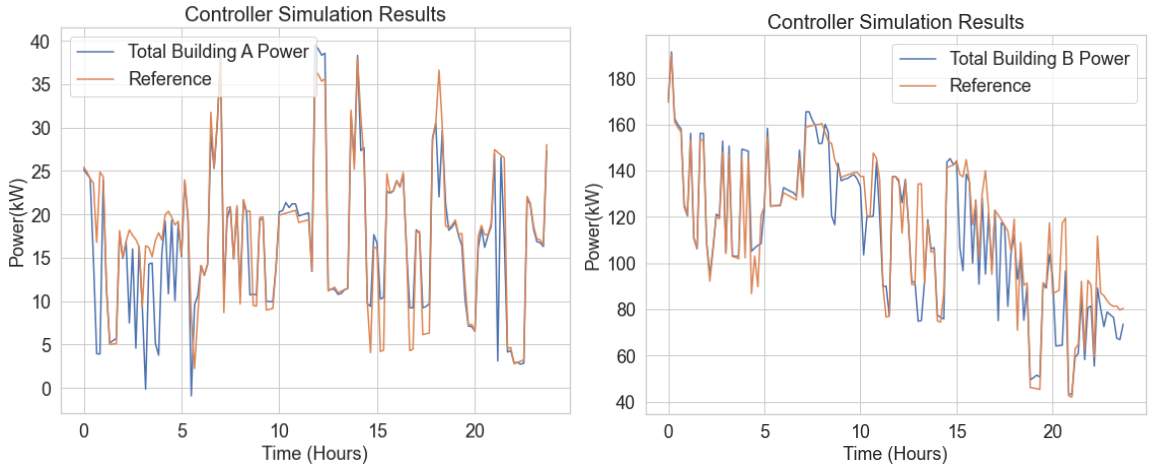

(a) Building A (b) Building B

Figure 2.11: Control results for (a) building A (b) building B

average normalized RMSE over multiple internal and solar heat gain profile scenarios is 10.5% for building A. For building B, the average normalized RMSE is 8.7%.

Fig. 2.12 shows that the temperatures in each zone of the two buildings are mostly within the specified limits. The variations in temperature during the early hours of the day for building A are due to the heating actions of the electric reheat coils, which are also modulated to make the building's electric power consumption track the reference signals. In Fig. 2.12(b), zone 3 (office zone) is the only zone with windows which explains why there is a significant increase in temperature as the solar irradiance increases (between 11 am and 7 pm). Also, the hot water temperature limits are generally satisfied in both buildings, as shown in Fig. 2.13. For EV charging, 36% and 7% of the energy budgets are used in buildings A and B, respectively.

2.7 Conclusions and Future Work

This chapter discusses a stochastic EBM for representing the overall flexibility in the power consumption of commercial buildings. The proposed stochastic EBM addresses gaps identified in existing works with EBM representations for flexible resources in commercial buildings. Different sources of uncertainties, including internal heat gains, solar heat gains, hot water consumption rate, and EV charging profiles,

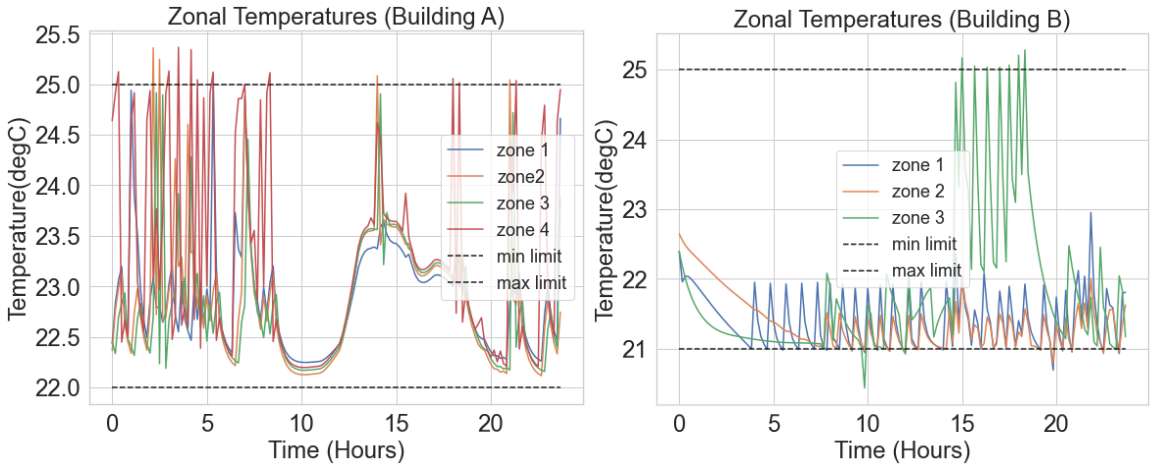

(a) Building A (b) Building B

Figure 2.12: Zone temperatures for (a) building A (b) building B

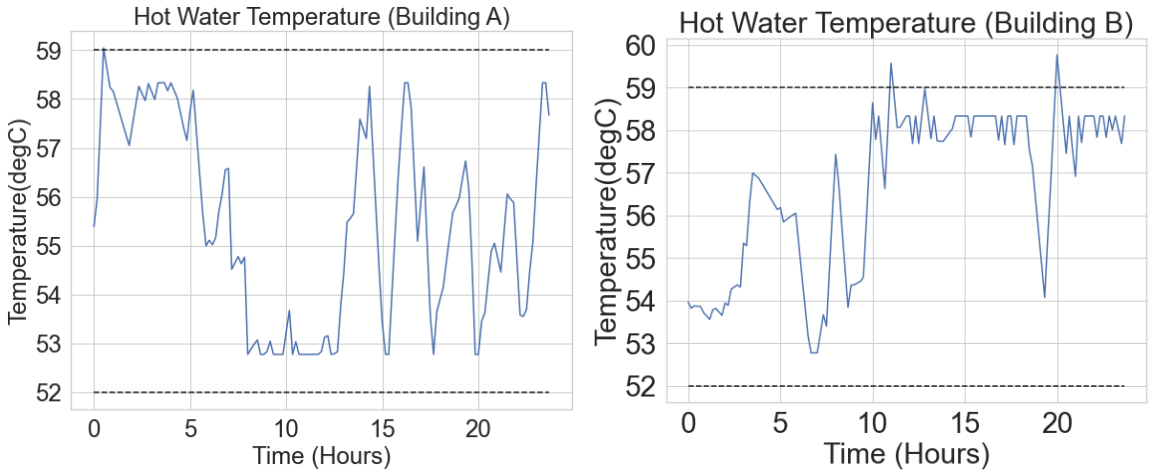

(a) Building A (b) Building B

Figure 2.13: Hot water temperature for (a) building A (b) building B

are captured in the proposed EBM. As such, the proposed model can be applied to stochastic resource scheduling problems where it will be very cumbersome to include detailed models of the flexibility associated with commercial buildings. Also, the illustrative use case shows that buildings can satisfactorily follow schedules generated from stochastic scheduling problems that model commercial buildings using the proposed stochastic EBM. For the two test buildings considered, we recorded an average tracking performance of over 90% across different scenarios of the internal heat gains, solar heat gains, and hot water consumption patterns. While the test buildings con-

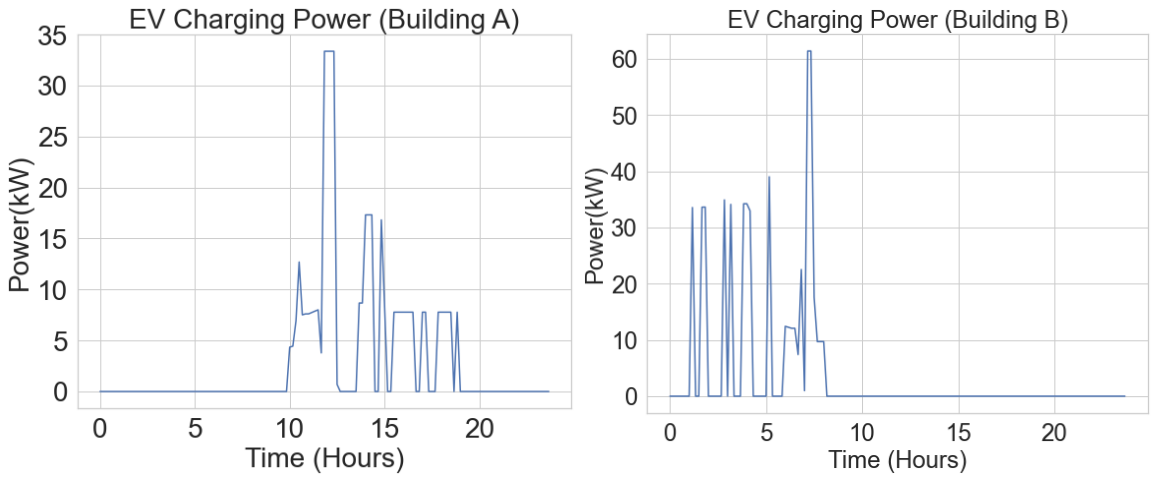

(a) Building A (b) Building B

Figure 2.14: EV charging power for (a) building A (b) building B

sidered were adapted from the commercial buildings database, the next step will be to use the proposed stochastic EBM to quantify the flexibility of real-world commercial buildings.

2.8 Appendix

Consider the generic convex stochastic optimization problem (2.36). $w(\gamma)$ and $x(\gamma)$ are scenario-dependent variables whose values depend on the specific realization of uncertainty γ, normally distributed with a zero mean. h, W, A, and B are deterministic parameters.

$$minimize\ E[w(\gamma)] \tag{2.36a}$$

subject to:

$$K + \gamma + x(\gamma) + Ww(\gamma) = h \tag{2.36b}$$

$$-w(\gamma) \leq 0 \tag{2.36c}$$

$$w(\gamma) - A \leq 0 \tag{2.36d}$$

$$-x(\gamma) \leq 0 \tag{2.36e}$$

$$x(\gamma) - B \leq 0 \tag{2.36f}$$

Considering the deterministic version, (2.36) becomes (2.37). v, u_1, u_2, u_3, and u_4 are the dual variables associated with the constraints.

$$minimize\, w \tag{2.37a}$$

subject to:

$$K + x + Ww = h : v \tag{2.37b}$$

$$-w \leq 0 : u_1 \tag{2.37c}$$

$$w - A \leq 0 : u_2 \tag{2.37d}$$

$$-x \leq 0 : u_3 \tag{2.37e}$$

$$x - B \leq 0 : u_4 \tag{2.37f}$$

Applying the Karush-Kuhn-Tucker (KKT) conditions to (2.36) yields a system of equations which when solved simultaneously produces $u_1 = u_2 = u_3 = 0$; $u_4 = \frac{1}{W}$; v_1 = -$\frac{1}{W}$; $x = B$; $w = \frac{h-K-B}{W}$ [26]. Note that the values of parameters h, K, B and W are such that constraints (2.36c) and (2.36d) are non-binding.

Considering (2.36) under two equally probable scenarios of γ produces (2.38).

$$minimize\, E[w] = \frac{w_1 + w_2}{2} \tag{2.38a}$$

subject to:

$$K + \gamma_1 + x_1 + Ww_1 = h : v_1 \tag{2.38b}$$

$$K + \gamma_2 + x_2 + Ww_2 = h : v_2 \tag{2.38c}$$

$$-w_1 \leq 0 : u_1 \tag{2.38d}$$

$$w_1 - A \leq 0 : u_2 \tag{2.38e}$$

$$-w_2 \leq 0 : u_3 \tag{2.38f}$$

$$w_2 - A \leq 0 : u_4 \tag{2.38g}$$

$$-x_1 \leq 0 : u_5 \tag{2.38h}$$

$$x_1 - B \leq 0 : u_6 \tag{2.38i}$$

$$-x_2 \leq 0 : u_7 \tag{2.38j}$$

$$x_2 - B \leq 0 : u_8 \tag{2.38k}$$

Applying KKT conditions to (2.38) yields $E[w] = \frac{h-K-B}{W}$ - $\frac{\gamma_1+\gamma_2}{2W}$. Since γ is normally distributed with a zero mean, the average value of γ_1, γ_2, ... , γ_n converges to 0 as n $\rightarrow \infty$ based on the law of large numbers. Hence, the summation $\gamma_1 + \gamma_2 +$ .... $+ \gamma_n$ also approaches 0 as n $\rightarrow \infty$. As such, the additional term $\frac{\gamma_1+\gamma_2}{2W}$ approaches 0 as more scenarios are included. Therefore the solution to the stochastic optimization problem approaches the solution to the deterministic problem as the number of scenarios increases. The same applies to the maximization problem. Thus, *Theorem* 1 is established.

REFERENCES

[1] Energy Information Administration, "Electric power monthly 2021," Electric Power Monthly, 2021. Available: https://www.eia.gov/electricity/monthly/current_month/march2021.pdf.

[2] S. O. Jensen, A. Marszal-Pomianowska, R. Lollini, W. Pasut, A. Knotzer, P. Engelmann, A. Stafford and G. Reynders, "IEA EBC annex 67 energy flexible buildings," *Energy and Buildings*, vol. 155, pp. 25–34, 2017.

[3] "An assessment of power flexibility from commercial building cooling systems in the united states," *Energy*, vol. 221, p. 119571, 2021.

[4] I. Beil, I. Hiskens and S. Backhaus, "Frequency regulation from commercial building HVAC demand response," *Proceedings of the IEEE*, vol. 104, no. 4, pp. 745–757, 2016. doi: 10.1109/JPROC.2016.2520640.

[5] H. Hao, Y. Lin, A. S. Kowli, P. Barooah, and S. Meyn, "Ancillary service to the grid through control of fans in commercial building hvac systems," *IEEE Transactions on Smart Grid*, vol. 5, no. 4, pp. 2066–2074, 2014. doi: 10.1109/TSG.2014.2322604.

[6] Y. Lin, P. Barooah, S. Meyn, and T. Middelkoop, "Experimental evaluation of frequency regulation from commercial building hvac systems," *IEEE Transactions on Smart Grid*, vol. 6, no. 2, pp. 776–783, 2015. doi: 10.1109/TSG.2014.2381596.

[7] Y. Shi, B. Xu, D. Wang, and B. Zhang, "Using battery storage for peak shaving and frequency regulation: Joint optimization for superlinear gains," *IEEE Transactions on Power Systems*, vol. 33, no. 3, pp. 2882–2894, 2018. doi: 10.1109/TPWRS.2017.2749512.

[8] H. Hao, B. M. Sanandaji, K. Poolla, and T. L. Vincent, "Aggregate flexibility of thermostatically controlled loads," *IEEE Transactions on Power Systems*, vol. 30, no. 1, pp. 189–198, 2015. doi: 10.1109/TPWRS.2014.2328865.

[9] H. Hao, A. Somani, J. Lian, and T. E. Carroll, Thomas, "Generalized aggregation and coordination of residential loads in a smart community," in *2015 IEEE International Conference on Smart Grid Communications (SmartGridComm)*, pp. 67–72, 2015. doi: 10.1109/SmartGridComm.2015.7436278.

[10] S. P. Nandanoori, I. Chakraborty, T. Ramachandran, and S. Kundu, "Identification and validation of virtual battery model for heterogeneous devices," in *2019*

IEEE Power Energy Society General Meeting (PESGM), pp. 1–5, 2019. doi: 10.1109/PESGM40551.2019.8973978.

[11] I. Chakraborty, S. P. Nandanoori, S. Kundu, and K. Kalsi, "Stochastic virtual battery modeling of uncertain electrical loads using variational autoencoder," in *2020 American Control Conference (ACC)*, pp. 1305–1310, 2020. doi: 10.23919/ACC45564.2020.9147609.

[12] D. Wu, H. Hao, T. Fu, and K. Kalsi, "Regional assessment of virtual battery potential from building loads," doi: 10.1109/TDC.2018.8440225.

[13] J. T. Hughes, A. DomÃnguez-GarcÃa, and K. Poolla, "Identification of virtual battery models for flexible loads," *IEEE Transactions on Power Systems*, vol. 31, no. 6, pp. 4660–4669, 2016. doi: 10.1109/TPWRS.2015.2505645.

[14] H. Hao, D. Wu, J. Lian, and T. Yang, "Optimal coordination of building loads and energy storage for power grid and end user services," *IEEE Transactions on Smart Grid*, vol. 9, no. 5, pp. 4335–4345, 2018. doi: 10.1109/TSG.2017.2655083.

[15] V. Adetola, F. Lin, S. Yuan, and H. Reeve, "Ramping services from grid-interactive buildings," in *2019 IEEE Conference on Control Technology and Applications (CCTA)*, pp. 624–629, 2019. doi: 10.1109/CCTA.2019.8920453.

[16] A. Abbas, R. Ariwoola, S. Kamalasadan and B. Chowdhury, "Evaluation of hybrid commercial building models for grid interactive building simulations," in *53rd North American Power Symposium*, pp. 1–6, 2021.

[17] H. Hao, D. Wu, J. Lian, and T. Yang, "Optimal coordination of building loads and energy storage for power grid and end user services," *IEEE Transactions on Smart Grid*, vol. 9, no. 5, pp. 4335–4345, 2018. doi: 10.1109/TSG.2017.2655083.

[18] D. N. Gujarati and D. C. Porter, *Basic Econmetrics*. New York: McGraw-Hill, 2009.

[19] P. Kepplinger, G, Huber, M. PreiÃinger and J. Petrasch, "State estimation of resistive domestic hot water heaters in arbitrary operation modes for demand side management," *Thermal Science and Engineering Progress*, vol. 9, pp. 94–109, 2019. doi: https://doi.org/10.1016/j.tsep.2018.11.003.

[20] D. M. Rosewater, D. A. Copp, T. A. Nguyen, R. H. Byrne, and S. Santoso, "Battery energy storage models for optimal control," *IEEE Access*, vol. 7, pp. 178357–178391, 2019. doi: 10.1109/ACCESS.2019.2957698.

[21] M. Deru, K. Field, D. Studer, K. Benne, B. Griffith, P. Torcellini, M. Halverson, D. Winiarski, B. Liu, M. Rosenberg, J. Huang, M. Yazdanian, and D. Crawley, "U.S. Department of Energy commercial reference building models of the national building stock," 2010.

[22] S. Wilcox and W. Marion, "Users manuals for TMY3 data sets," 2008. Available: https://www.nrel.gov/docs/fy08osti/43156.pdf .

[23] Gurobi Optimization, LLC, "Gurobi optimizer reference manual," 2021. Available: https://www.gurobi.com.

[24] New York Independent System Operator, "Energy market and operational data," 2022. Available: https://www.nyiso.com/energy-market-operational-data.

[25] M. Farivar and S. H. Low, "Branch flow model: Relaxations and convexificationâpart i," *IEEE Transactions on Power Systems*, vol. 28, no. 3, pp. 2554–2564, 2013. doi: 10.1109/TPWRS.2013.2255317.

[26] H. W. Kuhn and A. W. Tucker, "Nonlinear programming," in *Proceedings of the Second Berkeley Symposium on Mathematical Statistics and Probability*, pp. 481–492, 1950. Available: http://web.math.ku.dk/ moller/undervisning/MASO2010/kuhntucker1950.pdf.

CHAPTER 3: A STOCHASTIC OPTIMIZATION FRAMEWORK FOR REALIZING COMBINED VALUE STREAMS FROM CUSTOMER-SIDE RESOURCES

Due to numerous supporting policies aimed at decarbonizing electricity infrastructures in different regions of the world, customer-side resources are becoming increasingly valuable. Consequently, load-serving entities (LSEs) that typically have access to these customer-side resources can use them for multiple services simultaneously. This chapter discusses a stochastic optimization framework for using clusters of residential HVACs, electric water heaters (EWH), and behind-the-meter (BTM) batteries, spread around the LSE's distribution network, for energy arbitrage, peak shaving, and market-based frequency regulation simultaneously. Our framework captures the effects of controlling the consumption of the customer-side resources on the voltages in the LSE's distribution network. We also discuss two real-time dispatch algorithms capable of eliciting a fast response from the resources to frequency regulation signals from the market operator with minimal voltage violations. We evaluate the optimization models and dispatch algorithms using a HELICS-based co-simulation platform and real-world data from New York Independent System Operator (NYISO).

Nomenclature

Parameters

b	Index of BTM battery clusters
h	Index of HVAC clusters
j	Index of time windows for regulation capacity
k	Index of observed node voltages
s	Index of scenarios
t	Index of time steps
u	Index of inequality constraints
v	Index of equality constraints
w	Index of electric water heaters
y	Index of buses with observed node voltages
A	EWH total surface area
c, ρ	Specific heat capacity and density of water
$E_{h,total}$	Maximum energy consumption for HVAC cluster h
$E_{b,min/max}$	Battery energy limits
M_t	Regulation mileage
m	Mass of water in electric water heater
N	Time steps in each regulation capacity window
$p_{c,t}, p_{m,t}$	Regulation capacity and movement price at time t

$P_{base,h,t}$	HVAC cluster h base consumption
$P_{base,w,t}$	Electric water heater w base consumption
$P_{base,b,t}$	Battery cluster b base consumption
$P_{cluster,t}$	BTM cluster total forecasted base demand at time t
P_{max}	Maximum demand limit
$P_{h,max}$	Maximum power for HVAC cluster h
$P_{w,max}$	Maximum power for water heater cluster w
$P_{ch,b,max}$	Battery charging power limits
$P_{dis,b,max}$	Battery discharging power limits
$P_{sol,t}$	Solar heat gain at time t
$P_{ref,t}$	Total power reference at time t
pf_h	Aggregated power factor for HVAC cluster h
p_{kh}, q_{kh}	Active & reactive power voltage sensitivity for node k & cluster h
r_t,$\hat{r}_{t,J}$	Historical and real-time frequency regulation signal
R_e	Water heater thermal resistance
S_t	LSE's total forecasted base demand at time t
$SOC_{w,min/max}$	Cluster w equivalent min/max state-of-charge
T_a, T_{in}	Outdoor and indoor air temperature
T_{cw}	EWH inlet water temperature
$T_{i,h,min/max}$	HVAC cluster h equivalent minimum/maximum temperature

$T_{sp,h,t}$	HVAC thermostat setpoint for cluster h at time t
$T_{sp,w,t}$	EWH thermostat setpoint for cluster w at time t
$T_{w,max}$	Cluster w maximum hot water temperature
UL	Voltage unbalance limits
V_h	Total value (in $) of HVAC units in cluster h
$V_{base,k,t}$	Base voltage at node k at time t
$V_{min/max}$	Minimum and maximum voltage limits
$V_{UP,t-1}$	Most recent maximum voltage measurement
$V_{L,t-1}$	Most recent minimum voltage measurement
W_t	Hot water consumption at time t
α	Frequency regulation performance score
α_b	Battery cluster b self discharge rate
$\eta_{ch/dis,b}$	Battery charging/discharging efficiency
$\eta_{COP,h}$	HVAC cluster h COP
$\lambda_{m,t}, \lambda_{s,t}$	Market, retail electricity price respectively
λ_{TOU}	Time-of-Use rate
$\phi_{h/w/b}$	Cluster performance score
$\rho_{h/w/b,t}$	Cluster participation factor at time t

Variables

$batt_{ret,b}$	Battery cluster b total savings from local arbitrage

$E_{b,t}$	Battery cluster b energy state at time t
$P_{b,t}$	Battery cluster b power consumption at time t
$P_{b,\beta,t}$	Battery cluster b updated baseline consumption
$P_{ch,b,t}$	Battery charging power for cluster b at time t
$P_{dis,b,t}$	Battery discharging power for cluster b at time t
$P_{h,t}$	HVAC cluster h total consumption at time t
$P_{w,t}$	EWH cluster w power consumption at time t
$P_{w,\beta,t}$	EWH cluster w updated baseline consumption
$P_{up,t}$	Load increase at time t
$P_{shave,t}$	Load reduction at time t
$P_{reg,j}$	Regulation capacity for time window j
$T_{i,h,t}$	HVAC cluster h temperature at time t
$SOC_{w,t}$	EWH cluster w state-of-charge at time t
$V_{k,t}$	Voltage at node k and time t
$V_{y,avg,t}$	Average voltage at bus y at time t
$\Delta v_{k,t}$	Voltage change at node k and time t
$\Delta P, \Delta Q$	Active and reactive power changes

3.1 Introduction

3.1.1 Background and Motivation

The demand side of the grid, which has been traditionally dormant, is becoming increasingly active. This increasing activity is definitely connected to grid modernization and decarbonization trends that have catalyzed the proliferation of new and existing clean energy technologies at the customer side of the grid. Declining costs of sensory and computation devices have also made it cheaper to monitor customer-side resources and gain insights into how they interact with the grid providing the necessary framework for using these resources to support the overall grid. Furthermore, favorable policies have also played significant roles in encouraging these trends. For example, the New York Reforming the Energy Vision (NYREV) is a major initiative that is strongly encouraging the usage of Non-Wires Alternatives (NWA) and electrification of heating in New York state [1]. Also, FERC Order 841 and the more recent Order 2222 are two policies that are removing the barriers to the participation of energy storage and other distributed energy resources (DERs) in wholesale markets including energy markets, ancillary service markets and capacity markets [2]. In fact, a major stipulation of FERC Order 2222 is that a single DER or an aggregation of DERs can provide multiple services [2]. These services can be both at the transmission and distribution levels. As such, we focus on such service combinations in this work.

Extensive work has been done on the usage of different customer-side resources for single grid-level services. A detailed overview of the existing works on this topic may be found in [3]. For combined services, these can be considered from two broad perspectives. Firstly, a group of homogeneous resources can be used to provide multiple services. For example, in [4], authors consider the usage of an aggregate of electric water heaters (EWHs) for frequency regulation and voltage management in the presence of a high penetration of renewables. Previous knowledge of the control band of the

aggregation and regulation capacity requirements are assumed. However, this may not necessarily be applicable in typical contexts where the aggregator needs to decide its regulation capacity bids before submittal to the market operator for clearing or otherwise. Also, stochasticity associated with electricity prices and regulation market prices were not clearly captured in the aggregator's day-ahead scheduling problem. In another work, an aggregation of behind-the-meter (BTM) batteries is considered for frequency regulation while the batteries are individually used for end-user services like peak load reduction and PV curtailment simultaneously [5]. Also, stochasticity is not considered. In [6], electric vehicles are considered for combined frequency regulation and peak shaving.

The second broad perspective is the usage of a group of heterogeneous resources for multiple services. This theme is particularly found in works that represent single buildings as virtual power plants. In [7], the authors consider batteries and heating, ventilation and air-conditioning (HVAC) systems in commercial buildings for energy arbitrage, frequency regulation, and spinning reserve provision. However, since the resources are collocated within a single building, grid voltage impacts were not considered. Also, a perfect knowledge of prices and other system parameters is assumed without stochasticity. Furthermore, the work focuses on the day-ahead scheduling phase and as such does not propose any real-time control algorithm for resource dispatch.

From the preceding paragraphs, it can be logically inferred that a combination of both perspectives will be beneficial. The homogeneous resource standpoint allows for a justified reliance on aggregate models since each device/resource in the aggregation is essentially the same. On the other hand, the heterogeneous standpoint exploits potential benefits from complementary interactions of different resources. Combining both perspectives, a single resource aggregation can thus be seen as a heterogeneous cluster of several homogeneous clusters scattered around the distribution system.

This is particularly relevant in situations where a single load serving entity (LSE) also serves as an aggregator of DERs capable of simultaneously participating in wholesale markets and meeting local system needs as highlighted in the FERC Order 2222 [2]. Another implication of this perspective is that individual resource owners can elect to have specific resources in their buildings instead of the entire building responding to external signals, which will mostly be the case with residential customers.

This work, therefore, considers a heterogeneous resource aggregation made up of homogeneous aggregations of residential HVACs, EWH and BTM batteries. We consider frequency regulation, energy arbitrage and system peak load reduction (which can also be seen as distribution capacity expansion deferral) as the service combination of interest. Furthermore, our work can be seen as closing the gaps and building on the work presented in [4] and [7].

3.1.2 Contributions

Our major contributions are highlighted as follows.

1. We present a stochastic day-ahead scheduling model for an LSE with access to aggregations of residential HVACs, EWH and BTM batteries for combined market-based frequency regulation provision, energy arbitrage and peak shaving. Our formulation captures stochasticity in energy and regulation market prices and frequency regulation signals. Our formulation also captures the potential impact of resource control actions on system voltages based on the voltage sensitivity matrix approach.

2. Furthermore, our formulation captures the fact that individual BTM resources must have had pre-intended applications. We focus on arbitrage and illustrate how LSEs can estimate opportunity costs (i.e. value from local energy arbitrage) for a group of BTM battery owners .

3. We present two real-time control algorithms capable of eliciting fast resource

response given the requirements for frequency regulation with minimal violations of system voltage limits. It should be noted that our previous work, [8], considers only a deterministic day-ahead problem involving the usage of residential HVACs and EWH for frequency regulation and peak shaving without system voltage considerations. Also, real time control was not considered.

3.2 Resource Modeling

In this section, we discuss the modeling approaches considered for the customer-side resources, i.e., groups of residential HVACs, EWH and BTM batteries.

3.2.1 Residential HVAC Aggregation Model

Residential HVAC units are often modeled using first-order or second-order equivalent thermal parameter (ETP) models with binary variables capturing on/off status of the units [9]. However, when considering a large number of single units within a high-resolution multi-period optimization problem, it is clear that such an approach can quickly become intractable. As such, we adopt a first order ETP equivalent model which approximates the aggregated dynamics of a cluster of single units. This aggregated model captures the total power consumption of the HVAC units and the average temperature dynamics for all the HVAC units within the cluster. It is worth mentioning that clusters are assumed to be formed at nodes of the primary distribution network. However, multiple sub-clusters can be created for nodes that have a significant number of units with varying characteristics. To achieve such clustering, popular clustering algorithms such as the K-means and Gaussian Mixture Model (GMM) clustering algorithms can be applied [10].

The first-order aggregate model equation is shown in (3.1). The R and C parameters are obtained via a system identification procedure based on Pseudo Random Binary Sequence (PRBS) signals. Specifically, the HVAC units within each cluster are perturbed with the same setpoint offsets and total power consumption of the units

and the average temperature across the cluster are measured. The CTSM software, which is based on maximum likelihood estimation and Kalman filters, is then applied to obtain the respective R and C values [11]. η_{COP} is taken as the average of the COP values for each unit within the cluster.

$$T_{i,h,t+1} = T_{i,h,t}\left(1 - \frac{\Delta t}{R_h C_h}\right) + T_{a,t}\left(\frac{\Delta t}{R_h C_h}\right) - \eta_{\mathrm{COP},h} P_{h,t}\left(\frac{\Delta t}{C_h}\right) + P_{\mathrm{sol},,}\left(\frac{\Delta t}{C_h}\right) \tag{3.1}$$

3.2.2 Residential EWH Aggregation Model

As with the residential HVACs, an aggregate model is also adopted for the residential EWH. This model is also based on a first-order ETP model (also known as the single node model), which has been widely used in the existing literature [12]. The model equations are as shown in (3.2a) to (3.2e). The interested reader is referred to [12] and our previous work [8] for more details about the model.

$$SOC_W = \frac{T_{w_{avg}}}{T_{w_{\max}}} \tag{3.2a}$$

$$SOC_{w,t+1} = a_{w,t} SOC_{w,t} + \frac{(b_t P_{w,t} + e_{w,t})}{T_{w\max}} \tag{3.2b}$$

$$a_{w,t} = \exp\left(-\frac{\Delta t}{R_w C_w}\right), b_t = R_w\left(1 - a_{w,t}\right) \tag{3.2c}$$

$$e_{w,t} = \left(G R_w T_a + B R_W T_{cw}\right)\left(1 - a_{w,t}\right) \tag{3.2d}$$

$$R_w = \frac{1}{G+B}, B = \rho W_t c, G = \frac{A}{R_e}, C_w = mc \tag{3.2e}$$

3.2.3 BTM Battery Aggregation Model

For the batteries, the well-established energy reservoir model is adopted, as shown in (3.3a) - (3.3g) [13]. The self-discharging, charging, and discharging rates are taken

as weighted averages of the batteries within the cluster.

$$E_{b,t+1} = \alpha_b E_{b,t} + \eta_{ch,b} P_{ch,b,t} - \frac{1}{\eta_{dis,b}} P_{\text{dis, b,t}} \tag{3.3a}$$

$$P_{b,t} = \eta_{ch,b} P_{ch,b,t} - \frac{1}{\eta_{dis,b}} P_{dis,b,t} \tag{3.3b}$$

$$E_{b,\min} \leq E_{b,t} \leq E_{b,\max} \tag{3.3c}$$

$$0 \leq P_{ch,b,t} \leq P_{ch,b,\max} \tag{3.3d}$$

$$0 \leq P_{dis,b,t} \leq P_{\text{dis,b, max}} \tag{3.3e}$$

$$P_{b,t}^2 + Q_{b,t}^2 \leq S_b^2 \tag{3.3f}$$

$$ch_{ind,t} + dis_{ind,t} \leq 1 \tag{3.3g}$$

As previously highlighted, electricity consumers who have made investments in BTM batteries must have done so to fulfill certain objectives. As such, the LSE or aggregator needs to estimate the expected benefits for the BTM battery owners. The value of the expected benefits will form the minimum compensation that these resource owners will be willing to accept and should be captured in the LSE's scheduling problem. The assumption is that the resource owners use their batteries primarily for energy arbitrage. While we will show that local energy arbitrage can be an economically viable application for BTM batteries for the case studies considered, other applications can be considered depending on the conditions specific to the LSE.

3.3 Day-Ahead Scheduling Model

As earlier discussed, the LSE/aggregator uses the customer-side resources for market-based frequency regulation, energy arbitrage, and peak load reduction. We assume that the LSE participates in a competitive market environment, is a profit-making entity, and is also a price taker whose actions do not significantly influence market outcomes. We also assume that the LSE can forecast its overall day-ahead demand and can estimate, on a day-ahead basis, the expected base consumption for each

HVAC and EWH aggregation with acceptable accuracy levels. The possibility of easily getting fine-grain historical consumption data through increasingly reliable and cost-effective advanced metering infrastructure makes these assumptions even more valid. Furthermore, the day-ahead aggregated demand profile for each cluster of buildings providing BTM batteries can also be forecasted. Also, it is assumed that the LSE has access to historical market-based regulation signals, energy prices, and regulation market prices. This market-based information is assumed to constitute the stochasticity associated with the LSE's day-ahead scheduling problem. This section discusses the LSE's day-ahead scheduling problem based on these assumptions.

3.3.1 BTM Battery Base Profile and Benefits Estimation

To obtain the base demand profile and the expected benefits for the BTM batteries, the problem represented in (3.4) is solved. The expected benefits for the BTM batteries are taken as the lower compensation limit for the BTM battery owners.

$$minimize\ Y_{batt}$$

$$Y_{batt} = \sum_{t=1}^{T} \lambda_{TOU,t}(P_{cluster,t} + P_{b,t}) \tag{3.4a}$$

Subject to:

$$\text{(3.3a) - (3.3g)} \tag{3.4b}$$

$$P_{cluster,t} + P_{b,t} \geq 0 \tag{3.4c}$$

$$E_1 = E_T \tag{3.4d}$$

$$batt_{ret} = (\sum_{t=1}^{T} \lambda_{TOU,t} P_{cluster,t}) - Y_{batt} \tag{3.4e}$$

In problem (3.4), the objective function (3.4a) minimizes the cost of electricity for the BTM battery owners by taking advantage of time-of-use (TOU) rates represented by $\lambda_{TOU,t}$. Constraint (3.4c) ensures that the net demand is non-negative implying

that the buildings are not injecting electricity back to the grid and (3.4d) enforces energy balance for the batteries. Equation (3.4e) gives the expected base benefits for the aggregated BTM batteries. The expected base profile for the aggregated BTM batteries, $P_{base,b,t}$, equals $P_{b,t}$.

3.3.2 Service Combination Formulation

The LSE's day-ahead scheduling problem is as shown in problem (3.5).

$$maximize\ Y_{DA}$$

$$\begin{aligned} Y_{DA} = &\sum_{j=1}^{J} \sum_{t=1+(j-1)N}^{jN} \left[\left(\lambda_{s,t} - \lambda_{m,t} \right) \left(S_t + P_t - r_t P_{reg,j} \right) \right] \\ &+ \left[\sum_{j=1}^{J} P_{\mathrm{reg},j} \left(\sum_{t=1+(j-1)N}^{jN} \left(p_{c,t} + \alpha \left| M_t \right| p_{m,t} - 1.1 p_{c,t} (1-\alpha) \right) \right) \right] \\ &- \sum_{t=1}^{T} \sum_{h=1}^{H} b_h \left(T_{i,h,t} - T_{sp,h,t} \right)^2 \\ &- \sum_{t=1}^{T} \sum_{w=1}^{W} b_w \left(T_{i,w,t} - T_{sp,w,t} \right)^2 \\ &- \sum_{t=1}^{T} \sum_{b=1}^{B} b_b \left(P_{b,t} - P_{base,b,t} \right) - \sum_{b=1}^{B} batt_{ret,b} \\ &- \sum_{t=1}^{T} \sum_{h=1}^{H} \left(\frac{V_h}{E_{h,total}} \right) z_{h,t} \end{aligned} \tag{3.5a}$$

Subject to:

$$(3.1),\ \forall h \in H \tag{3.5b}$$

$$(3.2),\ \forall w \in W \tag{3.5c}$$

$$(3.3),\ \forall b \in B \tag{3.5d}$$

$$\begin{aligned} P_t - r_{t,j} P_{reg,j} = &\sum_{h=1}^{H} \left(P_{h,t} - P_{base,h,t} \right) \\ &+ \sum_{w=1}^{W} \left(P_{w,t} - P_{base,w,t} \right) + \sum_{b=1}^{B} \left(P_{b,t} - P_{base,b,t} \right) \end{aligned} \tag{3.5e}$$

$$P_t = p_{up,t} + p_{\text{shave},t} \tag{3.5f}$$

$$z_{h,t} = p_{rate,h,t} - \left\| P_{base,h,t} - P_{base,h,t-1} \right\|, \forall h \in H \tag{3.5g}$$

$$p_{rate,t} = \left\| P_{h,t} - P_{h,t-1} \right\|, \forall h \in H \tag{3.5h}$$

$$\sum_{t=1}^{T} (P_t - r_{t,j} P_{reg,j}) = 0 \tag{3.5i}$$

$$\sum_{t=1}^{T} \sum_{b=1}^{B} (P_{b,t} - P_{base,b,t}) \geq 0 \tag{3.5j}$$

$$0 \leq S_t + P_t - r_{t,j} P_{reg,j} \leq P_{\max} \tag{3.5k}$$

$$0 \leq S_t + P_t \leq P_{\max} \tag{3.5l}$$

$$p_{up,t} \geq 0, \;\; p_{shave,t} \leq 0 \tag{3.5m}$$

$$\begin{aligned} p_{shave,t} \geq & \sum_{h=1}^{H} (-P_{base,h,t}) + \sum_{w=1}^{W} (-P_{base,w,t}) \\ & + \sum_{b=1}^{B} (P_{dis,b,\max} - P_{base,b,t}) \end{aligned} \tag{3.5n}$$

$$\begin{aligned} p_{up,t} \leq & \sum_{h=1}^{H} (P_{h,max} - P_{base,h,t}) \\ & + \sum_{w=1}^{W} (P_{w,max} - P_{base,w,t}) + \sum_{b=1}^{B} (P_{ch,b,max} - P_{base,b,t}) \end{aligned} \tag{3.5o}$$

$$T_{i,h,min} \leq T_{i,h,t} \leq T_{i,h,max}, \forall h \in H \tag{3.5p}$$

$$SOC_{w,min} \leq SOC_{w,t} \leq SOC_{w,max}, \forall w \in W \tag{3.5q}$$

$$0 \leq P_{h,t} \leq P_{h,max}, \forall h \in H \tag{3.5r}$$

$$0 \leq P_{w,t} \leq P_{w,max}, \forall w \in W \tag{3.5s}$$

$$p_{rate,h,t} \geq P_{h,t} - P_{h,t-1}, \;\; p_{rate,h,t} \geq -(P_{h,t} - P_{h,t-1}) \tag{3.5t}$$

Since the LSE is a for-profit entity, the objective function (3.5a) maximizes the LSE's expected profit for the next operating day. The revenues include those from the sales of electricity and from participation in regulation markets represented by the first and second terms in (3.5a). The regulation market revenue term adopted

in this work is based on NYISO's operational information because the case studies considered are based on historical market data from NYISO [14]. It is also worth mentioning that energy arbitrage is implicitly captured in the first term in (3.5a). The third, fourth and fifth terms in the objective function represent the LSE's cost terms for the HVAC, EWH and BTM battery clusters. For the HVACs and EWHs, the cost is modeled as a quadratic function of the deviations of air and hot water temperatures from the desired setpoints. This quadratic nature captures the fact both upward and downward temperature deviations will impact the comfort of the resource owners. For the batteries, a linear function with a degradation cost parameter and an additional non-negativity constraint (3.5j) are considered. Constraint (3.5j) ensures that the batteries' resultant daily energy profile is at least equal to that obtained from problem 3.4 (i.e., with each BTM resource owner using its battery for energy arbitrage). However, the actual energy profile is dependent on the degradation cost term b_b which is obtained using a similar procedure presented in [15] and [16]. It is worth mentioning that the degradation cost is a function of the charging and discharging efficiencies of the batteries as implied by equation (3.3b). To capture additional degradation that can be induced on the HVAC units due to frequent switching resulting from fast changing frequency regulation signals, an additional degradation cost term $\sum_{t=1}^{T}\sum_{h=1}^{H}\left(\frac{V_h}{E_{h,total}}\right)z_{h,t}$ with additional constraints (3.5g) and (3.5h) are added to the model. Constraints (3.5g) and (3.5h) capture how changes in the new power profile of the HVAC cluster differs from the changes in the base profile which must have been previously established. A detailed discussion on the degradation cost term for the HVAC units is presented in our previous work [8] and can be referred to for further details. For convexity, (3.5h) is reformulated as (3.5t).

Constraints (3.5b) to (3.5d) represent the aggregated dynamics for the HVAC, water heater and BTM battery clusters. Constraint (3.5e) can be considered as some sort of power balance equation that ensures that total deviation of the HVAC, water

heater and BTM battery clusters from their respective base profiles at each time index is equal to the regulation requests and load changes to achieve peak load reduction and energy arbitrage. Constraint (3.5i) ensures that the energy consumption of the customer side resources are not increased excessively resulting in higher electricity bills for the resource owners. (3.5k) and (3.5l) captures the peak shaving requirements for the LSE under peak shaving only or when both peak shaving and frequency regulation are being considered. The maximum demand parameter P_{max} can defined based on predetermined system capacity requirements which will be the case if the LSE is considering capacity expansion deferral. P_{max} can also be based on the need to reduce market-based capacity charges, which is determined by varying mechanisms across different market environments. The specific mechanisms for defining the value of P_{max} are outside the scope of this work. Constraints (3.5m) - (3.5o) represent the limits on the changes in demand without the impact of the response to regulation signals. Constraints (3.5p) - (3.5s) capture predefined air and hot water temperature limits representing the comfort limits for the HVAC and EWH resource owners.

3.3.3 Voltage Constraints

Given that the LSE's resource clusters can be distributed throughout its network, there is a need to consider the effects of the LSE's scheduling on system voltages. In fact, as the penetration of BTM batteries increases and as the LSE gets access to more flexible loads, the need for considering system voltages in the scheduling problem will become more important. However, given the high resolution nature of frequency regulation signals which are captured in the model formulation, the use of typical distribution system power flow equations will quickly result in a computationally intensive model. As such, we adopt an approximate method based on the voltage sensitivity matrix approach. It is worth mentioning that the voltage sensitivity matrix approach would perform best when the penetration of controllable customer-side resources is relatively low (i.e., load changes not too far away from

linearization point, which is the case with most demand-side management programs) with lesser accuracy as the penetration of the controllable customer-side resources increases. However, since the overall model is stochastic, it can be assumed that the overall effect of the stochasticities associated with the other parameters would have a higher magnitude compared to the voltage errors. The voltage equations based on the voltage sensitivity matrix are represented in (3.6).

$$\begin{bmatrix} \Delta v_1 \\ \vdots \\ \Delta v_n \end{bmatrix} = \begin{bmatrix} p_{11} & \cdots & p_{1m} \\ \vdots & \ddots & \vdots \\ p_{n1} & \cdots & p_{nm} \end{bmatrix} \begin{bmatrix} \Delta P_1 \\ \vdots \\ \Delta P_m \end{bmatrix} + \begin{bmatrix} q_{11} & \cdots & q_{1m} \\ \vdots & \ddots & \vdots \\ q_{n1} & \cdots & q_{nm} \end{bmatrix} \begin{bmatrix} \Delta Q_1 \\ \vdots \\ \Delta Q_m \end{bmatrix} \tag{3.6}$$

As shown in (3.6), the changes in voltage at the observed nodes (indexed 1 to n) are dependent on changes in both active and reactive power consumption or injection at the actor nodes (indexed 1 to m). For a selected observed node k, the sensitivities are further defined explicitly in (3.7a) to (3.7e).

$$\Delta v_k = \Delta v_{pk} + \Delta v_{qk} \tag{3.7a}$$

$$\Delta v_{pk} = \sum_{i=1}^{m} p_{ki} \Delta P_i \tag{3.7b}$$

$$\Delta v_{qk} = \sum_{i=1}^{m} q_{ki} \Delta Q_i \tag{3.7c}$$

$$p_{ki} = \frac{\delta V_k}{\delta P_i} \tag{3.7d}$$

$$q_{ki} = \frac{\delta V_k}{\delta Q_i} \tag{3.7e}$$

The sensitivities p_{ki} and q_{ki} are obtained by changing the active and reactive power consumption/injection (ΔP_i, ΔQ_i) at the actor node i and observing the associated voltage changes at the observed node k. The resultant sensitivity is taken as the average of the sensitivities for both consumption and injection related changes. For the HVAC units being considered, reactive power consumption is associated with the

motoring components within the units. Given that residential HVAC units are mostly on/off units, the reactive power consumption is directly associated with the active power consumption. Assuming that the power factor for each unit is known, the aggregated power factor can be estimated and (3.7c) can be rewritten as (3.8b). The overall voltage change equation for the HVAC clusters can be written as (3.8c).

$$\Delta Q_h = \Delta P_h tan\left(cos^{-1} pf_h\right) \tag{3.8a}$$

$$\Delta v_{qk} = \sum_{h=1}^{H} q_{kh} \Delta P_h tan\left(cos^{-1} pf_h\right) \tag{3.8b}$$

$$\Delta v_k = \sum_{h=1}^{H} \Delta P_h \left(p_{kh} + q_{kh} tan\left(cos^{-1} pf_h\right)\right) \tag{3.8c}$$

For the EWH, it is assumed that the units are resistive. As such, there is no reactive power consumption associated with the EWH. For the BTM batteries, although the battery inverters can be used for reactive power support, we assume that this function is not active in this context. In our subsequent work, which will capture voltage management as a service on its own, reactive power support using BTM batteries will be captured. Combining these three resource types, the resulting voltage change equation for each node k for every time step t is as shown in (3.9). The voltage at each node is as shown in (3.9b), where $V_{base,k,t}$ represents voltage values obtained from system simulations using the LSE's total day-ahead forecasted base load profile. In addition, (3.9c) - (3.9d) capture additional constraints to keep the node voltages and voltage unbalance at each bus within acceptable limits. To improve computational efficiency, the voltage equations can be restricted to buses where the customer-side resources are located and other weak buses that would have been identified during a preliminary system analysis.

$$\Delta v_k = \sum_{h=1}^{H} (P_{h,t} - P_{base,h,t}) \left(p_{kh} + q_{kh} tan\left(cos^{-1} pf_h\right)\right)$$

$$+\sum_{w=1}^{W}(P_{w,t}-P_{base,w,t})(p_{kw})+\sum_{b=1}^{B}(P_{b,t}-P_{base,b,t})(p_{kb})\ \ \forall k\ in\ K \tag{3.9a}$$

$$V_{k,t}=V_{base,k,t}+\Delta v_{k,t} \tag{3.9b}$$

$$\frac{V_{y,k,t}-V_{y,avg,t}}{V_{y,avg,t}}\leq UL \tag{3.9c}$$

$$V_{min}\leq V_{k,t}\leq V_{max} \tag{3.9d}$$

3.3.4 Stochastic Model Formulation

As discussed earlier, the stochasticities considered are associated with $\lambda_{m,t}$, r_t, $p_{c,t}$ and $p_{m,t}$. As such, problem (3.5) including constraints (3.9a) - (3.9d) is reformulated as a convex stochastic program with a general form shown in (3.10) [17]. The choice of the stochastic optimization approach hinges on the premise that LSEs often have access to a wealth of system data, and market operators also provide an enormous amount of market data, making it possible for the LSE to generate realistic scenarios for the uncertain parameters. Under such conditions, even though the LSE is typically risk averse, the usage of robust optimization methods may produce solutions that are unnecessarily conservative compared to results from a stochastic optimization framework. Expression (3.10a) represents the expected value of (3.5a). Constraints (3.10b) and (3.10c) represent the inequality and equality constraints in problem (3.5) over different scenarios represented by set S. Also, x and q represent the decision variables and the parameters under different scenarios respectively. U and V represent the sets of inequality and equality constraints in problem (3.5) respectively.

$$minimize\ \ E[f_o(x,q)] \tag{3.10a}$$

Subject to:

$$f_{u,s}(x,q)\leq 0,\ \ \forall u\ \ in\ \ U,\forall s\ \ in\ \ S \tag{3.10b}$$

$$f_{v,s}(x)\leq 0,\ \ \forall v\ \ in\ \ V,\forall s\ \ in\ \ S \tag{3.10c}$$

To generate the needed scenarios for $\lambda_{m,t}$, r_t, $p_{c,t}$ and $p_{m,t}$, forecast models based on historical data and other exogenous variables are used to generate interval forecasts for each of the parameters. These interval forecasts provide a representation of the future distribution of these parameters which are then sampled randomly to generate different scenarios. For the regulation signals r_t, each historical daily profile is taken as an individual scenario. For computational feasibility, a scenario tree with a reduced set of scenarios is then constructed using the scenario tree construction algorithm presented in [18] which is based on the backward reduction algorithm and the Kantorovich distance metric [19].

3.4 Real Time Dispatch Algorithm

After solving the day-ahead problem, the LSE obtains its total expected net demand profile (i.e., $E[S_t + P_{t,s} - r_{t,j,s}P_{reg,j,s}]$) which forms the basis for its demand bids into the day-ahead energy market. Also, expected regulation capacity bids and the expected net demand profile for the customer-side resources being controlled are obtained. This expected net demand profile for the controlled resources forms the consumption baseline, $P_{baseline,t}$, which is submitted into the regulation market in addition to the regulation capacity bids. $P_{baseline,t}$ is calculated as shown in (3.11). It is worth mentioning that $E[P_{t,s}]$ represents the expected value of P_t over different scenarios s which is also obtained from the results of the day-ahead scheduling model.

$$P_{baseline,t} = \sum_{h=1}^{H} P_{base,h,t} + \sum_{w=1}^{W} P_{base,w,t} + \sum_{b=1}^{B} P_{base,b,t} + E[P_{t,s}] \tag{3.11}$$

After the day-ahead phase, the LSE will need to respond to real time regulation signals from the grid operator (which also often doubles as the market operator) while ensuring that its peak shaving and voltage related constraints are not violated. Fig. 3.1 illustrates the interaction between the LSE's day-ahead scheduling problem and its real-time control actions. This figure shows that the LSE solves the scheduling

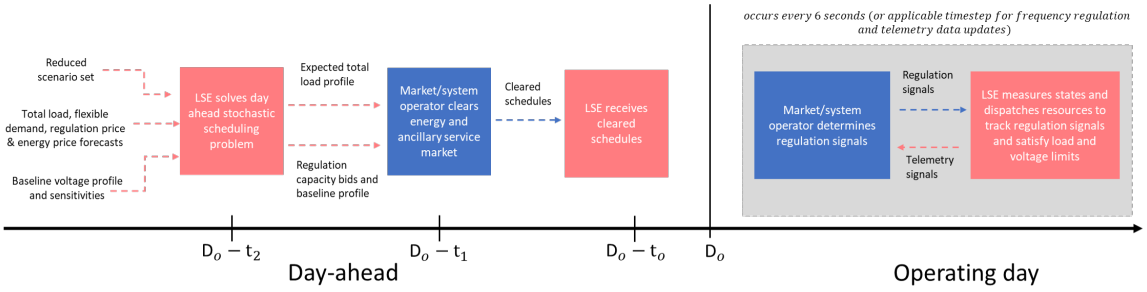

**Note that the LSE is a distribution utility which also serves as an aggregator of customer-side resources and operates the distribution network which is a possibility e.g., under policy frameworks like FERC Order 2222*

Figure 3.1: Illustration of LSE's day-ahead and real-time dispatch problems

problem in the day-ahead phase. This implies that the LSE will also generate the relevant load profile, price forecasts, stochasticities and the reduced scenario sets associated with the uncertainties in the day-ahead period. Furthermore, the base voltage profile and relevant voltage sensitivities will be obtained in the day-ahead phase. The outcomes of the LSE's scheduling problem, specifically expected load profile and regulation market bid information, are then provided to the market operator which uses that information to clear its energy and ancillary service markets. In the real time phase, the market operator provides dispatch signals which the LSE combines with other system variables to ensure that its peak load and voltage-related constraints are not violated. At the same time, the comfort-related limits associated with the resources being controlled must not be violated. To achieve this real time response, a hierarchical framework as shown in Fig. 3.2 is required. This is because while the grid operator assumes it is interacting with a single resource, the reality is that the resource is made up of several other individual homogeneous resource clusters with different characteristics. As such, the secondary level control divides the reference power among the individual homogeneous resource clusters while the primary level control deals with allocating response actions within each cluster.

To achieve an optimal division of the reference power among the resource clusters, a traditional approach would be a model predictive control (MPC) based approach. However, given the fast response requirements (e.g., 6 seconds for NYISO) for market-

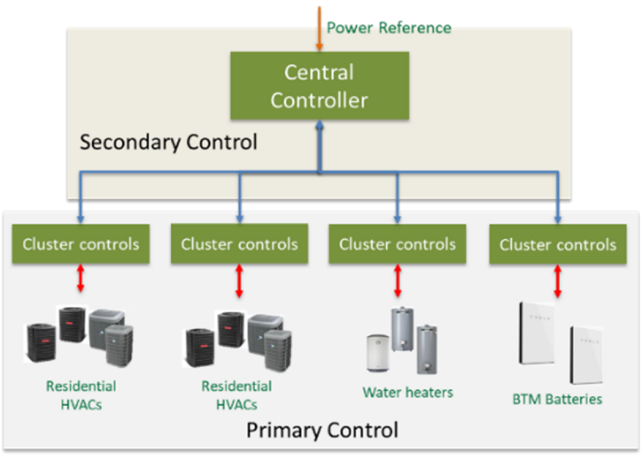

Figure 3.2: Hierarchical framework for real time resource dispatch.

based regulation products focused on fast responding resources like batteries and flexible loads, the traditional MPC-based routine might be too slow especially when several resource clusters and voltage constraints are being considered. This is because it might take too long to solve the optimization problem within the MPC routine. On the other hand, a dispatch algorithm could elicit faster responses at the expense of optimality. As such, we develop two dispatch algorithms - an MPC-based algorithm and a dynamic droop-based algorithm. These algorithms are further discussed in subsequent sections. At the primary control level, the widely studied temperature priority list (TPL) algorithm proposed in [9] is adopted for the HVAC and water heater clusters. For the BTM battery clusters, we develop an adaption of the TPL algorithm based on the state-of-charge (SOC) and size of each BTM battery within the cluster.

3.4.1 MPC-Based Dispatch Algorithm

Whenever a regulation signal is received from the grid operator, the total power reference for the resources is calculated using equation (3.12).

$$P_{ref,t} = P_{baseline,t} - \hat{r_{t,j}} P_{reg,j} \tag{3.12}$$

The MPC problem represented in (3.13) is then solved to obtain the power references for each individual homogeneous resource cluster at every time step. Given the high frequency nature of the regulation signals, the MPC is solved with a 1-hour horizon (i.e., 600 time steps if the regulation signal is received every 6 seconds). The most recent measurements of the required variables and parameters are used to initialize every run of the MPC routine.

$$minimize\,(P_{rt,t} - P_{ref,t})^2 \tag{3.13a}$$

Subject to:

$$(3.1),\ \forall h \in H \tag{3.13b}$$

$$(3.2),\ \forall w \in W \tag{3.13c}$$

$$(3.3),\ \forall b \in B \tag{3.13d}$$

$$P_{rt,t} = \sum_{h=1}^{H} P_{h,t} + \sum_{w=1}^{W} P_{w,t} + \sum_{b=1}^{B} P_{b,t} \tag{3.13e}$$

$$0 \leq S_t - P_{baseline,old,t} + P_{rt,t} \leq P_{\max} \tag{3.13f}$$

$$\begin{aligned}\Delta v_{k,t} = &\sum_{h=1}^{H} \left(P_{h,t} - P_{base_{h,t}}\right)\left(p_{kh} + q_{kh}\tan\left(\cos^{-1} pf_h\right)\right) \\ &+ \sum_{w=1}^{W} \left(P_{w,t} - P_{base_{w,t}}\right)\left(p_{kw}\right) \\ &+ \sum_{b=1}^{B} \left(P_{b,t} - P_{base_{b,t}}\right)\left(p_{kb}\right), \forall k \in K\end{aligned} \tag{3.13g}$$

$$V_{k,t} = V_{base,k,t} + \Delta v_{k,t} \tag{3.13h}$$

$$\frac{V_{y,k,t} - V_{y,avg,t}}{V_{y,avg,t}} \leq UL \tag{3.13i}$$

$$V_{\min} \leq V_{k,t} \leq V_{\max} \tag{3.13j}$$

3.4.2 Dynamic Droop-Based Dispatch Algorithm

The dynamic-droop based dispatch algorithm dynamically allocates the power reference among the different homogeneous clusters based on the previous performances of each cluster. Each cluster's performance is measured by $\varphi_{h/w/b}$ which is based on a normalized cumulative root mean square error value as shown in (3.14a). Depending on the availability of new measurements, $\varphi_{h/w/b}$ can be updated at different time intervals. However, faster updates will characterize an ideal situation. The participation factor, $\eta_{h/w/b}$, for each homogeneous cluster is then calculated as shown in (3.14b).

In (3.14b), the ratio $\frac{E[P_{h/w/b,t,s}]}{E[P_{h,t,s}]+E[P_{w,t,s}]+E[P_{b,t,s}]}$ represents the fraction of the expected power consumption for each homogeneous resource cluster with respect to the total expected power consumption of the resources. This ratio is also obtained from the results of the day-ahead stochastic optimization model. Given that $\rho_{h/w/b}$ changes over time, we consider it as some sort of dynamic droop co-efficient.

$$\varphi_{h/w/b} = 1 - \left(\frac{1}{P_{h/w/b,\max}} \sqrt{\frac{\sum_{t=1}^{I} \left(P_{h/w/b,t} - P_{ref,h/w/b,t}\right)^2}{I}} \right),\ \varphi_{h/w/b/b} \in [0,1] \tag{3.14a}$$

$$\rho_{h/w/b/b} = \varphi_{h/w/b,t} \frac{E[P_{h/w/b,t,s}]}{E[P_{h,t,s}] + E[P_{w,t,s}] + E[P_{b,t,s}]} \tag{3.14b}$$

After calculating the total power reference for the resources and the participation factors using (3.12) and (3.14b) respectively, the allowable limits on changes in voltage magnitude, with respect to predefined voltage limits (i.e.Δv_{up}, Δv_{down}), are obtained using (3.15).

$$\Delta v_{up} = V_{max} - max(V_{U,t-1}, V_{base,k,t}) \tag{3.15a}$$

$$\Delta v_{down} = V_{min} - min(V_{L,t-1}, V_{base,k,t}) \tag{3.15b}$$

Equation (3.15) is hinged on the premise that there are no other factors, such as high DER penetration levels, that could significantly alter voltage dynamics. Moreover, if such penetrations exists, they can be accounted for in the stochastic day-ahead scheduling problem. Furthermore, the introduction of the most recent voltage measurements (i.e., $V_{U(L),t-1}$) ensures that the algorithm reacts quickly to current system conditions by setting the appropriate voltage limits.

Afterward, the linear optimization problem (3.16) is solved to obtain the power references for each homogeneous resource cluster. Problem (3.16) is a much simpler problem and can be solved faster than (3.13). The objective function (3.16a) maximizes the weighted sum of the power consumption of the resources while the inequality constraint (3.16b) tries to match the total power consumption of the resources to the reference signal. Other constraints are similar to those described earlier. Also, (3.16) is solved for a single timestep and does not require any horizon as is the case with MPC. Furthermore, the parameters with index t - 1 in (3.15) refer to the most recent measurements while $E[P_{h,t,s}]$, $E[P_{w,t,s}]$, $E[P_{dis,b,t,s}]$ and $E[P_{ch,b,t,s}]$ are obtained from the stochastic day-ahead scheduling problem.

$$maximize \quad \sum_{h=1}^{H} \rho_{h,t} P_{h,t} + \sum_{w=1}^{W} \rho_{w,t} P_{w,t} + \sum_{b=1}^{B} \rho_{b,t} P_{b,t} \tag{3.16a}$$

Subject to:

$$\sum_{h=1}^{H} P_{h,t} + \sum_{w=1}^{W} P_{w,t} + \sum_{b=1}^{B} P_{b,t} \leq P_{ref,t} \tag{3.16b}$$

$$\Delta v_{U(L),t} = \sum_{h=1}^{H} \left(P_{h,t} - P_{base,h,t}\right) \left(p_{U(L)h} + q_{U(L)h} \tan\left(\cos^{-1} pf_h\right)\right)$$
$$+ \sum_{w=1}^{W} \left(P_{w,t} - P_{base,w,t}\right) \left(p_{U(L)w}\right) + \sum_{b=1}^{B} \left(P_{b,t} - P_{base,b,t}\right) \left(p_{U(L)b}\right) \tag{3.16c}$$

$$\Delta v_{U,t} \leq \Delta v_{up}, \;\; \Delta v_{L,t} \geq \Delta v_{\text{down}} \tag{3.16d}$$

$$0 \leq P_{h,t} \leq E P_{h,t,s}, \quad \forall h \in H \tag{3.16e}$$

$$0 \leq P_{w,t} \leq EP_{w,t,s}, \quad \forall w \in W \tag{3.16f}$$

$$0 \leq P_{ch,b,t} \leq EP_{ch,b,t,s}, \quad \forall b \in B \tag{3.16g}$$

$$0 \leq P_{dis,b,t} \leq EP_{dis,b,t,s}, \quad \forall b \in B \tag{3.16h}$$

3.4.3 Primary Control Algorithm for BTM Battery Cluster

For the distribution of control actions within BTM battery clusters, an adaption of the popular TPL algorithm often applied to thermostatically controlled load (TCLs) is adopted. The algorithm is described in Fig. 3.3.

TPL-Based Battery Dispatch Algorithm

Input: Battery state of charge, $\boldsymbol{soc_i}$ $\forall \boldsymbol{i}$; Power rating $\boldsymbol{P_{r,i}}$ $\forall \boldsymbol{i}$; Power reference, $\boldsymbol{P_{ref}}$
Output: Charging and discharging power reference of each battery, $\boldsymbol{P_{ch,i}}$and $\boldsymbol{P_{dis,i}}$

1. Obtain the most recent $\boldsymbol{soc_i}$ measurements
2. Sort $\boldsymbol{soc_i}$ in ascending order for charging responses
3. Sort $\boldsymbol{soc_i}$ in descending order for discharging responses
4. If charging request is received, $\boldsymbol{P_{ch,i}} = \left(\frac{\boldsymbol{1}}{\boldsymbol{soc_i}} / \sum_{\boldsymbol{i}} \frac{\boldsymbol{1}}{\boldsymbol{soc_i}}\right) \times \boldsymbol{P_{ref}}$
   If $\boldsymbol{P_{ch,i}} > \boldsymbol{P_{r,i}}$, then $\boldsymbol{P_{ch,i}} = \boldsymbol{P_{r,i}}$ and $\boldsymbol{P_{i+1,update}} = (\boldsymbol{P_{i,ch}} - \boldsymbol{P_{r,i}}) + \boldsymbol{P_{i+1}}$
5. If discharging request is received, $\boldsymbol{P_{dis,i}} = \left(\frac{\boldsymbol{soc_i}}{\sum \boldsymbol{soc_i}}\right) \times \boldsymbol{P_{ref}}$
   If $\boldsymbol{P_{dis,i}} > \boldsymbol{P_{r,i}}$, then $\boldsymbol{P_{dis,i}} = \boldsymbol{P_{r,i}}$ and $\boldsymbol{P_{i+1,update}} = (\boldsymbol{P_{i,dis}} - \boldsymbol{P_{r,i}}) + \boldsymbol{P_{i+1}}$

Figure 3.3: Battery dispatch algorithm

3.5 Case Studies

3.5.1 Simulation Data

The proposed framework was tested using the IEEE-37 bus test system [20]. It is assumed that the LSE has four homogeneous resource clusters across its distribution network as shown in Fig. 3.4. Residential units forming HVAC cluster 1 are connected to phase A of bus 702, while HVAC cluster 2 is on phase B of bus 701. Water Heater Cluster and BTM Battery Cluster are on phases C and B of buses 706 and 775 respectively. However, the resources are treated as a single resource by the transmission network/market operator. Out of the four homogeneous clusters, two

are HVAC clusters while the other two are the EWH and BTM battery clusters. The parameters for the four clusters are shown in Table I. The energy market and regulation market price data were obtained from NYISO's 2019 data repository while downsampled PJM RegD signals for 2019 were taken as the regulation signals [21]. A HELICS-based co-simulation testbed with GridLAB-D and Python federates, was used to run the real-time dispatch simulations [22]. The distribution network, HVACs, EWHs and batteries were simulated with GridLAB-D while the dispatch algorithms were implemented with Python. A Gurobi solver, within the CVX optimization tool, running on a 16-GB HP EliteOne 800 computer was used to solve the stochastic day-ahead model and the battery base profile and benefits estimation model [23]. A typical summer day is considered and the LSE's forecasted base demand profile, the BTM battery cluster's forecasted base demand profile and the TOU rates are shown in Fig. 3.5. The TOU rates are ConEdison's residential TOU rates [24]. Also, P_{max} was set at 3,400 kW.

Table 3.1: Resource cluster parameters

	HVAC (Cluster 1&2)	Water Heater (Cluster 3)	BTM Battery Cluster (Cluster 4)
No. of units	42	42	30
Parameters	$\mathrm{R}_h = 0.06^oC/kW$	$\mathrm{A} = 96\mathrm{m}^2$	$\alpha_b = 1$
Parameters	$\mathrm{C}_h = 45.25kWh/^oC$	$\mathrm{R}_e = 16$	$\eta_{ch} = 0.927$
Parameters	$\eta_{COP} = 4$	$\mathrm{C}_w = 33 \times 10^6 J/kg$	$\eta_{dis} = 1.08$
Total rating	180 kW	189 kW	150 kW / 405 kWh
Comfort/ Usage Limits	$\mathrm{T}_{i,min} = 66.95^oF$ $\mathrm{T}_{i,max} = 72.95^oF$	$\mathrm{SOC}_{min} = 0.895$ $\mathrm{SOC}_{max} = 1$	$\mathrm{SOC}_{min} = 0.2$ $\mathrm{SOC}_{max} = 1$

3.5.2 BTM Battery Base Profile Estimation Results

Problem (3.5) is solved using the parameters specified in Table 3.1 and the data in Fig. 3.5. From the results, $batt_{ret}$ equals \$484 for summer weekdays days and \$169 for all other the weekdays. Using the TOU rates and corresponding time schedules in [24], the estimated total annual electricity cost savings from arbitrage is \$72,290.

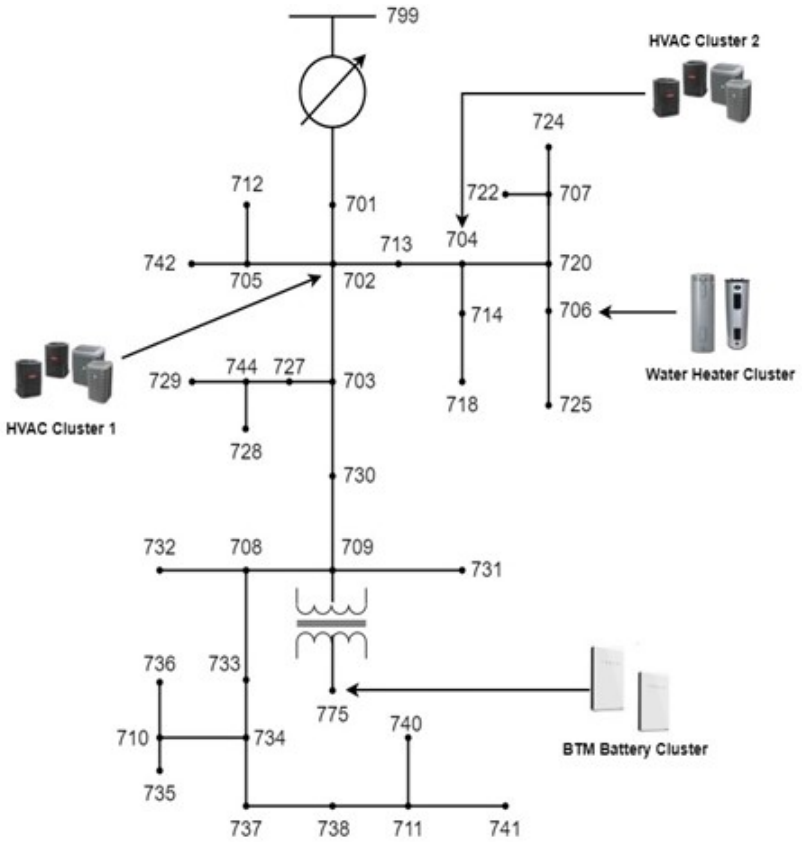

Figure 3.4: Test system

Using the unit cost of a Tesla Powerwall, the total cost of the batteries is $277,500 [25]. This shows that if the BTM battery owners use their batteries only for arbitrage, the cost price would have been recouped after four years which is much lesser than the 10-year warranty expiration period of the Powerwall [25]. For this scenario, energy arbitrage is a viable service from the perspective of the BTM battery owners.

3.5.3 Day-Ahead Model Results

Due to the high time resolution of the regulation signals (6 seconds) and the multiple scenarios considered, the model was solved in 9008.3 seconds (i.e., 2.5 hours). From the results, the LSE's expected profit is $9,146.10 which is 4.4% higher than the expected profits without any of the additional value streams (i.e., $8,744). Furthermore, the LSE's expected net demand profile is as shown in Fig. 3.6(a), while the baseline profile provided to the market operator, $P_{baseline,t}$, is shown in Fig. 3.6(b).

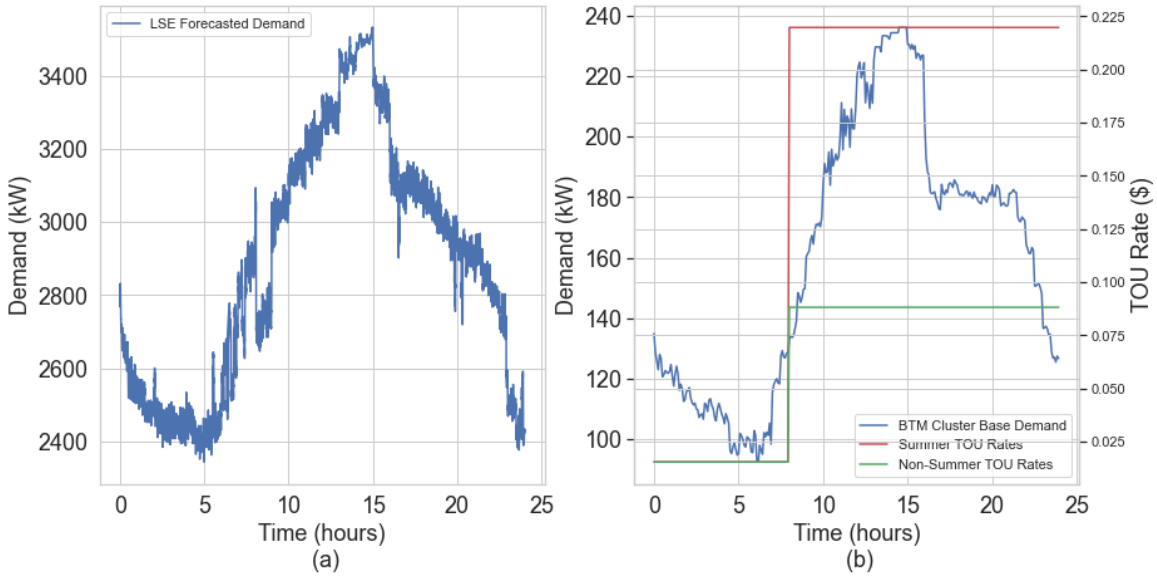

Figure 3.5: (a) LSE's total forecasted demand profile (b) TOU rates

The expected net demand profile reflects the effect of the anticipated response of the customer-side resources to the fast regulation signals and the peak demand limit. Also, the demand variations seem to be more pronounced during the late hours of the day (i.e., from 4pm to 11pm). During this period, the customer-side resources had a relatively higher base power consumption when compared with the early hours of the day. Also, the peak demand constraints were not active during this period. A combination of these factors implies increased flexibility which is demonstrated by the resultant increase in regulation capacity bids as shown in Fig. 3.7. This increased regulation capacity explains why more variations are noticed in the LSE's expected base demand during this period. Furthermore, the reduction in the expected regulation capacity during the peak demand period is chiefly because the same set of resources are being used to satisfy the peak demand constraints. As such, the capacity available for regulation is expected to reduce. For the early hours of the day, the lower regulation capacity bids is tied to lower base consumption of the resources.

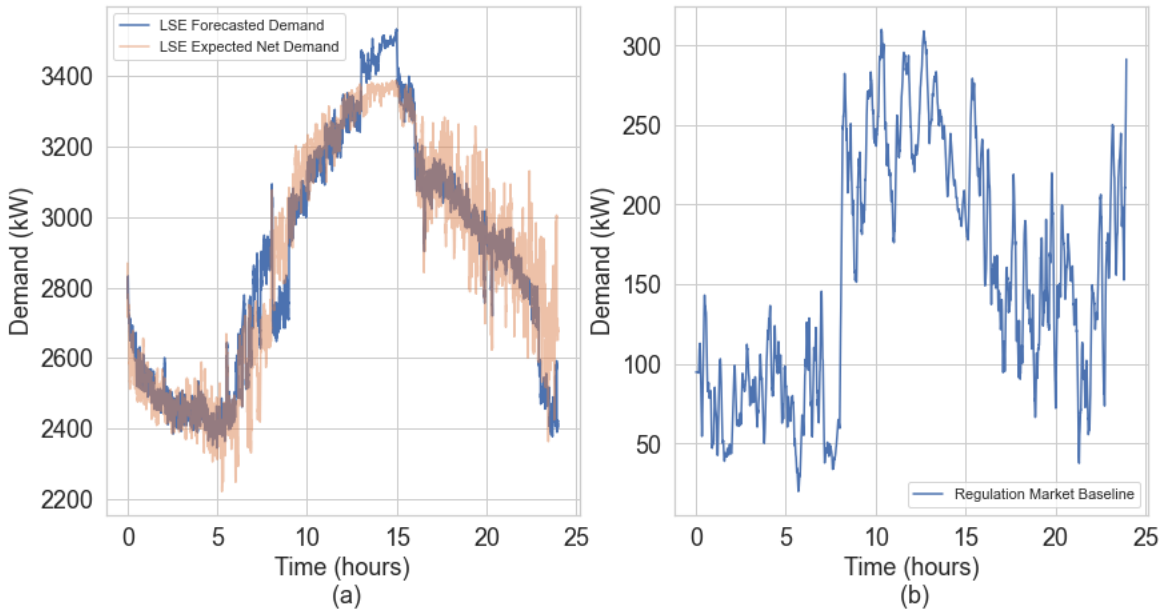

Figure 3.6: (a) LSE's expected net demand (b) Regulation market baseline

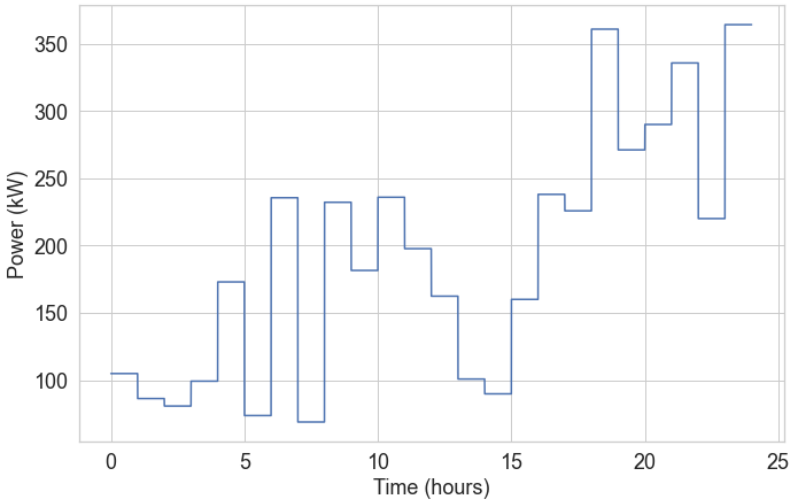

Figure 3.7: Expected regulation capacity bids

3.5.4 Real-Time Dispatch Results

The two dispatch algorithms discussed in Section IV are evaluated both qualitatively and quantitatively using three metrics - regulation performance score, voltage limit violations and computation time. Other performance measures relating to the thermal comfort limits are under the purview of the TPL-based algorithms used at the primary control level. As such, we do not focus on these metrics. Moreover, the

thermal comfort and SOC limits were all satisfied by the TPL-based algorithms at the primary control level. The regulation performance score is calculated using metrics defined in NYISO's accounting and billing manual [25]. The interested reader can refer to [25] for detailed discussions on the regulation performance metric. The computation time is taken as the average value of the execution times for each run of both algorithms. The hourly regulation performance scores for both the dynamic droop and MPC-based dispatch algorithms are shown in Fig. 3.8. Clearly the MPC-based algorithm outperforms the dynamic droop-based algorithm with respect to the regulation performance metric as shown in Fig. 3.8. This is because the MPC-based algorithm includes the aggregate models which represent the dynamics of the resources. Also, the dynamic droop-based algorithm constrains the power consumption of the resources with the expected schedule obtained from the day-ahead model to avoid voltage violations thereby making the algorithm conservative.

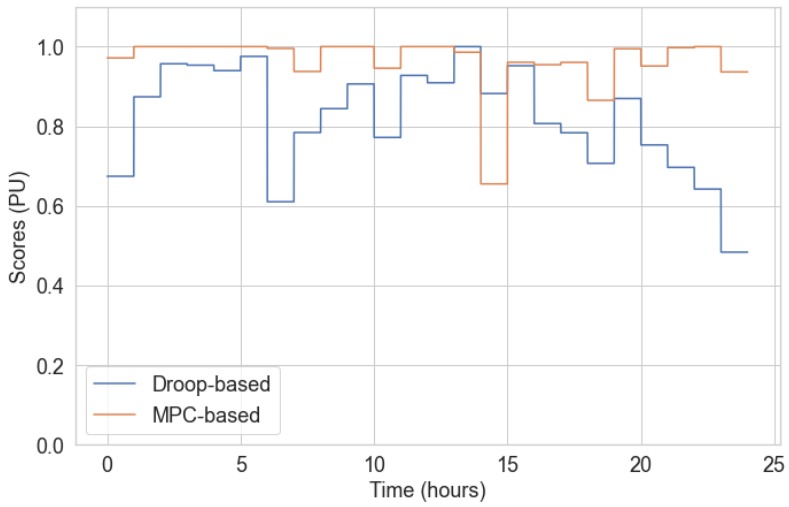

Figure 3.8: Regulation performance scores

For the voltages, the major violations were observed at phase B of bus 775 which is where the BTM batteries are connected. Subsequently, we refer to this node as the 'impact node'. In addition, phase B of the system is heavily loaded resulting in increased susceptibility of the voltages at the impact node to voltage violations. The base voltages (i.e., voltage without additional value streams) and the voltages under

MPC-based and dynamic droop-based dispatch at the impact node are shown in Fig. 3.9. It should be noted that the lower voltage limit was set at 0.94 pu because the base voltage at the impact node was already close to 0.94 pu.

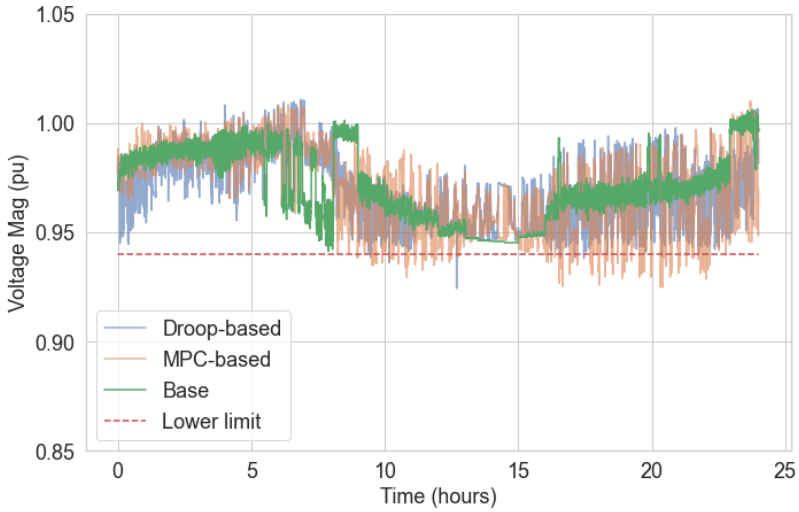

Figure 3.9: Voltages at impact node - bus 775.

With respect to voltage violations, the dynamic droop-based algorithm outperforms the MPC-based algorithm because the dynamic droop-based algorithm produces lesser voltage violations. This is because, although the dynamic droop-based algorithm does not explicitly capture the dynamics of the resources, it acts based on the worst case voltages measured in the previous time steps as shown in (3.15a) and (3.15b). However, the MPC-based algorithm, in its current form, is susceptible to model errors and errors in the voltage sensitivity matrix which forms the basis for the voltage constraints. Moreover, each voltage violation event in both cases is short-lived and may not cause significant problems in the system.

For the computation time, each run of the MPC-based algorithm solves in 4 seconds on average while each run of the dynamic droop-based algorithm solves in 0.1 seconds. The computation times are based on simulations performed on a Dell Optiplex 980 computer with 8 GB RAM and an Intel Core I7 processor with 2.80 GHz processing speed. Given that the regulation signals are received in 6-second intervals, the slower computation time of the MPC-based algorithm might be of concern. However, using

a much faster computer could alleviate these concerns at additional costs.

3.6 Conclusion

A stochastic framework for realizing combined value streams from different customer-side resources, including residential HVACs, EWHs and BTM batteries, has been rigorously discussed. Both day-ahead scheduling models and real-time dispatch algorithms were considered in the framework. Not only does our day-ahead model capture different value streams, it also includes stochasticities relating to energy and regulation market prices and regulation signals. Furthermore, we considered a dynamic droop-based and an MPC-based real-time dispatch algorithm. Our simulations show that combining multiple value streams is profitable for the LSE. However, the choice of real-time algorithms for dispatching the resources is also very important. Our simulations show that a droop-based dispatch algorithm will generally have shorter execution times when compared with an MPC-based dispatch algorithm at the expense of response accuracy and optimality. As such, the LSE might want to consider a trade-off between execution speed and performance accuracy of its dispatch algorithms depending on its exact system characteristics and operating market environment. In any case, our models and algorithms can be adapted to suit the exact system and market requirements.

REFERENCES

[1] New York State, "Reforming the energy vision REV," 2021. Available: https://www.ny.gov/sites/ny.gov/files/atoms/files/WhitePaperREVMarch2016.pdf, Accessed on: Feb. 3, 2021.

[2] Federal Energy Regulatory Commission, "FERC Order No. 2222: Fact Sheet," 2020. Available: https://www.ferc.gov/media/ferc-order-no-2222-fact-sheet.

[3] A. Abbas and B. Chowdhury, "Using customer-side resources for market-based transmission and distribution level grid services - a review," *International Journal of Electrical Power Energy Systems*, vol. 125, p. 106480, 2021. doi: https://doi.org/10.1016/j.ijepes.2020.106480.

[4] E. Vrettos and G. Andersson, "Combined load frequency control and active distribution network management with thermostatically controlled loads," in *2013 IEEE International Conference on Smart Grid Communications (SmartGridComm)*, pp. 247–252, 2013. doi: 10.1109/SmartGridComm.2013.6687965.

[5] O. Megel, J.L Mathieu, and G. Andersson, "Scheduling distributed energy storage units to provide multiple services," in *2014 Power Systems Computation Conference*, pp. 1–7, 2014. doi: 10.1109/PSCC.2014.7038358.

[6] C. D. White and K. M. Zhang, "Using vehicle-to-grid technology for frequency regulation and peak-load reduction," *Journal of Power Sources*, vol. 196, no. 8, pp. 3972–3980, 2011. doi: https://doi.org/10.1016/j.jpowsour.2010.11.010.

[7] H. Hao, D. Wu, J. Lian, and T. Yang, "Optimal coordination of building loads and energy storage for power grid and end user services," *IEEE Transactions on Smart Grid*, vol. 9, no. 5, pp. 4335–4345, 2018. doi:10.1109/TSG.2017.2655083.

[8] A. Abbas and B. Chowdhury, "Realizing combined value streams from utility-operated demand response resources," in *2020 52nd North American Power Symposium (NAPS)*, pp. 1–6, 2021. doi: 10.1109/NAPS50074.2021.9449749.

[9] N. Lu, "An evaluation of the hvac load potential for providing load balancing service," *IEEE Transactions on Smart Grid*, vol. 3, no. 3, pp. 1263–1270, 2012. doi: 10.1109/TSG.2012.2183649.

[10] M. A. Z. Alvarez, K. Agbossou, A. Cardenas, S. Kelouwani, and L. Boulon, "Demand response strategy applied to residential electric water heaters using dynamic programming and k-means clustering," *IEEE Transactions on Sustainable Energy*, vol. 11, no. 1, pp. 524–533, 2020. doi: 10.1109/TSTE.2019.2897288.

[11] R. Juhl, J. K. Moller, and H. Madsen, "CTSMR - Continuous time stochastic modeling in R," 2016. doi: arXiv:1606.00242.

[12] M. Liu, S. Peeters, D. S. Callaway and B. J. Claessens, "Trajectory tracking with an aggregation of domestic hot water heaters: Combining model-based and model-free control in a commercial deployment," *IEEE Transactions on Smart Grid*, vol. 10, no. 5, pp. 5686–5695, 2019. doi: 10.1109/TSG.2018.2890275.

[13] D. M. Rosewater, D. A. Copp, T. A. Nguyen, R. H. Byrne and S. Santoso, "Battery energy storage models for optimal control," *IEEE Access*, vol. 7, pp. 178357–178391, 2019. doi: 10.1109/ACCESS.2019.2957698.

[14] New York Independent System Operator, "Energy Market and Operational Data," 2020. Available: https://www.nyiso.com/energy-market-operational-data.

[15] Y. Shi, B. Xu, D. Wang, and B. Zhang, "Using battery storage for peak shaving and frequency regulation: Joint optimization for superlinear gains," *IEEE Transactions on Power Systems*, vol. 33, no. 3, pp. 2882–2894, 2018. doi: 10.1109/TPWRS.2017.2749512.

[16] A. Abbas and B. Chowdhury, "Comparison between flexible loads and grid-scale battery energy storage for value-added services," in *2021 IEEE Power Energy Society Innovative Smart Grid Technologies Conference (ISGT)*, pp. 1–5, 2021. doi: 10.1109/ISGT49243.2021.9372236.

[17] A. Ali, J. Z. Kolter, S. Diamond, and S. Boyd, "Disciplined convex stochastic programming: A new framework for stochastic optimization," in *Proc. 31st Conf. Uncertainty Artif. Intell.*, pp. 62–71, 2015.

[18] N. Growe-Kuska, H. Heitsch, and W. Romisch, "Scenario reduction and scenario tree construction for power management problems," in *2003 IEEE Bologna Power Tech Conference*, vol. 3, pp. 1–7, 2003. doi: 10.1109/ISGT49243.2021.9372236.

[19] A. J. Conejo, M. Carrion, and J. M. Morales, "Uncertainty characterization via scenarios," in *Decision Making Under Uncertainty in Electricity Markets*, pp. 157–194, Springer, 2010.

[20] W. H. Kersting, "Radial distribution test feeders," in *2001 IEEE Power Eng. Soc. Winter Meeting Columbus*, pp. 908–912, 2001.

[21] PJM, "PJM historical regulation market data," 2019. Available: http://www.pjm.com/markets-and-operations/ancillary-services.aspx.

[22] B. Palmintier, D. Krishnamurthy, P. Top, Philip, S. Smith, J. Daily, and J. Fuller, "Design of the HELICS high-performance transmission-distribution-communication-market co-simulation framework," in *2017 Workshop on Modeling and Simulation of Cyber-Physical Energy Systems (MSCPES)*, pp. 1–6, 2017. doi: 10.1109/MSCPES.2017.8064542.

[23] M. Grant and S. Boyd, "CVX: Matlab software for Disciplined Convex Programming," 2013.

[24] Consolidated Edision, "Time-of-Use rates." Available: https://www.coned.com/en/accounts-billing/your-bill/time-of-use-o, Accessed on: March 27,2021.

[25] New York Independent System Operator, "Manual 14: Accounting and billing manual," 2020. Available: https://www.nyiso.com/documents/20142/2923231/acctbillmnl.pdf/, Accessed on: April 26, 2021.

CHAPTER 4: STOCHASTIC OPTIMIZATION FRAMEWORK FOR REALIZING COMBINED VALUE STREAMS FROM CUSTOMER-SIDE RESOURCES - SELF SERVICE AND DISTRIBUTION SYSTEM OPERATIONS

Customer-side resources are becoming increasingly crucial in grid modernization and transitioning to a sustainable energy future. Although most load-serving entities (LSEs) typically consider customer-side resources for single applications, these resources can be used for multiple applications simultaneously. This chapter proposes a stochastic optimization framework to help LSEs capture multiple value streams from customer-side resources within their network. Specifically, we consider self-service applications - peak shaving, energy arbitrage, ramp rate reduction - and distribution system operational applications - loss reduction and voltage management. The framework is also adapted to handle the impacts of the activities of third-party aggregators on the LSE's network. We also evaluate the performance of two algorithms - decision rule-based and optimal real-time dispatch - for dispatching the customer-side resources in the face of different sources and levels of uncertainty. Simulations were run using modified IEEE test systems within the OpenDSS simulation tool. The results show the value of customer-side resources can be maximized when multiple applications are simultaneously considered, and that value increases with increasing levels of forecast uncertainties.

Nomenclature

Parameters

α_b	Battery self discharge rate
$\Delta P_{agg,i,t}$	Aggregator expected impact at node i at time t
Δt	Time step
ΔV	Voltage step
$\eta_{ch,b}$	Battery charging efficiency
η_{COP}	HVAC system co-efficient of performance
$\eta_{dis,b}$	Battery discharging efficiency
$\lambda_{capacitor}$	Capacitor switching price
λ_{cap}	Capacity price
$\lambda_{ramp,t}$	Price of additional reserve capacity for handling ramping concerns
$\lambda_{reactive,t}$	Reactive power price at time t
$\lambda_{real,t}$	Real power price at time t
λ_{reg}	Regulator switching price
A	Aggregated water heater total surface area
$E_{b,max}$	Maximum battery SOC
$E_{b,min}$	Minimum battery SOC
$I^2_{ij,min}, I^2_{ij,max}$	Line flow current rating
m	Total mass of water in water heater

$P_{abs,min}, P_{abs,max}$ Ramp rate limits

$P_{ch,b,max}$ Maximum battery charging rate

$P_{dis,b,max}$ Maximum battery discharging rate

$P_{der,base,t}$ Predicted DER output for time t

$P_{h,max}$ HVAC cluster power rating

$P_{L,i,t}$ Uncontrolled active power load at node i at time t

$P_{recons,base,t}$ LSE's predicted reconstituted load profile

$P_{substation}$ Substation active power limit

$P_{w,max}$ Water heater cluster power rating

$Q_{c,t}$ Capacitor reactive power

$Q_{L,i,t}$ Uncontrolled reactive power load at node i at time t

$Q_{substation}$ Substation reactive power limit

R_e Aggregated water heater thermal resistance

R_h HVAC thermal resistance

r_{ki} Line resistance between nodes k and i

$S_{der,max}$ DER apparent power rating

$S_{ij,max}$ Maximum line flow limit

$SOC_{w,min}, SOC_{w,max}$ Water heater cluster SOC limits

T_a Ambient temperature

$T_{i,h,min/max}$ Interior temperature limits

$T_{w,max}$	Maximum hot water temperature for water heater cluster
V_{min}^2, V_{max}^2	Voltage variable limits
x_{ki}	Line reactance between nodes k and i
$z_{1,t}$	Uncertainty associated with LSE's total demand (i.e. reconstituted load profile)
$z_{2,t}$	Uncertainty associated with LSE's DER at time t
$z_{agg,t}$	Uncertainty associated with LSE's prediction of aggregator's impact

Variables

$Cap_{c,t}$	Capacitor status at time t
$ch_{ind,t}$	Battery charging indicator at time t
$dis_{ind,t}$	Battery discharging indicator at time t
$E_{b,t}$	Battery SOC at time t
e_t	Slack variable
$I_{ki,t}$	Line current flow between nodes k and i
$P_{b,t}$	Battery power at time t
$P_{b0,t}, P_{b1,t}, P_{b2,t}, P_{b3,t}$	Battery cluster decision rule parameters for time t
$P_{bought,bid,t}$	Day-ahead active power bids at time t
$P_{bought,rt,t}$	Real time total power at time t
$P_{bought,t}$	Power consumption at substation
$P_{ch,b,t}$	Battery charging rate at time t

$P_{der,control,t}$ DER output control variable at time t

$P_{der,control0,t}, P_{der,control1,t}$ DER control decision rule parameters for time t

$P_{der,control2,t}, P_{der,control3,t}$ DER control decision rule parameters for time t

$P_{dis,b,t}$ Battery discharging rate at time t

$P_{h,t}$ HVAC cluster consumption at time t

$P_{h0,t}, P_{h1,t}, P_{h2,t}, P_{h3,t}$ HVAC cluster decision rule parameters for time t

$P_{ki,t}$ Active power flow between nodes k and i at time t

$P_{loss,t}$ Active power losses at time t

($P_{recons,rt,t}$ LSE's real-time reconstituted load profile

$P_{sol,t}$ Solar irradiation at time t

$P_{w,t}$ Total power consumption for water heater cluster at time t

$P_{w0,t}, P_{w1,t}, P_{w2,t}, P_{w3,t}$ Water heater cluster decision rule parameters for time t

$Q_{b,t}$ Battery reactive power

$Q_{h,t}$ HVAC cluster reactive at time t

$Q_{loss,t}$ Reactive power losses at time t

$Reg_{r,t}$ Regulator status at time t

S_b Battery inverter total apparent power rating

$SOC_{w,t}$ State of charge variable for water heater cluster at time t

$T_{i,h,t}$ Interior temperature for HVAC h at time t

$T_{w,avg}$ Average hot water temperature for water heater cluster

$V^2_{i,t}$ Voltage squared variable at node i at time t

$V_{sub,t}$ Substation squared voltage at time t

4.1 Introduction

4.1.1 Background and Motivation

The demand-side of the grid, which has been mostly passive, is becoming increasingly active. Furthermore, it is becoming more apparent that customer-side resources will play critical roles in grid modernization as well as a transition to a clean energy future. As expected, more policies, such as the FERC Order 2222, are being established to capture the full value of these customer-side resources [1]. However, most load-serving entities (LSEs) with direct access to these resources are still underutilizing these resources. LSEs typically use customer-side resources for single applications (mostly peak shaving) when multiple value streams can be simultaneously captured from the same set of resources. LSEs in this work refer to distribution utilities that provide electricity to end-users and operate the electricity distribution network.

In our previous work [2], we proposed a scenario-based stochastic optimization framework for LSEs to use customer-side resources on their network for combined self-service applications - peak shaving and energy arbitrage - and a transmission grid supporting application - frequency regulation. The resources of interest include clusters of residential heating, ventilation, and air-conditioning (HVAC) systems, water heaters, and behind-the-meter (BTM) batteries. This work introduces a new perspective to our previous work. Specifically, an additional self-service application - ramp rate reduction - is introduced, and the focus on transmission grid supporting applications is shifted to distribution system operational services. Loss reduction and voltage management are the distribution system operational applications of interest.

Peak shaving and energy arbitrage are well-established, high-savings applications that require no introduction. References [3–10] present different flavors of peak shav-

ing and energy arbitrage. Ramp rate reduction, however, can be considered nascent. This application is tied explicitly to increasing net-load variations, which is a consequence of the increasing penetration of intermittent renewable energy resources on the bulk power system. Authors in [11] studied an energy scheduling problem for prosumers, focusing on minimizing the system's overall peak ramp rate. Also, the authors in [12] developed an incentive mechanism based on Nash Bargaining to encourage the usage of microgrids for minimizing system ramp rates. Ramping concerns are motivating the creation of new flexibility products across deregulated electricity market environments in the United States. For example, the California Independent System Operator (CAISO) operates flexible ramping products designed to handle net-load variations in the form of both forecasted ramping movements and uncertainty movements [13]. These new products introduce additional system operating costs passed on to the market participants, i.e., LSEs. Therefore, a reduction in the ramp rate of each LSE's overall net-load profile will reduce such additional costs. Other deregulated electricity markets in the United States, such as the Midwest Independent System Operator (MISO), the Southwest Power Pool (SPP), and the New York Independent System Operator (NYISO), have similar market mechanisms or products to address ramping issues [14]. As distributed energy resources (DERs) penetration increases, the ramp rate reduction will become even more critical.

From the distribution system operations perspective, loss reduction and voltage management are two of the most important applications that could yield significant cost savings for LSEs [15]. In [16], the authors considered an optimal power scheduling framework to reduce losses and keep system voltages within limits using controllable loads. Although the controllable loads were not explicitly modeled and uncertainties were ignored, the paper showed an additional loss reduction of 1.08% with the controllable loads. In [17], the authors considered using customer-side resources for peak load reduction and loss minimization. The controllable loads are represented using neural

network-based models, which are embedded in recursively-solved optimal power flow problems. However, uncertainties were also not considered. Reference [18] proposes a multi-objective stochastic optimization problem that minimizes system losses and deviation of system voltages from nominal values by controlling the reactive power outputs of distributed photovoltaic generators. This framework captures uncertainties in the active power generation of the distributed solar PV resources and provides local control rules for each distributed PV inverter using linear decision rules. The latter provide a decentralized way of controlling the distributed solar PV inverters, which could become useful, especially when communication with a central controller is lost. The problem is reformulated to obtain the decision rules as an affinely adjustable robust optimization problem. This work considers uncertainties relating to load profiles and the outputs of solar PV resources operated by an LSE. However, the uncertainties are handled using a fusion of scenarios and affine decision rules. This approach allows us to take advantage of the decentralized and straightforward nature of the decision rules while avoiding excessive conservativeness in the results that typically accompanies robust optimization methods [19].

While an existing LSE can take advantage of the customer-side resources on its network for multiple applications, new policies are supporting the rise of aggregators who can also use customer-side resources on the LSE's network to provide services in deregulated markets environments. In such situations, the LSE's distribution system operations will have to consider the actions of the aggregator. This perspective is also considered in this work.

4.1.2 Contributions

In summary, the main contributions of this work are highlighted as follows.

1. We propose a novel stochastic optimization framework to help LSEs with solar PV resources and access to groups of residential HVACs, water heaters, and BTM batteries use these resources for combined self-service and distribu-

tion system operation applications simultaneously. The applications include peak shaving, energy arbitrage, ramp rate reduction, loss reduction, and voltage management. Also, the main sources of uncertainty are the solar PV output variations and variations in forecasted total load. The total load refers to the LSE's reconstituted load profile, which is the actual load at the substation level, excluding impacts of DERs and demand response. To the best of our knowledge, no other work captures such holistic perspectives.

2. The framework is extended to capture the presence of third-party aggregators using other customer-side resources on the LSE's network for market-based services. This contribution is significant given the rise of policies supporting the co-existence of third-party aggregators and LSEs with resources within the same power distribution network (e.g., FERC Order 2222).

3. Two algorithms based on linear decision rules and optimal real-time dispatch are proposed to dispatch the LSE's customer-side resources. A comparison of both algorithms in terms of computation time, accuracy, losses, and voltage limit violations using simulations in OpenDSS is also presented.

4. We also show that not only is it advantageous to use customer-side resources for multiple applications instead of single applications, but the expected value of customer-side resources also increases with an increasing level of uncertainty in forecasts.

4.2 Framework Description

Fig. 4.1 illustrates the overall framework. The flowchart on the left represents scenarios without the presence of a third-party aggregator on the LSE's distribution network. Under this scenario, the LSE solves a day-ahead stochastic optimization problem. The solutions to the optimization problem determine the LSE's demand bids for the day-ahead market participation. Based on the optimization problem results,

the LSE also generates rules to dispatch the customer-side resources in response to current system conditions and uncertainty realizations. Using such predefined rules for dispatching customer-side resources could be attractive compared to real-time optimization methods due to computational complexities arising from solving such large-scale optimization problems in real-time. A more detailed comparison between both dispatch methods is presented in the results section.

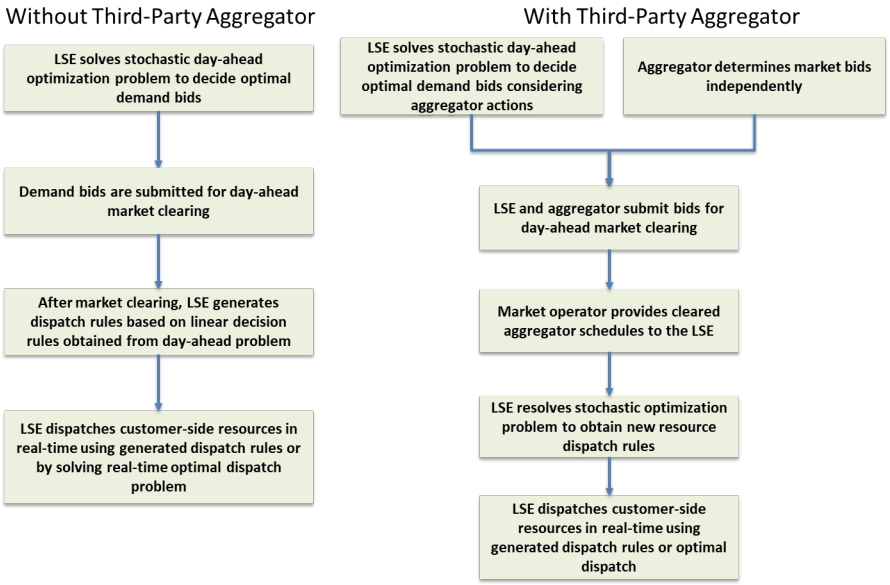

Figure 4.1: Overall framework illustration

On the other hand, when a third-party aggregator is present, the LSE solves the day-ahead optimization problem considering the aggregator's possible dispatch schedule as shown on the right of Fig. 4.1. The LSE can predict such schedules based on historical data and quantify uncertainties associated with such predictions. After market clearing, the market operator provides the cleared aggregator bids to the LSE. This information sharing is essential because the aggregator's dispatch profile will affect how the LSE operates its distribution network. In fact, such information-sharing considerations are captured in filings of major market operators in response to the recent FERC order 2222 [20]. Also, since the information sharing happens after market clearing, both entities can co-exist comfortably. After receiving the cleared aggre-

gator schedule from the market operator, the LSE repeatedly solves the rules-based optimization problem with the actual aggregator schedule to update its dispatch rules for the customer-side resources. The details of the stochastic optimization model are discussed subsequently.

4.3 Resource Modeling

This section presents the modeling approaches adopted for the customer-side resources.

4.3.1 Residential HVAC Aggregation Model

Residential HVAC units are often modeled using first-order or second-order equivalent thermal parameter (ETP) models with binary variables capturing the on/off status of the units [21]. However, when considering a large number of single units within a high-resolution multi-period optimization problem, it becomes clear that such an approach can quickly become intractable. As such, we adopt a first-order ETP equivalent model approximating the aggregated dynamics of a cluster of single units. This aggregated model captures the total power consumption of the HVAC units and the average temperature dynamics for all the HVAC units within the cluster. It is worth mentioning that clusters are assumed to be formed at nodes of the primary distribution network. However, multiple sub-clusters can be created for nodes with a significant number of units with varying characteristics. Popular clustering algorithms such as the k-means and Gaussian Mixture Model (GMM) can be applied to achieve such clustering [22].

The first-order aggregate model equation is shown in (4.1). The R and C parameters are obtained via a system identification procedure based on Pseudo-Random Binary Sequence (PRBS) signals. Specifically, the HVAC units within each cluster are perturbed with the same setpoint offsets, and the total power consumption of the units and the average temperature across the cluster are measured. The CTSM software, based on maximum likelihood estimation and Kalman filters, is then applied to

obtain the respective R and C values [23]. η_{COP} is taken as the average of the COP values for each unit within the cluster.

$$T_{i,h,t+1} = T_{i,h,t}\left(1 - \frac{\Delta t}{R_h C_h}\right) + T_{a,t}\left(\frac{\Delta t}{R_h C_h}\right) - \eta_{\mathrm{COP},h} P_{h,t}\left(\frac{\Delta t}{C_h}\right) + P_{\mathrm{sol},\,,}\left(\frac{\Delta t}{C_h}\right) \tag{4.1}$$

4.3.2 Residential Water Heater Aggregation Model

As with the residential HVACs, an aggregate model is also adopted for the residential water heaters. This model is also based on a first-order ETP model (also known as a single-node model), which has been widely used in the existing literature [24]. The model equations are shown in (4.2a) to (4.2e). The interested reader is referred to [24] and our previous work [25] for more details about the model. The water heaters are assumed to be electric.

$$SOC_W = \frac{T_{w_{avg}}}{T_{w_{\max}}} \tag{4.2a}$$

$$SOC_{w,t+1} = a_{w,t} SOC_{w,t} + \frac{(b_t P_{w,t} + e_{w,t})}{T_{w\,\max}} \tag{4.2b}$$

$$a_{w,t} = \exp\left(-\frac{\Delta t}{R_w C_w}\right), b_t = R_w\left(1 - a_{w,t}\right) \tag{4.2c}$$

$$e_{w,t} = \left(G R_w T_a + B R_W T_{cw}\right)\left(1 - a_{w,t}\right) \tag{4.2d}$$

$$R_w = \frac{1}{G + B}, B = \rho W_t c, G = \frac{A}{R_e}, C_w = mc \tag{4.2e}$$

4.3.3 BTM Battery Aggregation Model

For the batteries, the well-established energy reservoir model is adopted, as shown in (4.3a) - (4.3g) [26]. The self-discharging, charging, and discharging rates are taken as weighted averages of the batteries within the cluster.

$$E_{b,t+1} = \alpha_b E_{b,t} + \eta_{ch,b} P_{ch,b,t} - \frac{1}{\eta_{dis,b}} P_{\mathrm{dis,\ b,t}} \tag{4.3a}$$

$$P_{b,t} = \eta_{ch,b} P_{ch,b,t} - \frac{1}{\eta_{dis,b}} P_{dis,b,t} \tag{4.3b}$$

$$E_{b,\min} \leq E_{b,t} \leq E_{b,\max} \tag{4.3c}$$

$$0 \leq P_{ch,b,t} \leq P_{ch,b,\max} \tag{4.3d}$$

$$0 \leq P_{dis,b,t} \leq P_{\text{dis,b, max}} \tag{4.3e}$$

$$P_{b,t}^2 + Q_{b,t}^2 \leq S_b^2 \tag{4.3f}$$

$$ch_{ind,t} + dis_{ind,t} \leq 1 \tag{4.3g}$$

4.4 Stochastic Optimization Model

As discussed earlier, the LSE uses the customer-side resources for peak shaving, energy arbitrage, ramp rate reduction, loss reduction, and voltage management. It is assumed that the LSE participates in a competitive market environment. The LSE can forecast its overall day-ahead demand and generation from its solar PV resources along with the limits of uncertainties for both parameters. In scenarios with third-party aggregators, the LSE can also predict resource dispatch schedules and associated uncertainty limits from historical data. On a day-ahead basis, the expected base consumption for each HVAC and water heater aggregation can be predicted with acceptable accuracy levels. The availability of high-resolution historical consumption data through increasingly reliable and cost-effective advanced metering infrastructure validates these assumptions. Furthermore, the day-ahead aggregated demand profile for each cluster of buildings providing BTM batteries can also be forecasted. This section discusses the LSE's day-ahead scheduling problem based on these assumptions.

The solutions to the LSE's optimization problem provides day-ahead market bidding and real-time dispatch decisions. $P_{bought,t}$ and $Q_{bought,t}$ are the variables of interest for the day-ahead bids while $P_{der,control,t}$, $P_{h,t}$, $P_{b,t}$, $P_{w,t}$, $Q_{b,t}$, $Q_{der,t}$, $Reg_{r,t}$ and $Cap_{c,t}$ are the variables of interest for real-time operation.

Problem (4.4) shows a deterministic version of the LSE's optimization problem.

Problem (4.4) is solved for multiple scenarios of uncertainties $z_{1,t}$ and $z_{2,t}$. The day-ahead demand bids are then taken as the corresponding average values for each timestep across all scenarios.

$$\text{minimize } Y_{DA}$$

$$Y_{DA} = \lambda_{\text{cap}} \ \max\left(P_{\text{bought},t}\right) + \sum_{t=1}^{T} \lambda_{\text{real},t} P_{\text{bought},t} +$$

$$\sum_{t=1}^{T} \lambda_{\text{reactive},} Q_{\text{bought},t} + \sum_{t=1}^{T} \lambda_{\text{real},t} P_{\text{loss},t} + \sum_{t=1}^{T} \lambda_{\text{reactive},t} Q_{\text{loss},t}$$

$$+ \sum_{t=1}^{T} \lambda_{\text{ramp,t}} P_{abs,t} + \sum_{c=1}^{C} \sum_{t=1}^{T} \lambda_{\text{capacitor}} X_{c,t} + \sum_{r=1}^{R} \sum_{t=1}^{T} \lambda_{reg} X_{r,t} \tag{4.4a}$$

Subject to:

$$(1), \forall h \in H \tag{4.4b}$$

$$(2), \forall w \in W \tag{4.4c}$$

$$(3) \ , \forall b \in B \tag{4.4d}$$

$$P_{\text{der},t} = P_{\text{der,base},t} - P_{\text{der, control},t} \tag{4.4e}$$

$$P_{\text{der},t}^2 + Q_{\text{der},t}^2 \leq S_{\text{der,max}}^2 \tag{4.4f}$$

$$0 \leq P_{\text{der,control},t} \leq P_{\text{der,base},t} \tag{4.4g}$$

$$P_{\text{loss}} = \sum_{t} \sum_{i} \sum_{j} I_{ij,t}^2 r_{ij} \tag{4.4h}$$

$$Q_{\text{loss}} = \sum_{t} \sum_{i} \sum_{j} I_{ij,t}^2 x_{ij} \tag{4.4i}$$

$$P_{h,t} = P_{h0,t} + P_{h1,t} z_{1,t} + P_{h2,t} z_{2,t} + P_{h3,t} z_{1,t} z_{2,t}$$

$$\forall h \in H \tag{4.4j}$$

$$P_{w,t} = P_{w0,t} + P_{w1,t} z_{1,t} + P_{w2,t} z_{2,t} + P_{w3,t} z_{1,t} z_{2,t}$$

$$\forall w \in W \tag{4.4k}$$

$$P_{b,t} = P_{b0,t} + P_{b1,t} z_{1,t} + P_{b2,t} z_{2,t} + P_{b3,t} z_{1,t} z_{2,t}$$

$$\forall b \in B \tag{4.4l}$$

$$P_{\text{der,control}} = P_{\text{der,control0},t} + P_{\text{der,control1},t} z_{1,t} +$$

$$P_{\text{der,control2},t} z_{2,t} + P_{\text{der,control3},t} z_{1,t} z_{2,t} \tag{4.4m}$$

$$\sum_{k \in pr(i)} \left(P_{ki,t} - r_{ki} I_{ki,t}^2\right) - \sum_{j \in cr(i)} P_{ij,t} = P_{L,i,t} + P_{h,i,t}$$

$$+P_{w,i,t} + P_{b,i,t} + \Delta P_{agg,i,t} - P_{der,i,t} \quad \forall b, h, w \in i, \forall i \in N \tag{4.4n}$$

$$\sum_{k \in \text{pr}(i)} \left(Q_{ki,t} - x_{ki} I_{ki,t}^2\right) - \sum_{j \in cr(i)} Q_{ij,t} = Q_{L,i,t} + Q_{h,i,t}$$

$$+Q_{b,i,t} + \text{Cap}_{c,t} \times Q_{c,t} - Q_{\text{der,i,t}} \quad \forall b, h, c \in i, \forall i \in N \tag{4.4o}$$

$$V_{i,t}^2 - V_{j,t}^2 - 2\left(r_{ij} P_{ij,t} + x_{ij} Q_{ij,t}\right) + \left(r_{ij}^2 + x_{ij}^2\right) I_{ij,t}^2 = 0$$

$$\forall j \in \text{cr}(i) \tag{4.4p}$$

$$P_{ij,t}^2 + Q_{ij,t}^2 \leq S_{ij,\max}^2 \tag{4.4q}$$

$$P_{\text{bought},t}^2 + Q_{\text{bought},t}^2 \leq S_{\text{substation}}^2 \tag{4.4r}$$

$$\left\| \begin{array}{c} 2P_{ij,t} \\ 2Q_{ij,t} \\ I_{ij,t}^2 - V_{i,t}^2 \end{array} \right\|_2 \leq I_{ij,t}^2 + V_{i,t}^2 \tag{4.4s}$$

$$V_{sub,t} = 1 + \Delta V \times Reg_{r,t} \tag{4.4t}$$

$$P_{\text{bought},t+1} - P_{\text{bought},t} \leq P_{\text{abs, }t} \forall t \in T \tag{4.4u}$$

$$P_{\text{bought},t+1} - P_{\text{bought},t} \geq -P_{\text{abs},t} \forall t \in T \tag{4.4v}$$

$$P_{abs,\min} \leq P_{abs,t} \leq P_{abs,\max} \quad \forall t \in T \tag{4.4w}$$

$$\text{Reg}_{r,t+1} - \text{Reg}_{r,t} \leq X_{r,t} \quad \forall r \in R \tag{4.4x}$$

$$\text{Reg}_{r,t+1} - \text{Reg}_{r,t} \geq -X_{r,t} \quad \forall r \in R \tag{4.4y}$$

$$X_{r,\min} \leq X_{r,t} \leq X_{r,\max} \quad \forall r \in R \tag{4.4z}$$

$$\text{Cap}_{c,t+1} - \text{Cap}_{c,t} \leq X_{c,t} \quad \forall r \in R \tag{4.4aa}$$

$$\text{Cap}_{c,t+1} - \text{Cap}_{c,t} \geq -X_{c,t} \quad \forall r \in R \tag{4.4ab}$$

$$\mathrm{X}_{c,\min} \leq \mathrm{X}_{c,t} \leq \mathrm{X}_{c,\max} \quad \forall r \in R \tag{4.4ac}$$

$$T_{i,h,\min} \leq T_{i,h,t} \leq T_{i,h,\max} \quad \forall h \in H \tag{4.4ad}$$

$$\mathrm{SOC}_{w,\min} \leq SOC_{w,t} \leq SOC_{w,\max} \quad \forall w \in W \tag{4.4ae}$$

$$0 \leq P_{h,t} \leq P_{h,\max} \quad \forall h \in H \tag{4.4af}$$

$$0 \leq P_{w,t} \leq P_{w,\max} \quad \forall w \in W \tag{4.4ag}$$

$$0 \leq P_{\text{bought},t} \leq P_{\text{substation}} \quad \forall t \in T \tag{4.4ah}$$

$$0 \leq Q_{\text{bought},t} \leq Q_{\text{substation}} \quad \forall t \in T \tag{4.4ai}$$

$$V_{\min}^2 \leq V_{i,t}^2 \leq V_{\max}^2 \quad \forall i, \forall t \tag{4.4aj}$$

$$I_{ij,\min}^2 \leq I_{ij,t}^2 \leq I_{ij,\max}^2 \quad \forall i, \forall j, \forall t \tag{4.4ak}$$

Problem (4.4) minimizes the LSE's system operation costs. However, costs relating to compensations for the customer-side resources are excluded from the objective function. This is because the difference between the optimal values for Problem (4.4) with and without the customer-side resources will be used to indicate the maximum value of the resources. The first term in equation (4.4a) represents the peak demand-related charge. This represents costs relating to capacity and transmission infrastructure, which the LSE pays to meet its demand. These charges are often associated with the maximum demand of the LSE, and as such, these costs are minimized in Problem (4.4). The second and third terms represent energy arbitrage, while the fourth and fifth terms are loss terms. The sixth term and equations (4.4u) - (4.4w) represent convex relaxations capturing the ramp rate reduction application. The term $\lambda_{ramp,t}$ reflects additional unit costs incurred by the transmission system operator (which also doubles as the market operator) in addressing ramping concerns due to the high penetration of intermittent DERs. The seventh and eighth terms of the objective function represent costs associated with operating typical voltage management devices. These costs are expressed in terms of the initial costs and switching

operations over the lifetime of these devices [27]. To preserve convexity, the seventh and eighth terms in the objective function, which represent absolute value terms, are accompanied by equations (4.4x) - (4.4ac).

The output of the LSE's solar PV system can be adjusted as required. Also, we assume that the inverter associated with the LSE's solar PV resources can produce reactive power to support voltages in the distribution network. These possibilities are captured in (4.4e) to (4.4g).

Equations (4.4j) - (4.4m) represent linear decision rules which will be used to dispatch clusters of customer-side resources in a decentralized fashion. $z_{1,t}$ represents the uncertainties associated with the LSE's forecasted total load (i.e. reconstituted load), which can be obtained at the substation level, while $z_{2,t}$ represents the uncertainties associated with the output of the LSE's solar PV resource. Since both uncertainties can also be related, an interaction term $z_{1,t}\ z_{2,t}$ is introduced into the decision rules.

Equations (4.4n) to (4.4t) represent the power flow-related constraints. To preserve convexity and capture loss terms, a second-order conic programming (SOCP) relaxation of the power flow equations is adopted [28]. Constraints (4.4ad) to (4.4ak) represent comfort limits and other variable limit constraints.

4.5 Real Time Dispatch Algorithms

As highlighted in previous sections, dispatch setpoints for the customer-side resource clusters can be obtained from the linear decision rules from the solution to the LSE's optimal scheduling problem. Alternatively, an optimal real-time dispatch problem can be solved to obtain optimal dispatch setpoints for the resource clusters. The resources within each cluster can then be dispatched using methods discussed in our previous work [2].

4.5.1 Decision Rule-Based Dispatch Algorithm

Solving Problem (4.4) under multiple scenarios will produce different values of rule parameters (e.g., $P_{h0,t}$, $P_{w0,t}$). This variation can be harnessed to provide an edge

over typical robust optimization methods that essentially uses the same parameters under all realizations of the uncertainties. Specifically, machine learning models providing the most appropriate rule parameters under different uncertainty realizations are trained with the decision rule parameter values from different scenarios. Each rule parameter is expressed as a function of $z_{1,t}$, $z_{2,t}$, and $P_{bought,rt,t}$. For each rule parameter, linear regression, neural networks, and XGBoost machine learning models are considered [29]. The performances of these models are also compared with simply taking the average and median values of the rule parameters across all scenarios. After selecting the most suitable rule parameter value based on measured $z_{1,t}$, $z_{2,t}$, and $P_{bought,rt,t}$ values, equations (4.4j) - (4.4m) are used to calculate the setpoint for each cluster. The states of the capacitors and regulators are determined based on the most dominant states for each timestep across all scenarios.

Practically, the LSE's reconstituted load profile can be obtained in real-time using (4.5a). $z_{1,t}$ can then be estimated as the difference between the LSE's real-time reconstituted load profile and the predicted reconstituted load profile at time t as shown in (5b). $z_{2,t}$ is simply the difference the PV output in real-time and the day-ahead forecasted output at time t.

$$P_{recons,rt,t} = P_{bought,rt,t} + \sum_i P_{der,i,t} - \sum_i \Delta P_{agg,i,t} \tag{4.5a}$$

$$z_{1,t} = P_{recons,rt,t} - P_{recons,base,t} \tag{4.5b}$$

4.5.2 Real Time Optimal Dispatch Algorithm

The optimal real-time dispatch algorithm is similar to the day-ahead scheduling problem (4.4). The main difference between the two problems is that the objective of the real-time dispatch algorithm is to make the overall demand, as measured at the substation, track the day-ahead market bids, as shown in (4.6a). The capacitor and regulator states are set to the solutions from the day-ahead problem. Also, the term

e_t and constraints (4.6b) and (4.6c) are included to guarantee model feasibility.

$$minimize \sum_{t=1}^{T} [(P_{bought,bid,t} - P_{bought,rt,t})^2 + e_t] \tag{4.6a}$$

$$\text{Problem (4.4) constraints excluding (4.4j) - (4.4}\ell\text{)} \tag{4.6b}$$

$$0 \leq P_{bought,rt,t} \leq P_{bought,bid,t} + e_t \tag{4.6c}$$

4.6 Case Studies

4.6.1 Simulation Data

The proposed framework was tested using a modified version of the IEEE-33 bus test system [30]. We assumed that the LSE has three homogeneous resource clusters across each phase of its distribution network, as shown in Fig. 4.2. Residential units forming the HVAC cluster are connected to Node 12. The water heater and BTM battery clusters are on Node 7 and Node 3, respectively. The parameters for the resource clusters are shown in Table 4.1. The LSE's solar PV system is rated at 200 kVA per phase and connected to Node 18. The capacitors are rated at 50 kVAR per phase and are connected to nodes 8, 13, 22, 23, and 27.

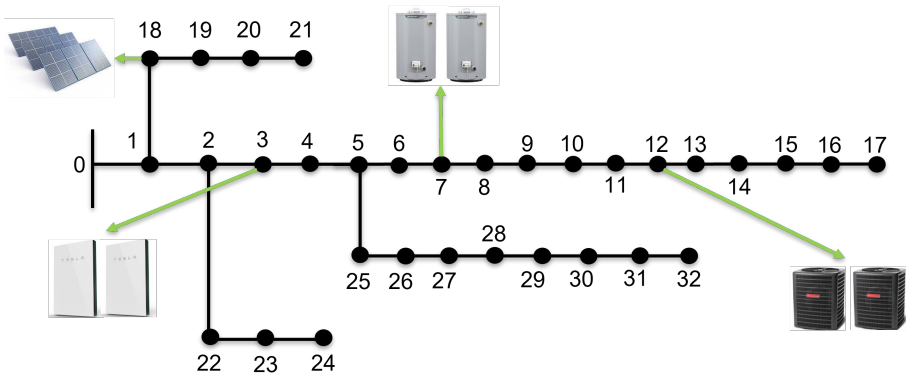

Figure 4.2: Test system description

The energy market prices and capacity cost data were obtained from NYISO's 2019 data repository [31]. $\lambda_{ramp,t}$ was set at \$25/MWh, based on the price at which NYISO procures additional reserve capacity to handle additional system ramping

concerns [32]. The operating costs for the capacitors ($\lambda_{capacitor}$) and regulators (λ_{reg}) are based on the analysis provided in [27]. The distribution network, HVAC cluster, water heater cluster, and battery cluster were simulated with OpenDSS, while the dispatch algorithms were implemented in Python. A Gurobi solver, within the CVX optimization tool, running on a 32-GB HP ProDesk 600 computer was used to solve the stochastic day-ahead model [33]. Also, the uncertainties $z_{1,t}$ and $z_{2,t}$ were assumed to be uniformly distributed with the minimum and maximum values equal to different percentages of the corresponding capacity. $P_{substation}$ was set at 1,500 kW per phase.

Table 4.1: Resource cluster parameters

	HVAC Cluster	Water Heater Cluster	BTM Battery Cluster
No. of units	42	42	30
Parameters	$R_h = 0.06^oC/kW$	A = 96m^2	$\alpha_b = 1$
Parameters	$C_h = 45.25kWh/^oC$	$R_e = 16$	$\eta_{ch} = 0.927$
Parameters	$\eta_{COP} = 4$	$C_w = 33 \times 10^6 J/kg$	$\eta_{dis} = 1.08$
Total rating	180 kW	189 kW	150 kW / 405 kWh
Comfort/ Usage Limits	$T_{i,min} = 66.95^oF$ $T_{i,max} = 72.95^oF$	$SOC_{min} = 0.895$ $SOC_{max} = 1$	$SOC_{min} = 0.2$ $SOC_{max} = 1$

4.6.2 Day Ahead Scheduling Results

Three simulation cases are considered to facilitate a thorough analysis of the proposed framework. The cases are as follows.

1. Optimal system operation without controlling customer-side resources (Base Case) - This case still involves solving Problem (4.4). However, the customer-side resources are excluded. This case represents the operation of a LSE that does not capture value from its customer-side resources

2. Peak shaving-focused system operation (Peak Shaving-Focused Case) - This case captures the perspective of an LSE focused on using its customer-side resources for peak shaving only. This case still involves solving Problem (4.4). However, the arbitrage and peak shaving terms are the only terms included in

the objective function.

3. Optimal system operation with customer-side resources (Combined Applications Case) - This case captures the usage of customer-side resources for multiple applications simultaneously.

Table 4.2 shows the LSE's system operation costs for the three simulation cases at different uncertainty levels associated with the load and solar PV output forecasts. Focusing on the results at the 5% uncertainty level, the usage of customer-side resources for multiple services simultaneously reduced the system operating costs by 11.8% and 12.9% respectively, compared to when the customer-side resources are ignored and when peak-shaving is the LSE's focus. Note that for the case where customer-side resources are ignored, the LSE still optimizes its operations considering the five value streams mentioned. This explains why the case without customer-side resources reflects lower operating costs compared to the peak-shaving-focused case.

Fig. 4.3(a) shows the LSE's expected day-ahead demand profile (single-phase) at a 5% uncertainty level with and without controlling customer-side resources. As expected, controlling customer-side resources produces a smoother demand profile with a reduced ramp rate. The average ramp rates for the demand profiles with and without the control of customer-side resources are 11.42 kW/hr and 68.08 kW/hr respectively. Also, Fig. 4.3(b), Fig. 4.4(a), and Fig. 4.4(b) show the average profiles for the HVAC, water heater, and BTM battery clusters, respectively. The increased power consumption of the HVAC cluster in the early hours of the day (3 to 6 am) represents pre-cooling effects. This makes it possible to reduce the consumption of the HVAC resources during the afternoon when electricity prices are expected to be more significant. Also, the batteries in the BTM battery cluster are expected to receive an additional charge in the early hours of the day when electricity is cheaper.

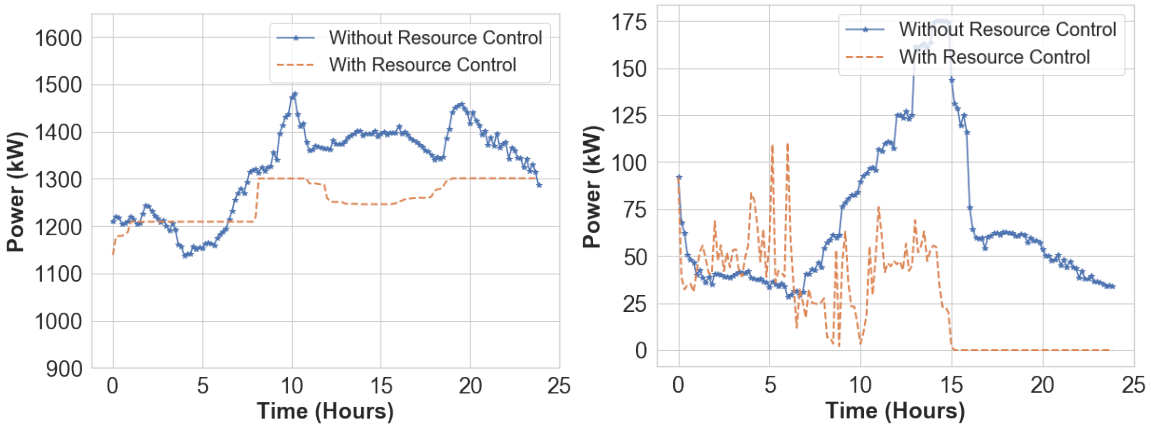

(a) LSE's expected load profile (b) HVAC cluster profile

Figure 4.3: (a) Expected total load profile (b) HVAC cluster profile

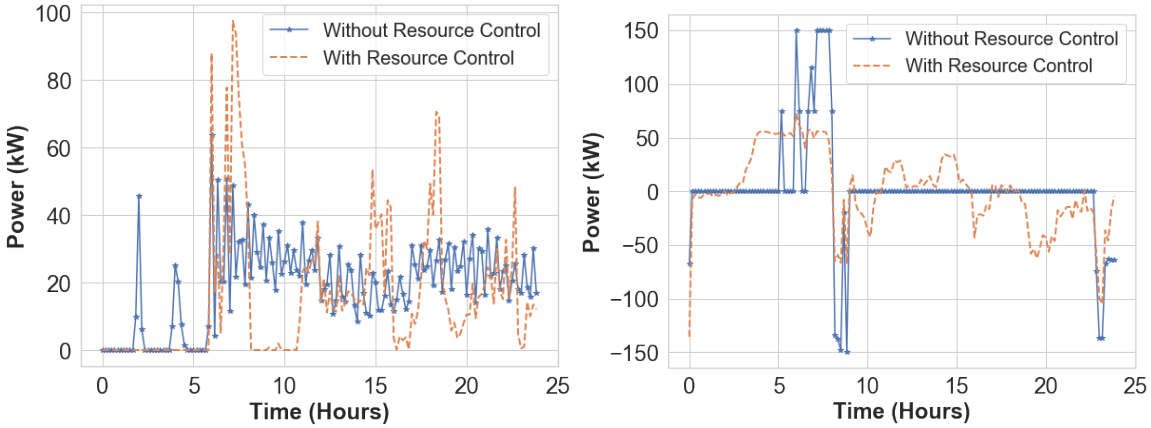

(a) Water heater cluster profile (b) Battery cluster profile

Figure 4.4: (a) Expected water heater cluster profile (b) Battery cluster profile

Table 4.2: LSE's operating costs

Uncertainty (%)	Base ($)	Peak Focused ($)	Comb. Apps. ($)	Resource Value ($)	Service Value ($)
0.5	1287.90	1316.01	1147.42	140.48	168.59
1	1290.22	1316.18	1147.74	142.48	168.44
2	1295.46	1316.69	1148.20	147.26	168.49
5	1301.84	1317.84	1148.46	153.38	169.38
10	1323.39	1327.63	1160.11	163.18	167.52
20	1365.12	1365.56	1200.55	164.57	165.01

4.6.3 Sensitivity Analysis

The column 'Resource Value' in Table 4.2 indicates the value of the customer-side resources, which is equal to the difference between values in the 'Base' and 'Comb. Apps' columns. On the other hand, the column 'Service Value' (equal to 'Peak Focused' - 'Comb. Apps') provides an indication of the value of the additional applications ignored (i.e. ramp rate reduction, loss reduction and voltage management). From a practical standpoint, the column 'Resource Value' provides the maximum compensation that can be allocated to all customer-side resources for the operating day under consideration. If permitted by existing regulations, the LSE can take a portion of the cost savings and pay the rest back to the owners of the customer-side resources. Such compensation structures are similar to concepts around the Performance-Based Regulation (PBR) framework being proposed in some regions of the United States [34]. Our subsequent work will focus on sharing the total compensation among individual customer-side resource clusters.

The values in the 'Resource Value' column increase with increasing levels of uncertainty, implying that the expected value of customer-side resource increases as load profiles and solar PV output becomes more uncertain. This observation is very logical because the customer-side resources are flexible and, as such, can serve to help the LSE minimize the impacts of forecast errors. Also, the rate of increase of the values in the 'Resource Value' column shows that the additional value of the customer-side eventually saturates. Again, this observation is logical, considering that there is so much the resources can do because of their physical capacity constraints. On the other hand, the 'Service Value' column appears to have an overall reduction trend. However, increases at specific points (such as at 5% uncertainty level), though minimal, make it difficult to draw conclusions about the downward trend observation. This implies that the expected added value of the other services (asides peak shaving and energy arbitrage) depends on the specific uncertainty realizations.

Table 4.3: ML model metrics for decision rule parameters

	Linear Regression	XGBoost	Neural Network	Mean	Median
P_{hvacn0}	17.5%	16%	17.6%	11.8%	12.3%
P_{hvacn3}	10.9%	6.9%	10.9%	10.2%	10.5%
P_{whn0}	13.8%	13.5%	14.3%	9.2%	9.7%
P_{whn3}	10.9%	6.9%	11.2%	10.2%	10.5%
P_{battn1}	6.5%	36.8%	6.5%	7.2%	6.5%
$P_{der,control,0}$	5.2%	6.3%	5.3%	5.1%	5.2%
$P_{der,control,1}$	0.3%	0.3%	1.4%	0.5%	0.3%
$P_{der,control,2}$	5.2%	5.8%	5.3%	5.1%	5.2%
$P_{der,control,3}$	5.2%	4.6%	5.2%	4.9%	5.2%
Q_{battn1}	9.7%	9.9%	9.7%	9.2%	9.3%
$Q_{der,0}$	23%	20.1%	23.5%	3.4%	3.5%

4.6.4 Real Time Dispatch with Decision Rules

As highlighted in previous sections, the day-ahead stochastic optimization problem's outcomes generate different rule parameter values. The relationship between these rule parameter values and the current uncertainty realizations and system conditions can be established using ML models. Such ML model representations make it easier to adapt the dispatch rules based on current system conditions.

Table 4.3 shows the error metric values for different ML models considered to provide a generalized representation of the rule parameters at the 5% uncertainty level. The error metric is a normalized root mean squared error (RMSE) value calculated by dividing RMSE by the maximum parameter value. The ML models were trained and tested using a 70%-30% split on data from 20 uncertainty scenarios, each with 144 data points (10-minute intervals). The model with the lowest error metric was selected for each rule parameter. Other parameters not included in the table either had constant values or clear segmentation that could be represented with simple IF-ELSE conditions.

Five uncertainty realizations (different from the 20 scenarios used to generate ML training and testing data) were generated to test the dispatch rules. Figure 4.5(a)

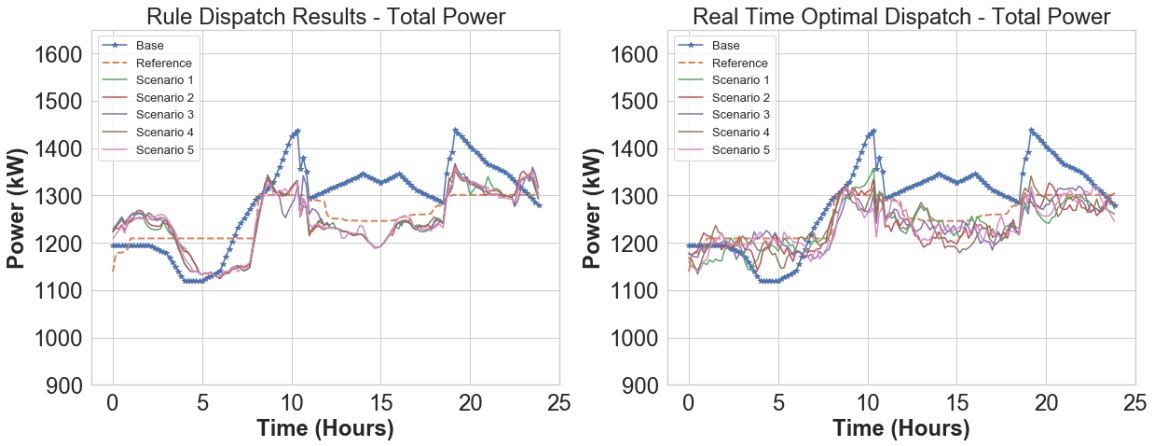

(a) Rule-based (b) Real-time optimal

Figure 4.5: (a), (b) Dispatch results - total power

shows the LSE's power profile for a single-phase across the five uncertainty scenarios using the generated decision rules. Figure 4.5(a) shows that while the decision-rules dispatch results showed some deviations from the expected demand profile generated by averaging the day-ahead scheduling results across 20 different uncertainty scenarios, the outcomes were significantly better than the base profile. Using the mean absolute percentage error (MAPE) as a metric to quantify the differences between the dispatch rules and the day-ahead bids, the mean MAPE value across the five test scenarios is 2.80%. The average reduction in energy costs across all five test scenarios with respect to the base profile is 3.9% compared to the 3.1% expected reduction. Also, the average decrease in capacity costs across all five test scenarios with respect to the base profile is 5.4% compared to the 9.5% expected reduction. Figures 4.6(a), 4.7(a), and 4.8(a) show the dispatch profiles for the HVAC, water heater, and BTM battery clusters, respectively. Figures 4.6(a) and 4.7(a) show that the cluster dispatch across different scenarios have minimal variations and are also similar to the expected profiles (Fig. 4.3 and Fig. 4.4) obtained from the day-ahead solutions.

Fig. 4.11(a) shows the system losses for the base case and the five test scenarios under the rules-based dispatch. The losses were reduced by 4.3%. Also, the voltage limits are satisfied across all five test scenarios.

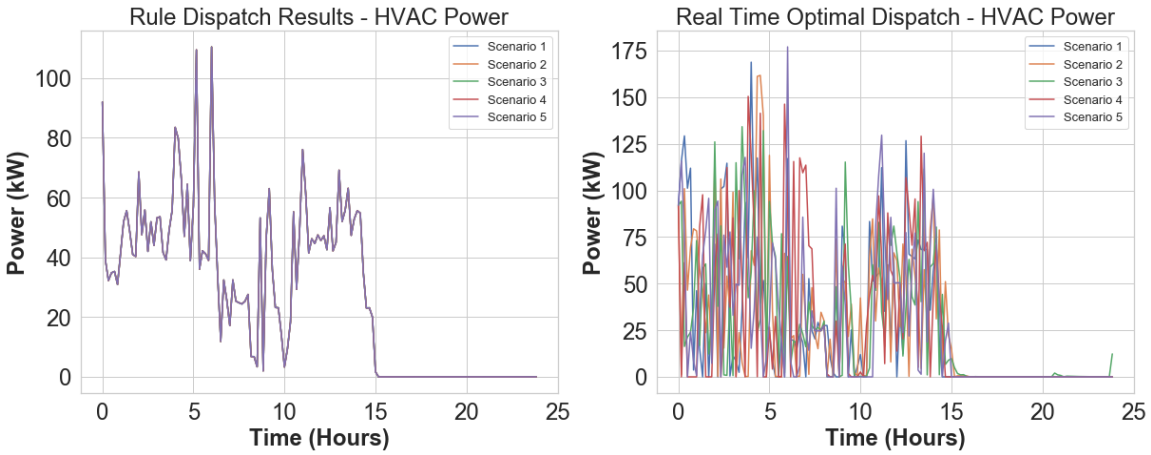

(a) Rule-based (b) Real-time optimal

Figure 4.6: (a), (b) Dispatch results - HVAC cluster

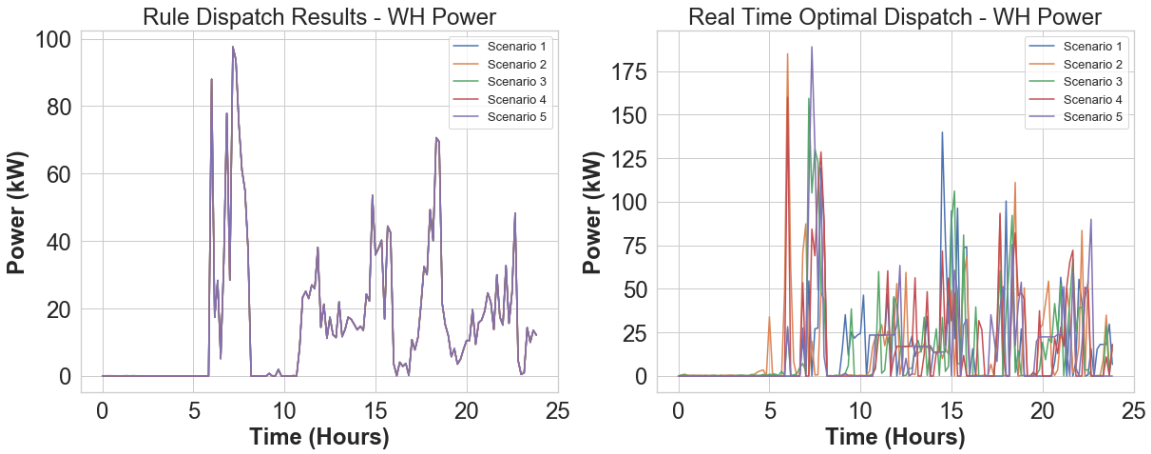

(a) Rule-based (b) Real-time optimal

Figure 4.7: (a), (b) Dispatch results - water heater cluster

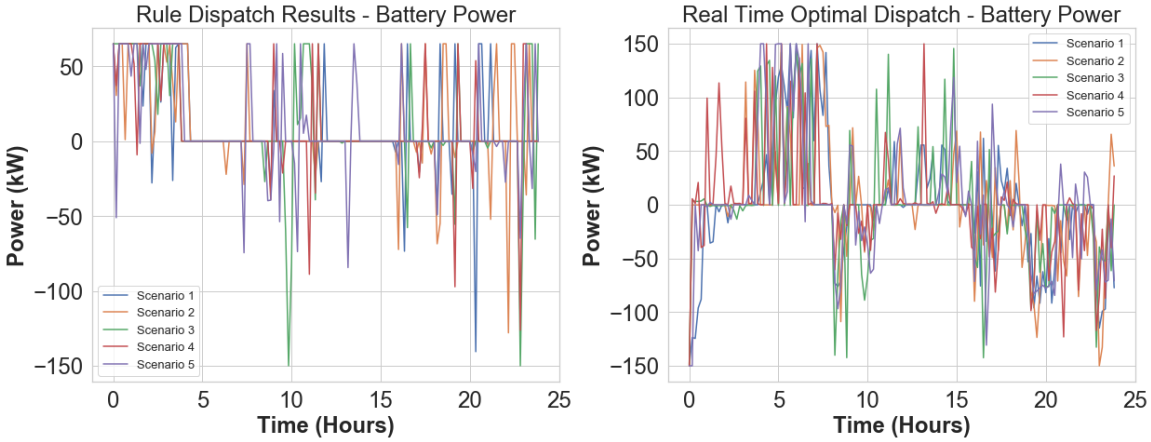

(a) Rule-based (b) Real-time optimal

Figure 4.8: (a), (b) Dispatch results - battery cluster

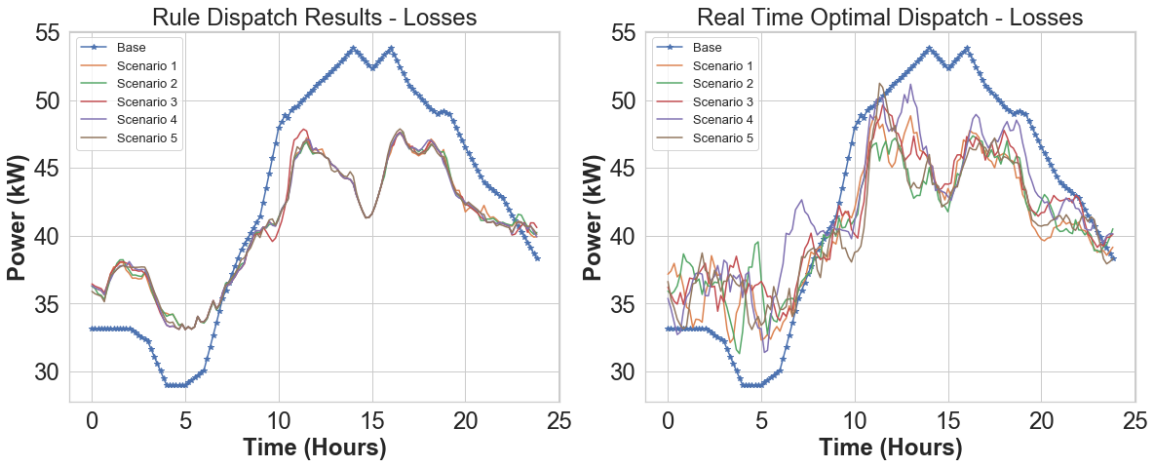

(a) Rule-based (b) Real-time optimal

Figure 4.9: (a), (b) Dispatch results - losses

4.6.5 Optimal Real-Time Dispatch

The real-time optimal dispatch problem was solved using the same uncertainty realizations for the rule-based dispatch case. Fig. 4.5(b) shows that the LSE's total load profiles under all five scenarios are close to the reference profile (i.e., expected day-ahead demand profile). The average MAPE between the reference profile and the actual profiles across all five scenarios is 1.94% which is about 0.86 percentage points less than the corresponding value for the rule-based dispatch case. The energy cost reduction is about 4.7% which represents a 0.8 percentage point improvement compared to the rule-based case. The capacity cost reduction follows the same vein with a 1.8 percentage point improvement over the rules-based case. However, the rule-based method outperforms the optimal dispatch method in terms of loss reduction by 0.8 percentage points. Figures 4.6(b), 4.7(b) and 4.8(b) show the dispatch profiles of the HVAC, water heater, and BTM battery clusters, respectively. More variations in the customer-side resource dispatch profiles indicate the overall dynamism of the optimal real-time dispatch. However, this dynamism comes with an additional 3-minute average computation time compared to the sub-second execution of the rules. While this is not an issue in the case studies considered in this work, the computation

times could be longer for distribution systems with numerous nodes.

Fig. 4.9(b) shows the system losses, which were reduced by 3.5% on average, with respect to the losses in the base case (i.e., without resource control). The voltage limits are also satisfied across all five test scenarios.

Table 4.4: Dispatch algorithm comparison

	MAPE	Energy Cost Reduction	Capacity Cost Reduction	Loss Reduction	Computation Time
Rule-based	2.8%	3.9%	5.4%	4.3%	<1s
RT optimal	1.94%	4.7%	7.2%	3.5%	3 mins

4.6.6 Case with Third Party Aggregator

Under new policy scenarios, third-party aggregators can aggregate customer-side resources on an LSE's network for participation in wholesale markets. However, such aggregations must be operated without adverse effects on the LSE's network. To preserve competitiveness and stifle market power effects, the market operator can make the aggregator's resource dispatch schedule available to the LSE only after market clearing. The LSE can only predict the aggregator's expected schedule while solving its day-ahead scheduling problem. The uncertainty associated with the day-ahead prediction of the aggregator's dispatch schedule, $z_{agg,t}$, provides another source of uncertainty. Since $z_{agg,t}$ will be revealed after market clearing, there is no need to capture $z_{agg,t}$ in the decision rules for real-time dispatch. However, the decision rule parameters for the rule-based dispatch should be re-estimated considering the revealed uncertainties post market clearing.

A third-party aggregator with a 20 kW flexibility capacity is assumed to be present on node 23. Also, the uncertainties associated with the LSE's prediction of the aggregator's actions are assumed to follow a uniform distribution with maximum and minimum values pegged at $\pm$ 10% of the expected profile. Under these conditions, using updated decision rules for dispatching the LSE's flexible resources produced 0.04

and 0.08 percentage point improvements in the MAPE metric and capacity charge savings over the usage of non-updated rules.

4.7 Conclusions and Future Work

This chapter discusses a framework for LSEs with solar PV resources and access to groups of residential HVACs, water heaters, and BTM batteries to capture multiple value streams from their resources. Specifically, we considered self-service applications for LSEs (peak shaving, energy arbitrage, and ramp rate reduction) and distribution system operation applications (voltage management and loss reduction). The framework captures uncertainties relating to load and solar PV output forecasts. Our results clearly show that LSEs can capture more value by using the same group of customer-side resources for multiple applications simultaneously. Specifically, the usage of customer-side resources for the suite of services reduced the system operating costs by 12.8% on average compared to a peak-shaving only application which is often the status quo. We also showed that the value of customer-side resources increases as uncertainties in the LSE's forecasts increases. For the cases considered, the value of customer-side resources ranged from 10% to 12% at different levels of forecast uncertainties.

Also, we compared and contrasted two real-time resource dispatch algorithms based on decision rules and the solution of a real-time optimization problem. Our results show that the real-time optimization-based algorithm performs better than the rule-based method across several metrics. However, the performance gains come at additional computation costs and lower system loss reductions. The additional computation time could be significant for LSEs with vast distribution networks. As such, appropriate trade-offs between both methods can be established based on specific system configurations.

The proposed framework has also been adapted to help LSEs capture the impacts of third-party aggregators on their distribution network. For decision rule-based dis-

patch, we showed that LSEs could obtain performance gains by updating the decision rules after additional information about the aggregator's actions has been revealed post market clearing. We believe that these perspectives and contributions provide holistic tools and methods for LSEs to navigate new policy scenarios that will significantly unlock the value associated with the flexibility of customer-side resources. In our subsequent work, we will consider how LSEs can compensate these customer-side resources for the multiple services provided.

REFERENCES

[1] Federal Energy Regulatory Commission, "FERC Order No. 2222: Fact Sheet," 2020. Available: https://www.ferc.gov/media/ferc-order-no-2222-fact-sheet.

[2] A. Abbas and B. Chowdhury, "A stochastic optimization framework for realizing combined value streams from customer-side resources," *IEEE Transactions on Smart Grid*, vol. 13, no. 2, pp. 1139–1150, 2022. doi: 10.1109/TSG.2021.3135155.

[3] Y. Shi, B. Xu, D. Wang, and B. Zhang, "Using battery storage for peak shaving and frequency regulation: Joint optimization for superlinear gains," *IEEE Transactions on Power Systems*, vol. 33, no. 3, pp. 2882–2894, 2018. doi: 10.1109/TPWRS.2017.2749512.

[4] M. J. E. Alam, K. M. Muttaqi, and D. Sutanto, "A controllable local peak-shaving strategy for effective utilization of PEV battery capacity for distribution network support," *IEEE Transactions on Industry Applications*, vol. 51, no. 3, pp. 2030–2037, 2015. doi: 10.1109/TIA.2014.2369823.

[5] J. Engels, B. Claessens, and G. Deconinck, "Optimal combination of frequency control and peak shaving with battery storage systems," *IEEE Transactions on Smart Grid*, vol. 11, no. 4, pp. 3270–3279, 2020. doi: 10.1109/TSG.2019.2963098.

[6] K. Kircher, A. Aderibole, L. K. Norford, and S. Leeb, "Distributed peak shaving for small aggregations of cyclic loads," *IEEE Transactions on Power Delivery*, pp. 1–1, 2022. doi: 10.1109/TPWRD.2022.3149446.

[7] Y. Guo, Q. Zhang, and Z. Wang, "Cooperative peak shaving and voltage regulation in unbalanced distribution feeders," *IEEE Transactions on Power Systems*, vol. 36, no. 6, pp. 5235–5244, 2021. doi: 10.1109/TPWRS.2021.3069781.

[8] J. L. Mathieu, M. Kamgarpour, J. Lygeros, and D. S. Callaway, "Energy arbitrage with thermostatically controlled loads," in *2013 European Control Conference (ECC)*, pp. 2519–2526, 2013. doi: 10.23919/ECC.2013.6669582.

[9] O. Gandhi, W. Zhang, C. D. RodrÃguez-Gallegos, M. Bieri, T. Reindl, and D. Srinivasan, "Analytical approach to reactive power dispatch and energy arbitrage in distribution systems with ders," *IEEE Transactions on Power Systems*, vol. 33, no. 6, pp. 6522–6533, 2018. doi: 10.1109/TPWRS.2018.2829527.

[10] M. R. Sarker, D. J. Olsen and M. A. Ortega-Vazquez, "Co-optimization of distribution transformer aging and energy arbitrage using electric vehicles,"

IEEE Transactions on Smart Grid, vol. 8, no. 6, pp. 2712–2722, 2017. doi: 10.1109/TSG.2016.2535354.

[11] H. K. Nguyen, A. Khodaei, and Z. Han, "Distributed algorithms for peak ramp minimization problem in smart grid," in *2016 IEEE International Conference on Smart Grid Communications (SmartGridComm)*, pp. 174–179, 2016. doi: 10.1109/SmartGridComm.2016.7778757.

[12] H. K. Nguyen, A. Khodaei and Z. Han, "Incentive mechanism design for integrated microgrids in peak ramp minimization problem," *IEEE Transactions on Smart Grid*, vol. 9, no. 6, pp. 5774–5785, 2018. doi: 10.1109/TSG.2017.2696903.

[13] California Independent System Operator, "Flexible ramping product," 2016. Available: http://www.caiso.com/informed/Pages/StakeholderProcesses/ CompletedClosedStakeholderInitiatives/FlexibleRampingProduct.aspx.

[14] E. D. Gur, "Flexible ramping product: Market design concept proposal," 2018. Available: https://www.nyiso.com/documents/20142/2545489/Flexible Ramping Product April 26 MIWG FINAL.pdf/0489ed61-472b-a320-9727-d51f32d8832c.

[15] T. P. Wagner, A.Y. Chikhani, and R. Hackam, "Feeder reconfiguration for loss reduction: an application of distribution automation," *IEEE Transactions on Power Delivery*, vol. 6, no. 4, pp. 1922–1933, 1991. doi: 10.1109/61.97741.

[16] Z. Ziadi, S. Taira, M. Oshiro and T. Funabashi, "Optimal power scheduling for smart grids considering controllable loads and high penetration of photovoltaic generation," *IEEE Transactions on Smart Grid*, vol. 5, no. 5, pp. 2350–2359, 2014. doi: 10.1109/TSG.2014.2323969.

[17] A. Mosaddegh, C. Canizares, and K. Bhattacharya, "Optimal demand response for distribution feeders with existing smart loads," *IEEE Transactions on Smart Grid*, vol. 9, no. 5, pp. 5291–5300, 2018. doi: 10.1109/TSG.2017.2686801.

[18] R. A. Jabr, "Linear decision rules for control of reactive power by distributed photovoltaic generators," *IEEE Transactions on Power Systems*, vol. 33, no. 2, pp. 2165–2174, 2018. doi: 10.1109/TPWRS.2017.2734694.

[19] Z. Li, R. Ding and A.C. Floudas, "A comparative theoretical and computational study on robust counterpart optimization: I. robust linear optimization and robust mixed integer linear optimization," *Industrial Engineering Chemistry Research*, vol. 50, no. 18, 2011. doi: 10.1021/ie200150p.

[20] New York Independent System Operator, "Compliance filing and request for flexible effective date," 2021. Available: https://nyisoviewer.etariff.biz/ViewerDocLibrary//Filing/Filing1805/Attachments/ 20210719 NYISO CmplncFlng Order No. 2222.pdf.

[21] N. Lu, "An evaluation of the hvac load potential for providing load balancing service," *IEEE Transactions on Smart Grid*, vol. 3, no. 3, pp. 1263–1270, 2012. doi: 10.1109/TSG.2012.2183649.

[22] M. A. Z. Alvarez, K. Agbossou, A. Cardenas, S. Kelouwani, and L. Boulon, "Demand response strategy applied to residential electric water heaters using dynamic programming and k-means clustering," *IEEE Transactions on Sustainable Energy*, vol. 11, no. 1, pp. 524–533, 2020. doi: 10.1109/TSTE.2019.2897288.

[23] R. Juhl, J. K. MÃžller and H. Madsen, "CTSMR - Continuous Time Stochastic Modeling in R," 2016.

[24] M. Liu, S. Peeters, D. S. Callaway and B. J. Claessens, "Trajectory tracking with an aggregation of domestic hot water heaters: Combining model-based and model-free control in a commercial deployment," *IEEE Transactions on Smart Grid*, vol. 10, no. 5, pp. 5686–5695, 2019. doi: 10.1109/TSG.2018.2890275.

[25] A. Abbas and B. Chowdhury, "Realizing combined value streams from utility-operated demand response resources," in *2020 52nd North American Power Symposium (NAPS)*, pp. 1–6, 2021. doi: 10.1109/NAPS50074.2021.9449749.

[26] D. M. Rosewater, D. A. Copp, T. A. Nguyen, R. H. Byrne and S. Santoso, "Battery energy storage models for optimal control," *IEEE Access*, vol. 7, pp. 178357–178391, 2019. doi: 10.1109/ACCESS.2019.2957698.

[27] T. Malakar and S. K. Goswami, "Active and reactive dispatch with minimum control movements," *International Journal of Electrical Power Energy Systems*, vol. 44, no. 1, pp. 78–87, 2013. doi: https://doi.org/10.1016/j.ijepes.2012.07.014.

[28] M. Farivar and S. H. Low, "Branch flow model: Relaxations and convexification - Part I," *IEEE Transactions on Power Systems*, vol. 28, no. 3, pp. 2554–2564, 2013. doi: 10.1109/TPWRS.2013.2255317.

[29] T. Chen and C. Guestrin, "XGBoost: A scalable tree boosting system," in *Proceedings of the 22nd ACM SIGKDD International Conference on Knowledge Discovery and Data Mining*.

[30] M.E. Baran and F. F. Wu, "Network reconfiguration in distribution systems for loss reduction and load balancing," *IEEE Transactions on Power Delivery*, vol. 4, no. 2, pp. 1401–1407, 1989. doi: 10.1109/61.25627.

[31] New York Independent System Operator, "Energy market and operational data," 2022. Available: https://www.nyiso.com/energy-market-operational-data.

[32] E. D. Avallone, "SENY reserve region enhancements," 2020. Available: https://www.nyiso.com/documents/20142/12170360/4_22_2020_Reserves_for_Resource_Flexibility_FINAL.pdf/ b2db3169-5d56-ec11-1541-c83bc5f58ed5.

[33] Gurobi Optimization, LLC, "Gurobi optimizer reference manual," 2021. Available: https://www.gurobi.com.

[34] State of Hawaii Public Utilities Commission, "Performance based regulation." Available: https://puc.hawaii.gov/energy/pbr/.

CHAPTER 5: AN ALTERNATIVE COMPENSATION MECHANISM FOR DEMAND-SIDE FLEXIBILITY CONSIDERING LOW AND MEDIUM INCOME (LMI) PARTICIPANTS

Load serving entities (LSEs) can realize combined value streams from different clusters of flexible customer-side resources on their networks. However, LSEs also need to know how to compensate the resource owners financially for the multiple services provided. At the same time, LSEs can introduce other compensation dimensions to incentivize participation by a unique customer segment, such as the low and medium-income (LMI) customer segment. Inspired by game-theoretic concepts, this work proposes a two-level compensation framework that rewards participants in an LSE's flexibility program based on the nature of the collective value produced by the resources. The proposed framework also includes a social compensation dimension that improves the credit ratings of LMI participants. The framework is illustrated using numerical simulations based on a modified IEEE 33-bus test system, electricity market prices from the New York Independent System Operator, NYISO, and simulated credit data.

Nomenclature

Parameters

α_b	Battery self discharge rate
$\Delta P_{agg,i,t}$	Aggregator expected impact at node i at time t
Δt	Time step
ΔV	Voltage step
$\eta_{ch,b}$	Battery charging efficiency
η_{COP}	HVAC system co-efficient of performance
$\eta_{dis,b}$	Battery discharging efficiency
$\lambda_{capacitor}$	Capacitor switching price
λ_{cap}	Capacity price
$\lambda_{ramp,t}$	Price of additional reserve capacity for handling ramping concerns
$\lambda_{reactive,t}$	Reactive power price at time t
$\lambda_{real,t}$	Real power price at time t
λ_{reg}	Regulator switching price
A	Aggregated water heater total surface area
Cr_{LMI}	LMI participant's credit improvement goal
$E_{b,max}$	Maximum battery SOC
$E_{b,min}$	Minimum battery SOC
$I^2_{ij,min}, I^2_{ij,max}$	Line flow current rating

K_1, K_2	Regression model parameters
m	Month index
m_w	Total mass of water in water heater
$P_{abs,min}, P_{abs,max}$	Ramp rate limits
$P_{b,i,base,t}$	Battery cluster base power consumption
$P_{ch,b,max}$	Maximum battery charging rate
$P_{dis,b,max}$	Maximum battery discharging rate
$P_{fin,m}$	Financial compensation for LMI participant at month m
$P_{h,i,base,t}$	HVAC cluster base power consumption
$P_{h,max}$	HVAC cluster power rating
$P_{L,i,t}$	Uncontrolled active power load at node i at time t
$P_{substation}$	Substation active power limit
$P_{w,i,base,t}$	Water heater cluster base power consumption
$P_{w,max}$	Water heater cluster power rating
$Q_{c,t}$	Capacitor reactive power
$Q_{L,i,t}$	Uncontrolled reactive power load at node i at time t
$Q_{substation}$	Substation reactive power limit
R_e	Aggregated water heater thermal resistance
R_h	HVAC thermal resistance
r_{ki}	Line resistance between nodes k and i

$S_{der,max}$	DER apparent power rating
$S_{ij,max}$	Maximum line flow limit
$SOC_{w,min}, SOC_{w,max}$	Water heater cluster SOC limits
T_a	Ambient temperature
$T_{i,h,min/max}$	Interior temperature limits
$T_{w,max}$	Maximum hot water temperature for water heater cluster
u	Credit model uncertainty
V^2_{min}, V^2_{max}	Voltage variable limits
x_{ki}	Line reactance between nodes k and i

Variables

$Cap_{c,t}$	Capacitor status at time t
$ch_{ind,t}$	Battery charging indicator at time t
Cr_m	LMI participant's credit rating at month m
$dis_{ind,t}$	Battery discharging indicator at time t
e	WCEM objective function variable
$E_{b,t}$	Battery SOC at time t
$I_{ki,t}$	Line current flow between nodes k and i
P_m	LMI participant's credit building commitment for month m
$P_{b,t}$	Battery power at time t
$P_{bought,t}$	Power consumption at substation

$P_{ch,b,t}$	Battery charging rate at time t
$P_{dis,b,t}$	Battery discharging rate at time t
$P_{h,t}$	HVAC cluster consumption at time t
$P_{ki,t}$	Active power flow between nodes k and i at time t
$P_{loss,t}$	Active power losses at time t
$P_{sol,t}$	Solar irradiation at time t
$P_{w,t}$	Total power consumption for water heater cluster at time t
$Q_{b,t}$	Battery reactive power
$Q_{h,t}$	HVAC cluster reactive at time t
$Q_{loss,t}$	Reactive power losses at time t
$Reg_{r,t}$	Regulator status at time t
S_b	Battery inverter total apparent power rating
$SOC_{w,t}$	State of charge variable for water heater cluster at time t
$T_{i,h,t}$	Interior temperature for HVAC h at time t
$T_{w,avg}$	Average hot water temperature for water heater cluster
$V_{i,t}^2$	Voltage squared variable at node i at time t
$V_{sub,t}$	Substation squared voltage at time t

5.1 Introduction

5.1.1 Background and Motivation

The role of flexible customer-side resources in transitioning to a low-carbon energy future cannot be overemphasized. These resources can handle multiple challenges associated with smart and low-carbon grids. For example, flexible customer-side resources can modify demand patterns such that the consumption of energy from clean sources is maximized [1]. Flexible customer-side resources can also respond to frequency control signals, thus maintaining the operational integrity of the grid [2]. As such, flexible customer-side resources are already unlocking multiple value streams for resource owners and load-serving entities (LSEs) with access to these resources. The numerous value streams can be combined and captured simultaneously by a single customer-side resource or an aggregation of homogeneous or heterogeneous resources.

In [3], behind-the-meter (BTM) batteries in commercial buildings are considered for combined peak shaving and frequency regulation. The authors show that not only does such a combination provide additional benefits for the BTM battery resource owner, but the benefits provided are also super-additive in nature. The super-additivity implies that the total benefit produced by combined frequency regulation and peak shaving is more than the summation of the individual benefits from frequency regulation and peak shaving. Reference [4] also examines the usage of an aggregation of residential water heaters for frequency regulation and voltage management in the presence of high penetration of intermittent renewable energy resources. In another work, an aggregation of behind-the-meter (BTM) batteries is considered for frequency regulation [1]. At the same time, each battery simultaneously provides end-user services like peak load reduction and PV curtailment. In [5], the authors consider batteries and heating, ventilation, and air-conditioning (HVAC) systems in commercial buildings for combined energy arbitrage, frequency regulation, and spinning reserve provision. In our previous work [6], we demonstrate how an LSE can

use aggregations of residential HVACs, BTM batteries, and residential water heaters for combined energy arbitrage, peak shaving, and frequency regulation in the face of multiple sources of uncertainty.

When an LSE or aggregator operates a demand-side flexibility program where many customer-side resources provide multiple value streams, the need for compensation allocation mechanisms becomes apparent. In such cases, the LSE can group similar customer-side resources into clusters and treat each cluster as a single resource to simplify complexities associated with modeling multiple resources in scheduling problems. Hence, the LSE's compensation sharing becomes a two-level problem involving cluster-level and sub-cluster level allocations. Since each resource cluster consists of resources with similar characteristics, sub-cluster level allocations can be uniform. However, cluster-level allocation depends on the nature of the collective value and the specific contributions of each resource cluster. The authors in [7] provide a detailed comparison of different value-sharing mechanisms for different types of energy communities. The mechanisms considered include equal sharing, production capacity-based sharing, consumption-based value allocation, supply-demand ratio (SDR) based sharing, marginal contribution-based sharing (also known as the Vickery-Clarke-Groves mechanism [8]), Shapley allocation mechanism, and Worst Case Excess Minimization mechanism. The Shapley allocation and Worst Case Excess Minimization mechanisms are deeply rooted in cooperative game theory. In [9], the authors proposed a cooperative game-based method for sharing profits and losses between an aggregation of spatially distributed wind farms bidding collectively into two-settlement energy markets. These wind farms work together to reduce variations in their total output, reducing penalties associated with bid quantity violations. Also, authors in [8] [10–12] apply cooperative game concepts to different energy management problems involving different entities forming a coalition. Although references [8–12] depend on the premise that each member of the coalition can realize some value on its own outside

any coalition, the LSE can still apply similar value-sharing concepts even if resource owners can only capture additional value by participating in the LSE's demand-side management program.

Furthermore, the compensation available to customer-side resources will affect the level of participation in the LSE's flexibility program. Hence, the LSE can introduce additional compensation dimensions to augment direct financial compensations. Such extra compensation dimensions can incentivize participation from a specific segment of resource owners. An example of such a participant segment is Low and Medium-Income (LMI) households. For example, a study on how different incentive mechanisms affect the participation of residential customers in traditional peak demand reduction programs conducted by researchers at the University of California at Los Angeles showed lower participation levels from low-income customers [13]. Although several factors could be responsible for this outcome, the introduction of incentives that are very relevant to low-income customers could improve their participation levels.

While income is not typically included in credit scoring models, studies have shown that there is at least a modest correlation between credit scores and income levels [14, 15]. Hence, lower-income households are generally more likely to have lower credit ratings. As such, an improvement to the credit ratings of an LMI household can produce ripple effects that can substantially improve the economic outcomes for such households. Therefore, a social compensation dimension that improves the credit ratings of LMI households in addition to financial compensation could further incentivize the participation of such households in the LSE's flexibility program. The LSE can improve the LMI household's credit rating by using a fraction of the LMI participant's monthly compensation as repayments towards credit builder loans over a certain period [16]. At the end of the period, the LMI participant gets back the total value of the credit builder loan in addition to improved credit ratings. However,

the LMI participants must be able to choose the maximum fraction of their monthly compensation for credit building apriori. Also, the LMI participants should be able to specify their credit improvement goals for a defined period. The LSE can then combine the maximum monthly commitment and credit improvement goals to determine the specific monthly commitments for each LMI participant interested in credit rating improvement. Generally, LMI households often share similar geographic locations making it feasible for the LSE to create aggregations of flexible customer-side resources belonging to LMI households.

5.1.2 Contributions

In summary, our main contributions are two-fold and are highlighted as follows.

1. Firstly, we propose a two-level compensation framework to help LSEs allocate compensations to multiple customer-side resource owners participating in the LSE's multi-value capturing flexibility program (referred to subsequently as flexibility program). The compensation framework is based on the nature of the collective value created by the resources. We posit that the collective value produced by customer-side resources can be either strictly sub-additive, strictly super-additive, or additive.

2. Secondly, we propose an additional social compensation dimension to incentivize the participation of LMI participants in the LSE's flexibility program. The social compensation dimension improves an LMI participant's credit ratings in addition to financial rewards. We also propose an optimization model that the LSE solves to give the LMI participants an estimation of their monthly commitments to achieve specified credit rating improvements at the end of the program cycle.

5.2 Assumptions and Framework Overview

This section provides an overview of the proposed compensation allocation framework. The major underlying assumptions are also outlined as follows.

1. The LSE has defined the main value streams of interest. Since the possible value streams will depend on regulations and specific conditions applicable to the LSE's jurisdiction, we do not focus on the specifics of LSEâs value stream definition procedure.

2. The LSE has defined resource clusters with similar flexible resources based on features applicable to the LSE's customers. Extensive work has been done on clustering flexible customer-side resources [17–19]. The LSE can cluster resources based on similar comfort requirements (e.g., thermostat deadband range for residential HVACs), resource ratings, resource locations, credit ratings of resource owners, etc.

3. More resource clusters will produce more value for the LSE. For example, if $V(x)$ represents the value produced by resource cluster x, then $V(x) < V(x, y) < V(x, y, z)$. Also, the value of each resource cluster is non-negative.

4. Like all other demand-side management programs operated by LSEs, each participant's monthly compensation over each program cycle is determined at the beginning of the program cycle.

5. The LSE can estimate resource owners' opportunity costs, where applicable. For example, the resource owners could have purchased a group of BTM batteries for local energy arbitrage. As such, the compensation provided to the BTM battery owners for participating in the LSE's flexibility program should be at least equivalent to the benefits from local energy arbitrage. For a group of residential HVACs, the net costs after participating in the LSE's flexibility program must

be at most equal to the total energy cost to maintain a certain level of thermal comfort.

6. Individual flexible resources cannot capture the LSE's combined value streams in isolation. For example, a residential HVAC system cannot capture combined peak shaving, energy arbitrage, ramp rate reduction, loss reduction, and voltage management unless it participates in the LSE's demand-side flexibility program.

7. The LSE has defined representative days for each operating season to estimate the total monthly compensation for the flexible resources. Each representative day has parameters such as expected load profile, expected resource profiles for each resource cluster, expected energy market prices, and any other parameter applicable to the LSE's value streams of interest.

Based on the preceding assumptions, the main components of the compensation allocation framework are defined as follows.

1. **Estimation of the collective value of all resource clusters and the marginal value of each resource cluster** - The LSE solves an optimization problem using parameters for each representative day to estimate the collective value of the flexible resources and marginal value of each resource cluster.

2. **Investigation of the nature of the collective resource value** - The LSE classifies the collective value of the flexible resources as either strictly sub-additive, strictly super-additive, or additive. Based on this classification, the most appropriate cluster-level compensation allocation mechanism is selected. The applicable compensation allocation mechanisms for each classification are discussed in detail in section 5.3.2.

3. **Estimation of each participant's monthly financial compensation** - The LSE allocates monthly compensations to the resource clusters based on the

appropriate allocation mechanism selected after investigating the nature of the collective resource value. Each cluster's total allocation is then shared equally among all participants since the participants have very similar characteristics.

4. **Estimation of prospective LMI participants' credit improvement commitments** - The LSE solves an optimization problem to estimate a prospective LMI participant's monthly commitment towards credit improvement to achieve a certain credit rating at the end of the program cycle. This provides the prospective LMI participant with additional information that could further incentivize participation in the LSE's flexibility program.

The overall framework is illustrated in Fig. 5.1. The proposed framework is intended for use at the design stage of the LSE's flexibility program to give prospective participants an indication of the benefits they stand to gain. Each component is discussed further in the subsequent section.

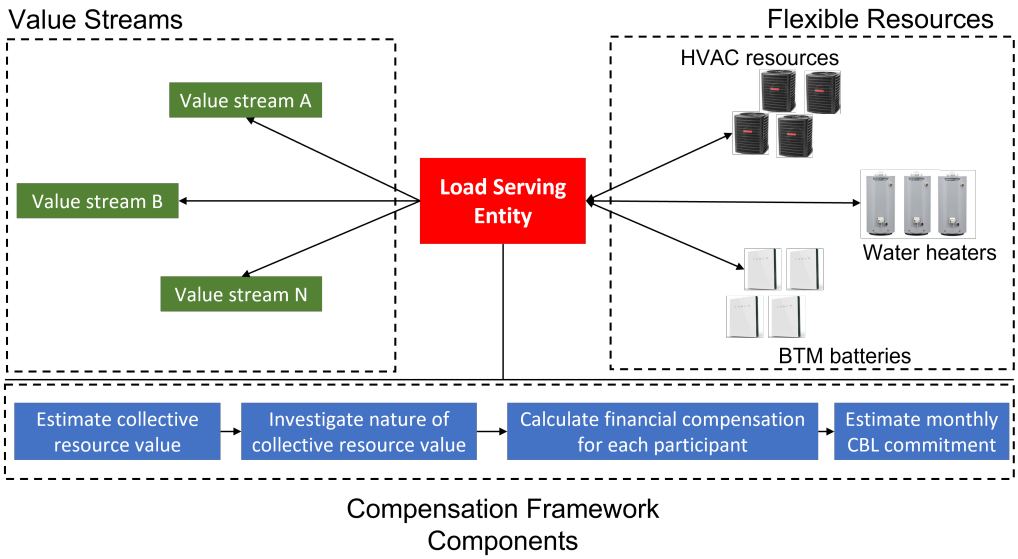

Figure 5.1: Overall framework illustration

5.3 Framework Details

5.3.1 Estimation of the Collective Value of All Resource Clusters and the Marginal Value of Each Resource Cluster

Consider the generic model (5.1), where $C(a, b, n)$ represents an LSE's cost function reflecting multiple value streams captured from resource clusters a, b, and n. Constraints (5.1b) to (5.1e) reflect the different characteristics of resource clusters a, b, and n and the characteristics of the LSE's network, if applicable.

$$minimize\ C(a, b, n) \tag{5.1a}$$

subject to:

$$Cluster\ a\ constraints \tag{5.1b}$$

$$Cluster\ b\ constraints \tag{5.1c}$$

$$Cluster\ n\ constraints \tag{5.1d}$$

$$Network\ constraints \tag{5.1e}$$

Let C^* and C^*_{base} be the optimal values of model (5.1) with and without resource clusters a, b, and n, respectively. Also, let C^*_a, C^*_b and C^*_n be the optimal values of model (5.1) with only cluster a, cluster b and cluster n, respectively. Hence, the collective value of the resource clusters, each resource cluster's marginal value, and other possible combinations can be calculated as shown in (5.2), where $V(s)$ denotes the value of resource cluster s. Note that similar expressions can be obtained in the case where the LSE maximizes some profit value.

$$V(a, b, n) = C^*_{base} - C^* \tag{5.2a}$$

$$V(a) = C^*_{base} - C^*_a \tag{5.2b}$$

$$V(b) = C^*_{base} - C^*_b \tag{5.2c}$$

$$V(c) = C^*_{base} - C^*_c \tag{5.2d}$$

$$V(a,b) = C^*_{base} - C^*_{a,b} \tag{5.2e}$$

$$V(a,c) = C^*_{base} - C^*_{a,c} \tag{5.2f}$$

$$V(b,c) = C^*_{base} - C^*_{b,c} \tag{5.2g}$$

Let us consider a specific application where the LSE's flexible resources are clusters of residential HVACs, water heaters, and BTM batteries. The HVAC, water heater, and BTM battery clusters are represented by models (5.3), (5.4), and (5.5). The interested reader is referred to our previous work [6] for a detailed explanation of the models.

5.3.1.1 HVAC Model

The aggregated HVAC model is as shown in (5.3).

$$\begin{aligned} T_{i,h,t+1} = T_{i,h,t}\left(1 - \tfrac{\Delta t}{R_h C_h}\right) + T_{a,t}\left(\tfrac{\Delta t}{R_h C_h}\right) - \\ \eta_{\mathrm{COP},h} P_{h,t}\left(\tfrac{\Delta t}{C_h}\right) + P_{\mathrm{sol},,}\left(\tfrac{\Delta t}{C_h}\right) \end{aligned} \tag{5.3}$$

5.3.1.2 Water Heater Model

The aggregated water heater model is as shown in (5.4).

$$SOC_W = \frac{T_{w,avg}}{T_{w_{\max}}} \tag{5.4a}$$

$$SOC_{w,t+1} = a_{w,t} SOC_{w,t} + \frac{(b_t P_{w,t} + e_{w,t})}{T_{w\,\max}} \tag{5.4b}$$

$$a_{w,t} = \exp\left(-\frac{\Delta t}{R_w C_w}\right), b_t = R_w\left(1 - a_{w,t}\right) \tag{5.4c}$$

$$e_{w,t} = \left(G R_w T_a + B R_W T_{cw}\right)\left(1 - a_{w,t}\right) \tag{5.4d}$$

$$R_w = \frac{1}{G+B}, B = \rho W_t c, G = \frac{A}{R_e}, C_w = mc \tag{5.4e}$$

5.3.1.3 BTM Battery Model

The aggregated battery model is as shown in (5.5).

$$E_{b,t+1} = \alpha_b E_{b,t} + \eta_{ch,b} P_{ch,b,t} - \frac{1}{\eta_{dis,b}} P_{\text{dis, b,t}} \tag{5.5a}$$

$$P_{b,t} = \eta_{ch,b} P_{ch,b,t} - \frac{1}{\eta_{dis,b}} P_{dis,b,t} \tag{5.5b}$$

$$E_{b,\min} \leq E_{b,t} \leq E_{b,\max} \tag{5.5c}$$

$$0 \leq P_{ch,b,t} \leq P_{ch,b,\max} \tag{5.5d}$$

$$0 \leq P_{dis,b,t} \leq P_{\text{dis,b, max}} \tag{5.5e}$$

$$P_{b,t}^2 + Q_{b,t}^2 \leq S_b^2 \tag{5.5f}$$

$$ch_{ind,t} + dis_{ind,t} \leq 1 \tag{5.5g}$$

Assuming the LSE combines peak shaving, energy arbitrage, ramp rate reduction, voltage management, and loss reduction as value streams of interest, model (5.1) becomes (5.6).

$$minimize\ C$$

$$C = \lambda_{\text{cap}}\ \max\left(P_{\text{bought},t}\right) + \sum_{t=1}^{T} \lambda_{\text{real},t} P_{\text{bought},t} +$$
$$\sum_{t=1}^{T} \lambda_{\text{reactive},} Q_{\text{bought},t} + \sum_{t=1}^{T} \lambda_{\text{real},t} P_{\text{loss},t} + \sum_{t=1}^{T} \lambda_{\text{reactive},t} Q_{\text{loss},t}$$
$$+ \sum_{t=1}^{T} \lambda_{\text{ramp,t}} P_{abs,t} + \sum_{c=1}^{C} \sum_{t=1}^{T} \lambda_{\text{capacitor}} X_{c,t} + \sum_{r=1}^{R} \sum_{t=1}^{T} \lambda_{reg} X_{r,t} \tag{5.6a}$$

Subject to:

$$(5.3),\ \forall h \in H \tag{5.6b}$$

$$(5.4),\ \forall w \in W \tag{5.6c}$$

$$(5.5)\ ,\forall b \in B \tag{5.6d}$$

$$P_{\text{loss}} = \sum_t \sum_i \sum_j I_{ij,t}^2 r_{ij} \tag{5.6e}$$

$$Q_{\text{loss}} = \sum_t \sum_i \sum_j I_{ij,t}^2 x_{ij} \tag{5.6f}$$

$$\sum_{k \in pr(i)} \left(P_{ki,t} - r_{ki} I_{ki,t}^2\right) - \sum_{j \in cr(i)} P_{ij,t} = P_{L,i,t} + P_{h,i,t}$$

$$+P_{w,i,t} + P_{b,i,t} \quad \forall b, h, w \in i, \forall i \in N \tag{5.6g}$$

$$\sum_{k \in \text{pr}(i)} \left(Q_{ki,t} - x_{ki} I_{ki,t}^2\right) - \sum_{j \in cr(i)} Q_{ij,t} = Q_{L,i,t} + Q_{h,i,t}$$

$$+Q_{b,i,t} + \text{Cap}_{c,t} \times Q_{c,t} \quad \forall b, h, c \in i, \forall i \in N \tag{5.6h}$$

$$V_{i,t}^2 - V_{j,t}^2 - 2\left(r_{ij} P_{ij,t} + x_{ij} Q_{ij,t}\right) + \left(r_{ij}^2 + x_{ij}^2\right) I_{ij,t}^2 = 0$$

$$\forall j \in \text{cr}(i) \tag{5.6i}$$

$$P_{ij,t}^2 + Q_{ij,t}^2 \leq S_{ij,\max}^2 \tag{5.6j}$$

$$P_{\text{bought},t}^2 + Q_{\text{bought},t}^2 \leq S_{\text{substation}}^2 \tag{5.6k}$$

$$\left\| \begin{array}{c} 2P_{ij,t} \\ 2Q_{ij,t} \\ I_{ij,t}^2 - V_{i,t}^2 \end{array} \right\|_2 \leq I_{ij,t}^2 + V_{i,t}^2 \tag{5.6l}$$

$$V_{sub,t} = 1 + \Delta V \times Reg_{r,t} \tag{5.6m}$$

$$P_{\text{bought},t+1} - P_{\text{bought},t} \leq P_{\text{abs},\,t} \forall t \in T \tag{5.6n}$$

$$P_{\text{bought},t+1} - P_{\text{bought},t} \geq -P_{\text{abs},t} \forall t \in T \tag{5.6o}$$

$$P_{abs,\min} \leq P_{abs,t} \leq P_{abs,\max} \quad \forall t \in T \tag{5.6p}$$

$$\text{Reg}_{r,t+1} - \text{Reg}_{r,t} \leq X_{r,t} \quad \forall r \in R \tag{5.6q}$$

$$\text{Reg}_{r,t+1} - \text{Reg}_{r,t} \geq -X_{r,t} \quad \forall r \in R \tag{5.6r}$$

$$X_{r,\min} \leq X_{r,t} \leq X_{r,\max} \quad \forall r \in R \tag{5.6s}$$

$$\text{Cap}_{c,t+1} - \text{Cap}_{c,t} \leq X_{c,t} \quad \forall r \in R \tag{5.6t}$$

$$\text{Cap}_{c,t+1} - \text{Cap}_{c,t} \geq -X_{c,t} \quad \forall r \in R \tag{5.6u}$$

$$\mathrm{X}_{c,\min} \leq \mathrm{X}_{c,t} \leq \mathrm{X}_{c,\max} \quad \forall r \in R \tag{5.6v}$$

$$T_{i,h,\min} \leq T_{i,h,t} \leq T_{i,h,\max} \quad \forall h \in H \tag{5.6w}$$

$$\mathrm{SOC}_{w,\min} \leq SOC_{w,t} \leq SOC_{w,\max} \quad \forall w \in W \tag{5.6x}$$

$$0 \leq P_{h,t} \leq P_{h,\max} \quad \forall h \in H \tag{5.6y}$$

$$0 \leq P_{w,t} \leq P_{w,\max} \quad \forall w \in W \tag{5.6z}$$

$$0 \leq P_{\text{bought},t} \leq P_{\text{substation}} \quad \forall t \in T \tag{5.6aa}$$

$$0 \leq Q_{\text{bought},t} \leq Q_{\text{substation}} \quad \forall t \in T \tag{5.6ab}$$

$$V^2_{\min} \leq V^2_{i,t} \leq V^2_{\max} \quad \forall i, \forall t \tag{5.6ac}$$

$$I^2_{ij,\min} \leq I^2_{ij,t} \leq I^2_{ij,\max} \quad \forall i, \forall j, \forall t \tag{5.6ad}$$

$$\sum_t (P_{h,i,t}) \leq \sum_t (P_{h,i,base,t}) \ \forall i \tag{5.6ae}$$

$$\sum_t (P_{w,i,t}) \leq \sum_t (P_{w,i,base,t}) \ \forall i \tag{5.6af}$$

$$\sum_t (P_{b,i,t}) \leq \sum_t (P_{b,i,base,t}) \ \forall i \tag{5.6ag}$$

The cost function in (5.6a) reflects all the costs associated with the LSE's value streams of interest. The first term represents capacity-related charges which can include capacity costs and transmission costs, while the second and third terms are energy costs. The losses are captured in the fourth and fifth terms. The sixth term and equations (5.6n) - (5.6p) represent convex relaxations capturing the ramp rate application. The seventh and eighth terms of the objective function represent costs associated with operating typical voltage management devices. These costs are expressed in terms of the initial costs and switching operations over the lifetime of these devices [20]. To preserve convexity, the seventh and eighth terms in the objective function, which represent absolute value terms, are accompanied by equations (5.6q) - (5.6v). Constraints (5.6g) to (5.6l) represent second-order conic relaxation-based power flow equations [21]. Constraint (5.6m) approximates the impact of the

voltage regulator located at the substation. Constraints (5.6ae) - (5.6ag) ensures that the energy costs incurred by the participants in the LSE's flexibility program do not exceed the costs they would have incurred if they did not participate. These constraints are tied to Assumption 5 and ensure that the participants are not worse off for participating in the LSE's program. Other constraints reflect comfort and operational limits associated with the flexible resources and the LSE's network.

Solving problem (5.6) with and without flexible resources provides the collective and marginal resource values illustrated in (5.2). These values indicate the maximum compensation allocated to each resource cluster. If existing regulations allow the LSE to recover costs associated with setting up the flexibility program, the participants will not get the maximum compensation allocation. Also, if regulations allow the LSE to keep a portion of the collective value for itself (e.g., Performance Based Regulation in Hawaii [22]), the participants will not get the maximum compensation allocation.

5.3.2 Investigation of the Nature of the Collective Resource Value

Using the results from (5.2), the LSE can investigate the nature of the collective value of the resource clusters. Understanding the collective resource value provides a basis for selecting the appropriate compensation allocation mechanism for the resource clusters. The following theorems are established to guide collective resource value investigation.

Theorem 1: *The collective value of a group of flexible resource clusters capturing multiple value streams for an LSE within the context of a flexibility program can be either strictly super-additive or strictly sub-additive or additive.*

Using definitions established in (5.2), Theorem 1 can be expressed mathematically as shown in (5.7a) to (5.7c).

$$\textbf{Strictly Sub-Additive: } V(a) + V(b) + V(n) > V(a, b, n) \tag{5.7a}$$

$$\textbf{Strictly Super-Additive: } V(a) + V(b) + V(n) < V(a, b, n) \tag{5.7b}$$

$$\textbf{Additive: } V(a) + V(b) + V(n) = V(a, b, n) \tag{5.7c}$$

The nature of the collective resource value depends on the value streams captured, resource characteristics, and applicable system constraints. Based on the three categories outlined in Theorem 1, Theorems 2 - 4 establish applicable compensation allocation mechanisms.

Theorem 2: *For a strictly sub-additive collective resource value, there is no completely fair compensation allocation mechanism that provides compensations equal to or greater than the marginal value of each resource cluster. In other words, other resource clusters suffer if a resource cluster is allocated its marginal value.*

Theorem 2 can be proven using game-theoretic concepts of balance and convexity. While the details of these concepts are not the focus of this work, we present the following definitions to set the stage for subsequent discussions. The reader can consult [9] and [12] for interesting discussions about these concepts.

Definition 1 (Balanced Map): *A map* $\gamma : S \rightarrow$ *[0,1] is balanced if* $\forall s \in \{a, b, n\}$, $\sum_{S \subset \{a,b,n\}} \gamma(S) 1\{s \in S\} = 1$, *where* $1\{.\}$ *is an indicator function. This implies that a balanced map assigns a weight to every resource cluster combination S such that the summation of weights for every combination containing a particular resource cluster is 1.*

Definition 2 (Balanced Game): *A game is balanced if for any balanced map* γ, $\sum_{S \subset \{a,b,n\}} \gamma(S) V(S) \leq V(a, b, n)$.

Definition 3 (Convex Game): *A game is convex if it satisfies the condition:* $V(S) + V(\Upsilon) \leq V(S \cup \Upsilon) + V(S \cap \Upsilon)$, $\forall\ S, \Upsilon \subset \{a, b, n\}$. *This implies that the marginal value of the resource clusters in a resource cluster combination increases as the combination grows in size.*

Specifically, we can check for the balance and convexity of the game involving the pseudo-coalition formed by the flexible resource clusters [12]. We use the term 'pseudo-coalition' because, according to Assumption 6, the resources cannot capture the value streams of interest in isolation. In other words, the resource clusters need to participate in the LSE's flexibility program to capture the value streams. The LSE determines the value created by each resource in its flexibility program. If the pseudo-coalition's game is both unbalanced and non-convex, then Theorem 2 holds. The proof is in the appendix.

Since there are no completely fair allocation mechanisms for sub-additive collective resource value, the compensations are allocated based on ratios of the total marginal value, as shown in (5.8). $x(a)$, $x(b)$, and $x(n)$ are the maximum financial compensation allocations for resource clusters a, b and n, respectively.

$$x(a) = \frac{V(a)}{V(a) + V(b) + V(n)} \times V(a, b, n) \tag{5.8a}$$

$$x(b) = \frac{V(b)}{V(a) + V(b) + V(n)} \times V(a, b, n) \tag{5.8b}$$

$$x(n) = \frac{V(n)}{V(a) + V(b) + V(n)} \times V(a, b, n) \tag{5.8c}$$

Theorem 3: *For a strictly super-additive collective resource value, totally fair compensation allocation mechanisms exist if the game involving the pseudo-coalition formed by the resource clusters is either balanced or convex.*

Again, Theorem 3 is based on game-theoretic concepts relating to the non-emptiness of the core of a game if conditions of balance or convexity are satisfied. A non-empty core implies the existence of a totally fair way of allocating the collective resource value. The interested reader can refer to [9] and [12] for an interesting discussion of these concepts. From Theorem 3, we can deduce that the applicable compensation allocation mechanism depends on the outcomes of checks for balance and convex-

ity. The applicable compensation mechanisms are selected based on the following conditions.

1. If the game involving the pseudo-coalition formed by the resource clusters is proven to be balanced and not convex, use the Worst-Case-Excess-Minimization (WCEM) mechanism [9]. For the three-cluster illustration (equation sets 5.1 and 5.2), WCEM solves the optimization problem (5.9) to obtain the best compensation allocations for each resource cluster.

$$minimize\ e \tag{5.9a}$$

Subject to:

$$e + x(a) - V(a) \geq 0 \tag{5.9b}$$

$$e + x(b) - V(b) \geq 0 \tag{5.9c}$$

$$e + x(n) - V(n) \geq 0 \tag{5.9d}$$

$$e + x(a) + x(b) - V(a,b) \geq 0 \tag{5.9e}$$

$$e + x(b) + x(n) - V(b,n) \geq 0 \tag{5.9f}$$

$$e + x(a) + x(n) - V(a,n) \geq 0 \tag{5.9g}$$

$$x(a) + x(b) + x(n) = V(a,b,n) \tag{5.9h}$$

$$x(a) \geq V(a) \tag{5.9i}$$

$$x(b) \geq V(b) \tag{5.9j}$$

$$x(n) \geq V(n) \tag{5.9k}$$

2. If the game involving the pseudo-coalition formed by the resource clusters is proven to be convex and not balanced, use the Worst-Case-Excess-Minimization (WCEM) mechanism or Shapley allocation mechanism [23]. The Shapley allocation mechanism is based on calculating the well-known Shapley values [23]. Hence, the allocated compensation for each resource cluster in the three-cluster

illustration equals its Shapley value, as shown in (5.10). However, if there are multiple clusters, trade-offs between using efficient algorithms for estimating the Shapley values (see [24]) and solving more complex optimization problems resulting from WCEM will need to be considered. For example, ten resource clusters will yield an optimization problem with at least $2^{10} - 1$ constraints.

$$x(s) = \sum_{S \subset \{a,b,n\} \setminus \{s\}} \frac{|S|!(3 - |S| - 1)!}{3!} [V(S \cup \{s\}) - V(S)] \quad \forall s \in \{a, b, n\} \tag{5.10}$$

3. If both balance and convexity conditions are satisfied, both WCEM and Shapley allocation mechanisms are applicable. However, if none of the balance and convexity conditions are satisfied (i.e., empty core), the allocation mechanism for the sub-additive case can be applied.

Theorem 4: *For an additive collective resource value, each resource cluster's maximum compensation equals its marginal value.*

From Theorem 4, the resource cluster compensations for the three-cluster illustration are shown in (5.11).

$$x(a) = V(a) \tag{5.11a}$$

$$x(b) = V(b) \tag{5.11b}$$

$$x(n) = V(n) \tag{5.11c}$$

5.3.3 Estimation of Each Participant's Monthly Financial Compensation

The collective resource value is shared among the different resource clusters using the applicable compensation allocation mechanism. If the LSE defines multiple representative days to capture seasonal variations in the collective value of the resources,

the applicable compensation mechanism for each season is selected. Each cluster's allocated compensation is then shared uniformly among the individual resources in the cluster. The uniform sub-cluster level allocation is based on Assumption 2, i.e., the resources in each cluster are very similar and connected to the same node on the LSE's network, if applicable.

5.3.4 Estimation of Prospective LMI Participants' Credit Improvement Commitments

Credit ratings are numerical indicators constructed to predict a borrower's credit risk. Generally, borrowers with higher credit scores have easier access to credit facilities and more favorable loan terms. Hence, the credit score could significantly impact a household's financial well-being. While income is not directly captured in credit scoring, studies have shown that there is at least a moderate correlation between income and credit ratings [14, 15]. This implies that, on average, LMI consumers are more likely to have lower credit ratings. As such, tools or programs that increase the credit ratings of LMI households could improve their overall financial well-being.

One of the widespread methods employed for credit rating improvement, especially in the United States, is the concept of credit builder loans (CBLs) [16]. CBLs are short-term installment contracts on small amounts in which the lender eliminates its credit risk by inverting the sequence of origination and repayment [16]. In other words, the loans are only released to the borrower after the loan's value has been fully paid over a defined period. In essence, CBLs operate more like savings instead of loans. However, credit reporting treats CBLs as standard installment loans, per industry agreements between CBL providers and the major credit bureaus [16].

In relation to the LSE's flexibility program, a fraction of an LMI participant's monthly financial compensation can be set aside as monthly payments for a CBL over the program cycle (e.g., 12 months). Under such conditions, the LSE can make the payment directly to the CBL provider on behalf of the LMI participant. At

the end of the program cycle, the LMI participant gets the total value of the CBL and improved credit ratings. This mechanism hinges on the assumption that the LSE can establish partnerships with third-party CBL providers, which is not far-fetched. The partnership between Duke Energy and Ford to reduce monthly lease payments made by Ford's F-150 electric truck leasees participating in Duke Energy's pilot Vehicle-to-Grid (V2G) program is an example of such a third-party partnership [25]. Duke Energy essentially makes payments to Ford on behalf of the V2G program participants.

Since the proposed framework is applied at the program design stage, the prospective LMI participant specifies their current credit rating, Cr_0, the maximum fraction of their monthly compensation to commit to credit building, F, and their intended credit improvement goals, Cr_{LMI}. The LSE uses this information as input into the optimization problem (5.12) to decide the LMI participant's monthly payments, P_m, to commit to a CBL.

$$minimize \ (E[Cr_{M,u}] - Cr_{LMI})^2 \tag{5.12a}$$

subject to:

$$Cr_{M,u} = K_1 Cr_0 + K_2 \sum_{m=1}^{M} P_{m,u} + u \ \forall \, u \, in \, U \tag{5.12b}$$

$$0 \leq P_{m,u} \leq F \times P_{fin,m} \ \forall \, u \, in \, U \tag{5.12c}$$

The objective function (5.12a) tries to make the LMI participant's expected credit rating at the end of the program cycle M as close as possible to the specified goal. The expectation operator ($E[.]$) indicates that there is some uncertainty associated with the actual credit score improvements. This uncertainty (u), which is mainly due to the participant's credit behavior, is captured in the regression-based relationship between the participant's current credit score, monthly CBL payments, and credit

score improvements (constraint (5.12b)). The exact nature of the uncertainty can be characterized using anonymized customer credit data. Constraint (5.12c) ensures that the monthly payments do not exceed the maximum fraction specified by the LMI participant. Note that the credit improvement is based on the assumption that the LMI participant does not default on other payment commitments different from the CBL. This caveat could be captured in the terms and conditions of the program.

5.4 Case Studies

5.4.1 Simulation Data

We assumed that the LSE's network is a modified version of the IEEE-33 bus test system [26]. As shown in (5.6) and Fig. 5.2, the LSE has three homogeneous resource clusters across each phase of its distribution network. Residential units forming the HVAC cluster are connected to Node 12. The HVAC resources are assumed to belong to the LMI households. The water heater and BTM battery clusters are on Node 7 and Node 3, respectively. The parameters for the resource clusters are shown in Table 5.1. The LSE also operates a solar PV system (rated at 200 kVA per phase) connected to Node 18. The capacitors are rated at 50 kVAR per phase and are connected to nodes 8, 13, 22, 23, and 27.

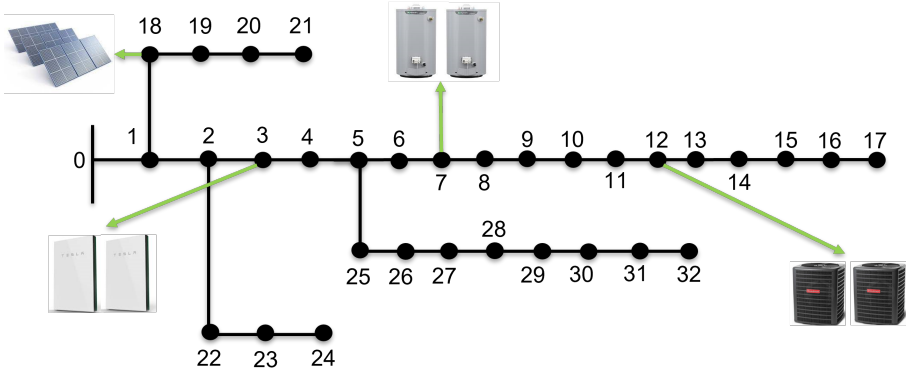

Figure 5.2: LSE's network and resource clusters

The energy market prices and capacity cost data were obtained from NYISO's 2019 data repository [27]. $\lambda_{ramp,t}$ was set at \$25/MWh, based on the price at which

NYISO procures additional reserve capacity to handle additional system ramping concerns [28]. The operating costs for the capacitors ($\lambda_{capacitor}$) and regulators (λ_{reg}) are based on the analysis provided in [20]. All optimization problems were solved using a Gurobi solver, within the CVX optimization tool, running on a Microsoft Surface laptop [29]. The regression model parameters (K_1 and K_2) describing the relationship between credit improvements and CBL payments were obtained using simulated credit data from Credit Land [30]. Note that the LSE can obtain real anonymized credit data from credit bureaus or CBL providers for real-world deployments.

Table 5.1: Resource cluster parameters

	HVAC Cluster	Water Heater Cluster	BTM Battery Cluster
No. of units	42	42	30
Parameters	$R_h = 0.06^oC/kW$	A = 96m^2	$\alpha_b = 1$
Parameters	$C_h = 45.25kWh/^oC$	$R_e = 16$	$\eta_{ch} = 0.927$
Parameters	$\eta_{COP} = 4$	$C_w = 33 \times 10^6 J/kg$	$\eta_{dis} = 1.08$
Total rating	180 kW	189 kW	150 kW / 405 kWh
Comfort/ Usage Limits	$T_{i,min} = 66.95^oF$ $T_{i,max} = 72.95^oF$	$SOC_{min} = 0.895$ $SOC_{max} = 1$	$SOC_{min} = 0.2$ $SOC_{max} = 1$

5.4.2 Compensation Allocation and Credit Rating Improvement Results

Two simulation cases are considered to illustrate variations in the nature of the collective value of the flexible resources.

1. LSE controls flexible resources and also operates a solar PV system (Flexible Resources and PV)

2. LSE controls flexible resources only (Flexible Resources Only)

5.4.2.1 Flexible Resources and PV

The collective resource value and the marginal value of the resource clusters in the LSE's flexibility program for a single summer representative data are shown in Table

5.2.

Table 5.2: Collective and marginal resource value

Resource Cluster	Flexible Resources and PV ($)	Flexible Resources Only ($)
V(HVAC)	67.06	69.38
V(WH)	10.33	5.36
V(Batt)	67.87	65.92
V(HVAC,WH)	76.69	76.13
V(HVAC,Batt)	132.2	138.9
V(Batt,WH)	75.12	72.95
V(HVAC,WH,Batt)	139.05	144.95

Table 5.2 shows that a combination of the three resource clusters produces the highest value for the LSE, as expected. However, the collective value from the three resource clusters is lower than the value for the Flexible Resources Only case. Again, this observation is logical, considering the solar PV resource reduces the LSE's energy cost and could provide additional low-cost voltage support.

Also, from Table 5.2, the summation of $V(HVAC)$, $V(WH)$, and $V(Batt)$ equals \$145.26, which is greater than the collective resource value, \$139.05. Hence, the collective value is sub-additive. Applying the allocation mechanism shown in (5.8), the maximum financial compensation allocations for the HVAC, water heater, and BTM battery clusters are \$64.19, \$9.89, and \$64.97, respectively. As discussed earlier, if the LSE is allowed by existing regulations to recover its program setup cost and keep some of the value for itself, the resource cluster compensation will be less than the maximum allocation.

For the HVAC cluster, which is also assumed to be the LMI participants' cluster, each participant's estimated monthly financial compensation based on the single representative day is \$39.48 (assuming the resources are used 310 days in a year).

The initial credit ratings of the HVAC resource owners are assumed to follow a normal distribution with a mean of 560 points, and a standard deviation of 65 points

based on the survey conducted in [16]. Also, we assume that the credit improvement goals have a mean of 700 points and a standard deviation of 10 points. The specified maximum compensation percentage has a mean of 25% and a standard deviation of 5%. The expected credit rating improvements for the 42 participants in the LMI resource cluster and the corresponding monthly commitment for CBLs are shown in Fig. 5.3 and Fig. 5.4, respectively.

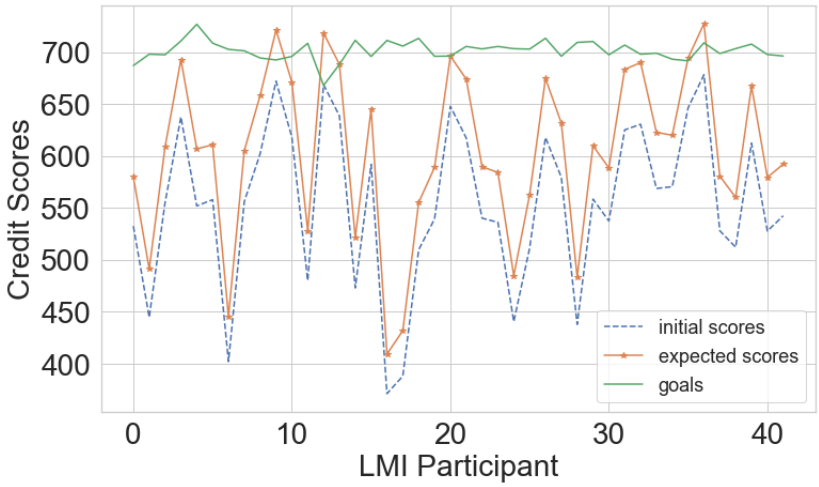

Figure 5.3: Illustrative credit ratings (Flexible Resources and PV)

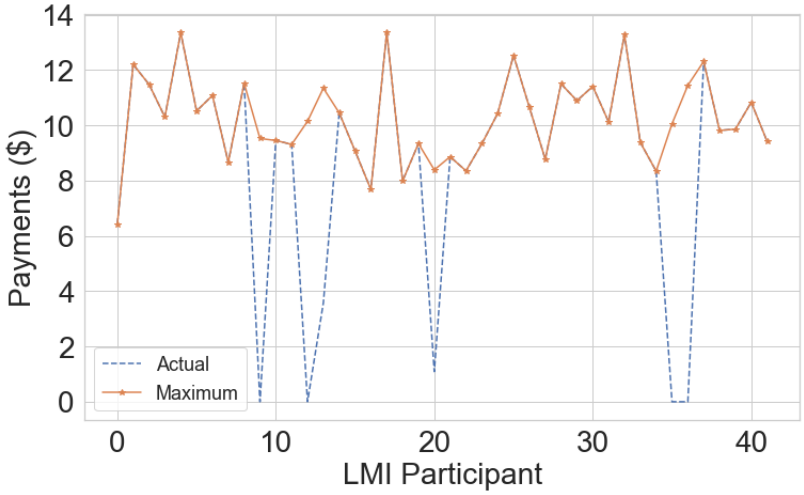

Figure 5.4: Monthly CBL commitments (Flexible Resources and PV)

Fig. 5.3 and Fig. 5.4 show that most of the participants have their monthly CBL commitments equal to their maximum limits, while their credit scores at the end of the program cycle are still less than their improvement goals. The average points

deficit across all 42 participants is 97.2 points. This implies that the participants in this illustration will have to increase their maximum commitment limits to improve the likelihood of achieving the set goals. Also, if the LSE uses the resources for services with higher value (e.g., frequency regulation), the participants can receive higher financial compensation, which can also improve their final credit scores through increased monthly CBL commitment capacity. For participants 10, 13, and 37 that exceeded their goals, their CBL commitments were negligible, implying that they could meet their credit improvement goals by continuing their consistent credit-building habits independent of taking advantage of the CBL. Also, participants 14 and 21 will be able to meet their goals with minimal CBL commitments.

5.4.2.2 Flexible Resources Only

For this case, the collective resource value and the marginal value of the resource clusters are also shown in Table 5.2. The summation of $V(HVAC)$, $V(WH)$, $V(Batt)$ equals \$140.66, which is less than the collective resource value, \$144.95. Hence, the collective value is super-additive. Checking for balance and convexity using definitions 2 and 3, the pseudo-coalition is balanced but non-convex. As such, the WCEM mechanism is applicable. The financial compensation allocations for the HVAC, water heater, and BTM battery clusters are \$70.77, \$5.71, and \$68.28, respectively, using WCEM. For each LMI participant (i.e., HVAC cluster member), the estimated monthly financial compensation based on the single representative day is \$43.52 (assuming the resources are used for 310 days in a year).

The expected credit improvement outcomes and monthly CBL commitments for this case are shown in Fig. 5.5 and Fig. 5.6, respectively. The patterns are similar to the Flexible Resources and PV case outcomes. However, the average credit points deficit was reduced to 96.3 points.

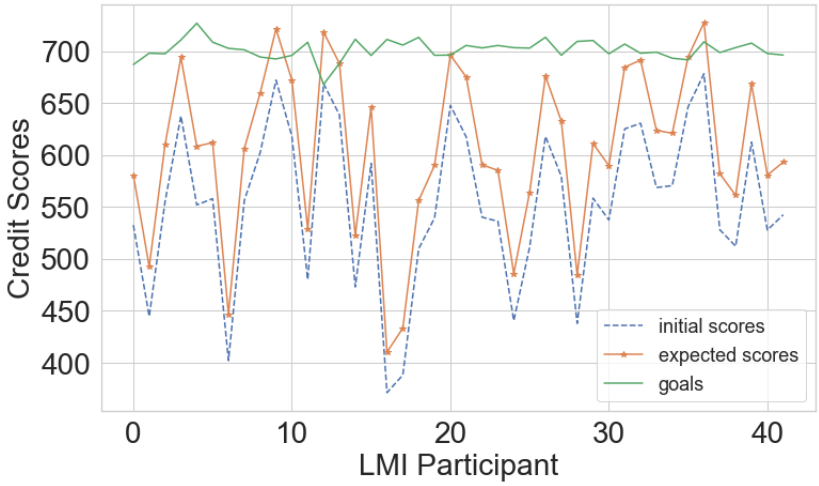

Figure 5.5: Illustrative credit ratings (Flexible Resources only)

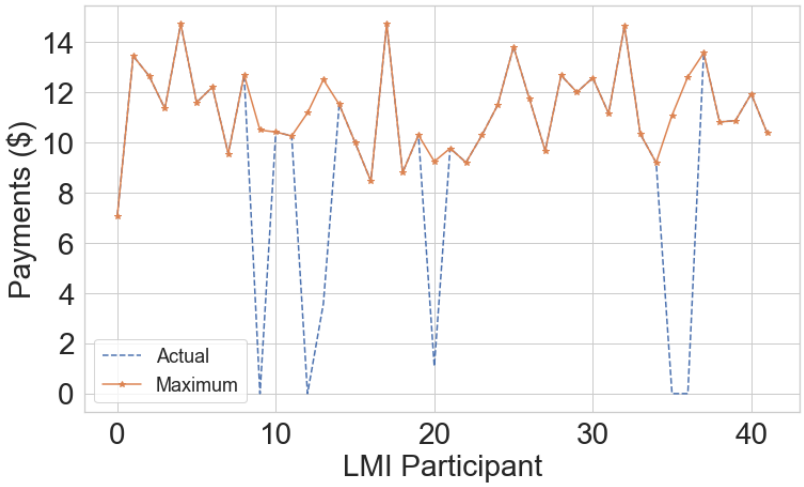

Figure 5.6: Monthly CBL commitments (Flexible Resources only)

5.5 Conclusions

This paper discusses a two-level compensation allocation framework that can be employed by an LSE using clusters of flexible customer-side resources on its network for multiple value streams. We posit that the collective resource value produced by flexible resources is either strictly sub-additive, strictly super-additive, or additive. We discuss applicable compensation mechanisms based on game-theoretic concepts depending on the classification. Also, we introduce the concept of social compensation mechanisms which the LSE can introduce to augment financial compensation and incentivize a unique customer segment to participate in the flexibility program.

Specifically, we propose improvements to credit ratings as an additional compensation dimension to encourage LMI customers to participate in the LSE's flexibility program. Illustrative case studies were also presented to show how the LSE can apply the proposed framework and compensation mechanisms. We focused on a single representative day in order to critically examine the case study outcomes. In practice, we expect that the LSE will estimate the resource value for different representative days representing different seasons of the year. Furthermore, while the illustrative credit score improvement outcomes are based on simulated credit data, the LSE can obtain anonymized real-world CBL data from credit unions to obtain more realistic outcomes for its LMI customers.

5.6 Appendix

The proof for Theorem 2 depends on the notion of balance and convexity of a game. We can prove that a game involving a pseudo-coalition with a sub-additive collective resource value is balanced or not by showing that there is at least a set of balanced weights that violates the condition in Definition 2.

Considering the three cluster example, we can assign the weight $\frac{1}{2}$ to each of the combinations $\{a\}$, $\{b\}$, $\{n\}$ and $\{a, b, n\}$. This mapping satisfies the balanced map definition (Definition 1). Writing out the expression on the left side of Definition 2 produces (5.13)

$$\frac{V(a) + V(b) + V(n) + V(a,b,n)}{2} > \frac{V(a,b,n) + V(a,b,n)}{2}$$
$$(since\, V(a) + V(b) + V(n) > V(a,b,n)) \tag{5.13}$$

Therefore,

$$\frac{V(a) + V(b) + V(n) + V(a,b,n)}{2} > V(a,b,n) \tag{5.14}$$

Therefore, Definition 2 is violated, implying that the game involving the resource clusters is not balanced. This result applies to pseudo-coalitions containing multiple resource clusters.

For convexity to hold, $V(a,b,n)$ - $V(a,n) \geq V(a,b)$ - $V(a)$ or $V(a,b)$ - $V(a) \geq V(b)$ must be true. Note that the number of conditions for a set of resource clusters equals $n-1$, where n is the number of resource clusters. To disprove convexity, we need to show that at least one of the following counter arguments holds.

Condition 1: $V(a,b,n)$ - $(V(a,n) + V(a,b)$ - $V(a)) < 0$

Condition 2: $V(a,b)$ - $(V(a) + V(b)) < 0$

The validity of either Condition 1 or Condition 2 depends on the relationship between $V(a) + V(b)$ and $V(a,b)$. Note that any two resource cluster combinations can be selected. Also, a larger number of clusters will require considering more cluster combinations.

If $V(a) + V(b) > V(a,b)$ (or any other two cluster combination), Condition 2 can be easily proven. It is clear that the left hand side (LHS) of Condition 2 is a negative value if $V(a) + V(b) > V(a,b)$.

If $V(a) + V(b) \leq V(a,b)$ (or any other two cluster combination), Condition 1 is provable. A term greater than or equal the LHS of Condition 1 can be obtained as shown in (5.15).

$$\begin{aligned} & V(a,b,n) - (V(a,n) + V(a,b) - V(a)) \\ \leq\ & V(a,b,n) - (V(a) + V(n)) - (V(a) + V(b)) + V(a) \end{aligned} \tag{5.15}$$

The RHS of (5.15) can be simplified further to obtain (5.16).

$$\begin{aligned} & V(a,b,n) - (V(a,n) + V(a,b) - V(a)) \\ \leq\ & V(a,b,n) - (V(a) + V(b) + V(n)) \end{aligned} \tag{5.16}$$

From Theorem 1, we know that under strict sub-additivity, $V(a) + V(b) + V(n) > V(a, b, n)$. Therefore the RHS of (5.16) is negative (i.e. less than 0). If the RHS of (5.16) is negative, then a smaller or equivalent value $V(a, b, n)$ - $(V(a, n) + V(a, b)$ - $V(a))$ is also negative. Thus, Condition 2 is satisfied.

Hence, a game involving a coalition of resource clusters yielding a sub-additive resource value is both unbalanced and non-convex. As such, Theorem 2 holds.

REFERENCES

[1] O. Megel, J.L Mathieu, and G. Andersson, "Scheduling distributed energy storage units to provide multiple services," in *2014 Power Systems Computation Conference*, pp. 1–7, 2014. doi: 10.1109/PSCC.2014.7038358.

[2] I. Beil, I. Hiskens, and S. Backhaus, "Frequency regulation from commercial building hvac demand response," *Proceedings of the IEEE*, vol. 104, no. 4, pp. 745–757, 2016. doi: 10.1109/JPROC.2016.2520640.

[3] Y. Shi, B. Xu, D. Wang, and B. Zhang, "Using battery storage for peak shaving and frequency regulation: Joint optimization for superlinear gains," *IEEE Transactions on Power Systems*, vol. 33, no. 3, pp. 2882–2894, 2018. doi: 10.1109/TPWRS.2017.2749512.

[4] E. Vrettos and G. Andersson, "Combined load frequency control and active distribution network management with thermostatically controlled loads," in *2013 IEEE International Conference on Smart Grid Communications (SmartGridComm)*, pp. 247–252, 2013. doi: 10.1109/SmartGridComm.2013.6687965.

[5] H. Hao, D. Wu, J. Lian, and T. Yang, "Optimal coordination of building loads and energy storage for power grid and end user services," *IEEE Transactions on Smart Grid*, vol. 9, no. 5, pp. 4335–4345, 2018. doi: 10.1109/TSG.2017.2655083.

[6] A. Abbas and B. Chowdhury, "A stochastic optimization framework for realizing combined value streams from customer-side resources," *IEEE Transactions on Smart Grid*, vol. 13, no. 2, pp. 1139–1150, 2022. doi: 10.1109/TSG.2021.3135155.

[7] A. Kulmala, M. Baranauskas, A. Safdarian, J. Valta, P. Järventausta, and T. Bjorkqvist, "Comparing value sharing methods for different types of energy communities," in *2021 IEEE PES Innovative Smart Grid Technologies Europe (ISGT Europe)*, Oct. 2021. doi: 10.1109/ISGTEurope52324.2021.9640205.

[8] C. Gerwin, R. Mieth, and Y. Dvorkin, "Compensation mechanisms for double auctions in peer-to-peer local energy markets," *Current Sustainable/Renewable Energy Reports*, vol. 7, pp. 165–175, Dec. 2020. doi: 10.1007/s40518-020-00165-1.

[9] E. Baeyens, E. Y. Bitar, P. Khargonekar, and K. Poolla, "Coalitional aggregation of wind power," *IEEE Transactions on Power Systems*, vol. 28, no. 4, pp. 3774–3784, 2013. doi: 10.1109/TPWRS.2013.2262502.

[10] C. Feng, F. Wen, S. You, Z. Li, F. Shahnia, and M. Shahidehpour, "Coalitional game-based transactive energy management in local energy communities,"

IEEE Transactions on Power Systems, vol. 35, no. 3, pp. 1729–1740, 2020. doi: 10.1109/TPWRS.2019.2957537.

[11] P. Chakraborty, E. Baeyens, P. Khargonekar, K. Poolla, and P. Varaiya, "Analysis of solar energy aggregation under various billing mechanisms," *IEEE Transactions on Smart Grid*, vol. 10, no. 4, pp. 4175–4187, 2019. doi: 10.1109/TSG.2018.2851512.

[12] L. Han, T. Morstyn, and M. McCulloch, "Incentivizing prosumer coalitions with energy management using cooperative game theory," *IEEE Transactions on Power Systems*, vol. 34, no. 1, pp. 303–313, 2019. doi: 10.1109/TPWRS.2018.2858540.

[13] J. Gattaciecca, K. Trumbull, S. Krumholz, K. McKanna and J. R. DeShazo, "Identifying effective demand response program designs for residential customers," Project Report CEC-500-2020-072, UCLA Luskin Center for Innovation, November 2020. Available: https://innovation.luskin.ucla.edu/wp-content/uploads/2021/01/Identifying-Effective-Demand-Response-Program-Designs-for-Residential-Customers.pdf.

[14] R. Beer, F. Ionescu, and G. Li, "Are income and credit scores highly correlated?," *FEDS Notes*, August 2018. Available: https://doi.org/10.17016/2380-7172.2235.

[15] S. Albanesi, G. De Giorgi, and J. Nosal, "Credit growth and the financial crisis: A new narrative," Working Paper 23740, National Bureau of Economic Research, August 2017. doi: 10.3386/w23740.

[16] J. Burke, J. Jamison, D. Karlan, K. Mihaly, and J. Zinman, "Credit building or credit crumbling? a credit builder loanâs effects on consumer behavior, credit scores and their predictive power," Working Paper 26110, National Bureau of Economic Research, July 2019. doi: 10.3386/w26110.

[17] P. Faria, J. SpÃnola, and Z. Vale, "Aggregation and remuneration of electricity consumers and producers for the definition ofÂ demand-response programs," *IEEE Transactions on Industrial Informatics*, vol. 12, no. 3, pp. 952–961, 2016. doi: 10.1109/TII.2016.2541542.

[18] M. A. Z. Alvarez, K. Agbossou, A. Cardenas, S. Kelouwani, and L. Boulon, "Demand response strategy applied to residential electric water heaters using dynamic programming and k-means clustering," *IEEE Transactions on Sustainable Energy*, vol. 11, no. 1, pp. 524–533, 2020. doi: 10.1109/TSTE.2019.2897288.

[19] S. Lin, F. Li, E. Tian, Y. Fu, and D. Li, Dongdong, "Clustering load profiles for demand response applications," *IEEE Transactions on Smart Grid*, vol. 10, no. 2, pp. 1599–1607, 2019. doi: 10.1109/TSG.2017.2773573.

[20] T. Malakar and S. K. Goswami, "Active and reactive dispatch with minimum control movements," *International Journal of Electrical*

Power Energy Systems, vol. 44, no. 1, pp. 78–87, 2013. Available: https://www.sciencedirect.com/science/article/pii/S0142061512003742.

[21] M. Farivar and S. H. Low, "Branch flow model: Relaxations and convexification - part i," *IEEE Transactions on Power Systems*, vol. 28, no. 3, pp. 2554–2564, 2013. doi: 10.1109/TPWRS.2013.2255317.

[22] State of Hawaii Public Utilities Commission, "Performance based regulation." Available: https://puc.hawaii.gov/energy/pbr/.

[23] L. Shapley, "Cores of convex games," *Int. J. Game Theory*, vol. 1, no. 1, pp. 11–26, 1971.

[24] G. O'Brien, A. El Gamal, and R. Rajagopal, "Shapley value estimation for compensation of participants in demand response programs," *IEEE Transactions on Smart Grid*, vol. 6, no. 6, pp. 2837–2844, 2015. doi: 10.1109/TSG.2015.2402194.

[25] Duke Energy, "Illuminating possibility: Duke Energy and Ford Motor Company plan to use F-150 Lightning electric trucks to help power the grid," 2022. Available:https://news.duke-energy.com/releases/illuminating-possibility-duke-energy-and-ford-motor-company-plan//-to-use-f-150- lightning-electric-trucks-to-help-power-the-grid.

[26] M.E. Baran and F. F. Wu, "Network reconfiguration in distribution systems for loss reduction and load balancing," *IEEE Transactions on Power Delivery*, vol. 4, no. 2, pp. 1401–1407, 1989. doi: 10.1109/61.25627.

[27] New York Independent System Operator, "Energy market and operational data," 2022. Available: https://www.nyiso.com/energy-market-operational-data.

[28] E. D. Avallone, "SENY Reserve Region Enhancements," 2020. Available: https://www.nyiso.com/documents/20142/12170360/ 4_22_2020 _Reserves_for_Resource_Flexibility_FINAL.pdf/b2db3169-5d56-ec11-1541-c83bc5f58ed5.

[29] Gurobi Optimization, LLC, "Gurobi optimizer reference manual," 2021. Available: https://www.gurobi.com.

[30] Credit Land, "Credit score simulator." Available: https://www.credit-land.com/tools/credit-score-simulator.php.

CHAPTER 6: CONCLUSIONS AND FUTURE WORK

This dissertation presented various tools that LSEs can leverage to capture multiple value streams from flexible customer-side resources within their jurisdictions. In Chapter 2, a novel stochastic equivalent battery model (EBM) that provides a simple and effective representation of the overall flexibility associated with a commercial building was discussed extensively. Also, an illustrative example of how the stochastic EBM can be applied to resource scheduling problems was presented. Under situations where the LSE has access to multiple commercial buildings, the proposed stochastic EBM model provides a simple and effective way of modeling the flexibility associated with each building. The stochastic nature of the model allows LSEs to model and examine how different uncertainties in building operating patterns can affect the overall flexibility achievable from each commercial building.

Also, in Chapter 3, a detailed stochastic scheduling model to help LSEs capture energy arbitrage, peak shaving, and market-based frequency regulation from homogeneous aggregations of residential heating, ventilation and air conditioning (HVAC) resources, water heaters, and behind-the-meter batteries was presented. Uncertainties relating to energy and regulation market signals and prices were considered. The scheduling model also captures the all-important consideration that participants, especially owners of behind-the-meter batteries, would require compensations beyond their opportunity costs to be incentivized to release their resources to the LSE. Although the scheduling model included elements unique to the New York Independent System Operator (NYISO) operating jurisdictions, it can be adapted to other electricity market environments. In addition to the scheduling model, a dynamic droop and a model predictive control (MPC) based real-time dispatch algorithm capable of

providing fast responses to high frequency regulation signals were also discussed and compared. Depending on unique operating conditions and requirements, the LSE can decide which of the two dispatch algorithms is more suitable.

Furthermore, Chapter 4 addresses day-ahead planning and operations for value streams relating to distribution system operations. Specifically, a stochastic scheduling model that captures energy arbitrage, peak shaving, ramp rate reduction, loss reduction, and voltage management using homogeneous aggregations of residential HVACs, water heaters, and behind-the-meter batteries was presented. Real-time dispatch algorithms based on linear decision rules (LDR) and model predictive control were also discussed. A unique perspective involving the presence of third-party aggregators on the LSEs network was also considered. In the near future, we expect policy trends to encourage the rise of multiple third-party aggregators that will also use resources on the LSE's network for multiple applications. As such, LSEs can use the proposed models and dispatch algorithms under such conditions.

Chapter 5 addresses issues relating to compensation for customer-side resources offering their flexibility to the LSE. Specifically, a practical step-wise framework that the LSE can employ to evaluate the financial compensations for each flexible resource owner was presented. In addition to direct financial compensations, a novel social compensation dimension was introduced as a tool for incentivizing flexibility from a unique customer segment. Discussions relating to how LSEs can use credit rating improvements as additional incentives to encourage flexibility from low and medium-income customers were also presented.

6.1 Main Contributions

In summary, the main contributions of this dissertation are as follows.

1. A novel stochastic equivalent battery model that represents the overall flexibility associated with the power consumption of a multi-zonal commercial building, including HVAC, water heater, battery, and EV charging resources, was devel-

oped. The flexibility limits in the model are time-varying and are quantified using a combination of model-based functional simulations and optimization techniques. The procedure for generating the stochastic flexibility limits has also been implemented as a Python package. The model's novelty stems from the inclusion of both dominant uncertainties associated with the operating pattern of the building and time-dependent flexibility limits.

2. A novel stochastic day-ahead resource scheduling model for a load-serving entity with access to aggregations of residential HVACs, water heaters, and behind-the-meter batteries for combined market-based frequency regulation provision, energy arbitrage, and peak shaving was also developed. The scheduling model captures stochasticity in energy and regulation market prices and frequency regulation signals which was non-existent prior to this work. The scheduling model also captures the potential impact of resource control actions on system voltages based on the voltage sensitivity matrix approach.

3. A novel stochastic day-ahead scheduling model for a load-serving entity with solar photovoltaic resources and access to groups of residential HVACs, water heaters, and behind-the-meter batteries for combined peak shaving, energy arbitrage, ramp rate reduction, loss reduction, and voltage management was developed. Uncertainty sources, including solar PV output variations and variations in forecasted total load, were captured.

4. A two-level game theory-based compensation framework was developed to help load serving entities allocate financial compensations to multiple customer-side resource owners participating in multi-value capturing flexibility programs. While the use of cooperative game theory for compensation allocation is not novel, the unique application to the case where an LSE uses multiple customer-side resources for multiple applications is novel.

5. A novel social compensation dimension to incentivize the participation of low and medium-income (LMI) customers in the flexibility programs is proposed. The social compensation dimension improves LMI participants' credit ratings in addition to financial rewards for providing their flexible resources for multiple value streams. Before this work, such compensation dimensions within the context of demand-side management programs were non-existent.

6.2 Future Work

Although several tools to aid load-serving entities in realizing multiple value streams from flexible customer-side resources within their jurisdictions have been proposed in this dissertation, there are still open research questions to be addressed. The following are some suggestions regarding areas for further research building on the concepts presented in this dissertation.

1. **Analysis of the impact of different flexible resource mixes and comfort limits on the overall flexibility of commercial buildings in different climate regions**

This represents a logical extension of the stochastic equivalent battery model (EBM) proposed in this dissertation. Different comfort limits, resource combinations, and weather conditions will result in varying flexibility limits for commercial buildings. Hence, examining how these different conditions affect the overall building flexibility will be beneficial. Subsequently, a set of representative flexibility limits for commercial buildings with different flexible resource mixes, comfort limits, and climate conditions can be established. Such representative limits can provide benchmarks for other regional or country-wide studies looking to fully capture the flexibility associated with commercial buildings.

2. **Long-term planning considerations**

The planning models proposed in this study are for the day-ahead time horizon. However, planning processes for LSEs cover multiple time scales. As such, there is a

need to consider long-term planning perspectives.

Long-term planning for using flexible customer-side resources for multiple value streams is multi-faceted. However, a major perspective relates to the LSE's need to understand how capturing multiple value streams from its customer-side resources will affect its long-term plans. For example, regulated electric utilities in the United States are often required to file integrated resource plans (IRP) that span multiple years. An electric utility that intends to capture multiple value streams from its customer-side resources must capture such perspectives in its IRP. Such electric utilities will benefit from further research on the right approach for including the impacts of multi-value flexibility programs in their IRPs.

3. **Frameworks and metrics for quantifying maximum beneficial flexibility penetrations**

As the popular saying goes, too much of anything is bad. While more demand-side flexibility is advantageous, there will be penetration levels beyond which negative effects overshadow the benefits. Therefore, LSEs will benefit from research that establishes clear frameworks and metrics to quantify maximum beneficial flexibility penetrations. Such frameworks and metrics will guide LSEs on what level of customer-side flexibility penetration to pursue.

4. **Pilot projects to test the proposed social compensation mechanism**

While the building blocks of the proposed social compensation dimension have been established in this dissertation, there is still a need for actual pilot studies to test how LMI customers respond to such compensation strategies.

APPENDIX A: BIOGRAPHY

Akintonde's professional career is dedicated to leveraging scientific methods and data-driven insights to build solutions catalyzing the energy transition and securing Africa's sustainable energy future. He holds a Bachelor's degree, with First Class honors, in Electronic and Electrical Engineering from Obafemi Awolowo University, Ile-Ife. He also holds a Master's degree in Electrical Engineering from the University of North Carolina at Charlotte. He has published several papers and presented his work at multiple conferences, including those organized by the Power and Energy Society (PES) of the Institute of Electrical and Electronic Engineers (IEEE). He also serves as a reviewer for multiple power and energy-related academic journals.

APPENDIX B: COPYRIGHT STATEMENT

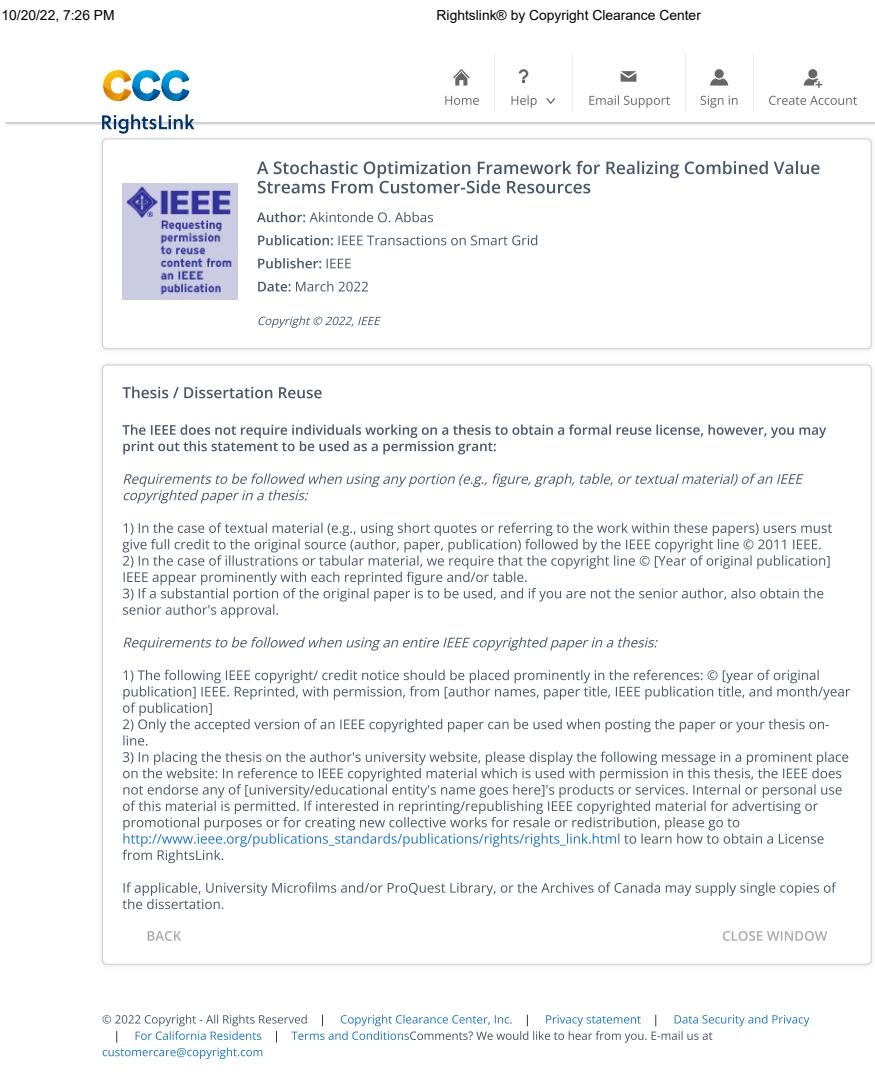

Figure B.1: IEEE copyright certificate for chapter 3